THE CHARACTERIZATION OF METHYLENE BLUE IN DETECTING BACTERIAL CONTAMINATION WITH THE UPDATED DESIGN OF THE RAPID CULTURE NANOWELL DEVICE

THE CHARACTERIZATION OF METHYLENE BLUE IN DETECTING BACTERIAL CONTAMINATION WITH THE UPDATED DESIGN OF THE RAPID CULTURE NANOWELL DEVICE

By:

CELINE SZE NEE LING, H. B. Sc

A Thesis

Submitted to the School of Graduate Studies

In Partial Fulfillment of the Requirements

For the Degree

Masters of Applied Science

McMaster University

MASTERS OF APPLIED SCIENCE (2019)	McMaster University
(Biomedical Engineering)	Hamilton, Ontario, Canada
TITLE	The Characterization of Methylene Blue in detecting bacterial contamination with the updated design of the Rapid Culture Nanowell Device
AUTHOR	Celine Sze Nee Ling, H. B. Sc. (McMaster University)
SUPERVISOR	Professor P. R. Selvaganapathy School of Biomedical Engineering
NUMBER OF PAGES	xiv, 111

Abstract

With approximately 24,500 preterm children born annually in Canada and an estimated shortage of 6 million ounces of breast milk, the distribution of donor milk must be time-sensitive yet safe to efficiently meet this demand. Donor human milk banks take the greatest precautions to protect their users, but some of these microorganisms manage to circumvent the employed methods. The consumption of contaminated donor milk has the potential to be fatal particularly to the vulnerable, immunocompromised premature infants. The tools used by milk banks to ensure safe distribution rely heavily on the culture plate. It has been the gold standard in screening for microbiological specimens due to its wide availability, low cost, and simplicity. However, the procedural times for bacterial culture plates are tedious and long, lasting a minimum of 48 hours. Advances in microfluidics, particularly in combination with the concept of monitoring metabolites to indicate bacterial viability, hold much promise to significantly reducing the long processing times of culture plates. Combining the concept of compartmentalized culture and a chromogenic optical dye for the detection of metabolic changes as a diagnostic sensor would simplify the identification and quantification of microbial presence. The updated Rapid Culture Detection system is a nanowell device fabricated using polydimethylsiloxane (PDMS) that uses the oxygen-sensitive redox indicator Methylene Blue to determine the presence of bacteria. Preliminary studies have shown to detect bacteria in as little as 3.33 hours using these nanowells compared to the 24 hours required for microwell liquid culture (620%). Initial studies have also been conducted with human milk, indicating a slower detection than in LB media. The novel easy-to-use and low-cost Rapid Culture Detection system is a promising alternative detection tool for protecting infants from pathogenic illnesses caused by contaminated human milk and shortening the time required to access lifesaving nutrition.

Acknowledgements

I'd like to thank my supervisor Dr. Ponnambalam Ravi Selvaganapathy for his guidance throughout this journey. You have made me question how things work and to always go back to the fundamentals; revising the process on how to learn and to breakdown a problem into solvable parts.

A million thanks go out to the past and present members of the Selvaganapathy lab: Aditya Aryasomayajula, Aliakbar Mohammadzadeh, Alireza Shahin, Devon Jones, Harpreet Matharoo, Jun Yang, Juncong Liu, Leo Hsu, Melizeth Bolaños, Mohammadhossein Dabaghi, Monika Sliwiak, Neda Saraei, Nidhi Jain, Parker Bondi, Rana Attalla, Reza Ghaemi, Rong Wu, Shayan Liaghat, and Sreekant Damodara. You have each played a part in completing this thesis by sharing your knowledge or lending a listening ear. To Reza and Mohammadhossein, I cannot thank you enough for your help and ingenuity as you guided me in the world of Mechanical Engineering. To Nidhi, thank you for believing in me and my work. To Rana, it is nearly impossible to put into words how much of an impact you have had throughout my research career. Thank you for guiding and inspiring in me. You are a true role model and friend for life.

I'd like to extend my thanks to Dr. Herb Schellhorn and his lab, particularly Ethan Pascos, Deepinder Sharma, Paul Naphtali, Mahi Mohiuddin, and Bansri Patel, for their expertise and support in the microbiology realm. I also want to acknowledge our collaborator PATH and our funding sponsors. Many thanks to all the technicians in the Biointerfaces Institute and the Mechanical Engineering Machine Shop – all your generous advice and support have propelled me to the finish line of this Masters Degree. To Nehad Hirmiz, thank you for sharing your extensive ImageJ and image processing knowledge and willingness to point me in the right direction.

To my beloved BME office-mates and hometown friends, you were the sunshine through the clouds caused by experimental mishaps and many uncertainties. I thank you from the bottom of my heart. Thank you to my parents and brother for your never-ending support, encouragement, patience, and most of all, your belief in me. You have helped me pass this finish line. Lastly, to everyone else not yet mentioned who has touched my life during this chapter, thank you.

To sum it up, you have all played a part in this milestone. It takes a village. Thank you.

Table of Contents

Abstract iii
Acknowledgements iv
List of Figures viii
List of Tables xii
Abbreviations xiii
Nomenclature xiv
Chapter 1 – Motivation and Organization 1
1.1 Motivation 1
1.2 Organization of Thesis 3
1.3 Contributions 4
Chapter 2 – Introduction 6
2.1 Foodborne Illnesses and Bacterial Contamination of Human Milk 6
2.2 Human Milk 7
2.2.1 Composition of Human Milk 8
2.2.2 Benefits of Human Milk 11
2.3 Human Milk Banking 12
2.3.1 Bacterial Contamination 13
2.3.1.1 Growth Phases of Bacteria 15
2.3.1.2 Bacterial Metabolism 17
2.3.2 Milk Banking Safety Protocols 18
2.3.2.1 Pasteurization and its Effects 18
2.3.2.2 Standard plate count using culture plates 21
2.4 Bovine Dairy Industry Methods of Detection: Dye Reduction 24
2.4 Current Microfluidic Biomedical Devices 26
2.5 Summary 28
Chapter 3 – Working Principle, Device Design, Materials, and Methods 30
3. 1 Working Principle 30
3.2 Device Design 32
3.2.1 Device Criteria 32
3.2.1 Device fabrication method: 3D Print vs Lithography 33
3.2.2 Device indicator material: Fluorescent vs Optical Dyes 34
3.2.3 Device imaging system 35

3.3 Materials 35
3.3.1 Consumable Reagents 35
3.3.2 Characterization Elements 36
3.3.3 Microfluidic Device 36
3.3.4 Bacteria 36
3.4 Methods 37
3.4.1 Fabrication of Nanowell Device 37
3.4.1.1 Master Mould Fabrication of Photolithography Device Mould 37
3.4.1.2 Master Mould Fabrication of 3D Printed Mould 38
3.4.1.3 Nanowell casting 39
3.4.1.4 Surface treatment 40
3.4.2 Sample Preparation 41
3.4.2.1 Bacteria preparation 41
3.4.2.2 Indicator Media Preparation 42
3.4.2.3 Human Milk Preparation 43
3.4.3 Sample Loading and Experimental Set-up in Nanowell device 44
3.4.3.1 Sample Loading 44
3.4.3.2 Experimental Set-up 44
3.4.4 Dissolved Oxygen Measurement 45
3.4.5 Imaging 45
3.4.5.1 Imaging in Tecan Plate Reader 46
3.4.5.2 Imaging with Cell Phone 46
3.4.5.3 Imaging with Fluorescent Microscope 47
3.4.5.4 Imaging with DSLR-Macroscope system 48
3.4.6 Image Processing and Data Extraction 49
3.4.7 Data Analysis 50
3.4.7.1 Relative Grey Scale Measurement 50
3.4.7.2 Statistical Analysis 50
Chapter 4 – Results & Discussion 51
4.1 Characterization of the use of Methylene Blue as an optical dissolved oxygen indicator for metabolism 51
4.1.1 Relationship between the colouration of Methylene Blue redox states and Mean Gray Value extracted from images 51
4.1.2 Effect of metabolism on Methylene Blue saturation 54

4.2 Colour change of MB in PDMS nanowell 57
4.3 Effect of the Method of Mould Fabrication on the effectiveness of MB as an optical sensor within the re-designed Rapid Culture Nanowell Device 58
4.4 Development of Imaging Set-up 61
4.4.1 Exploration of imaging modalities for MB characterization in microwells 62
4.4.2 Comparison of DSLR-Macroscope system to Tecan Plate Reader system 65
4.4.2 Exploration of imaging modalities for MB characterization in nanowells 68
4.5 Characterization of MB as optical metabolic indicator in microwells 69
4.5.1 Effect of MB quality on rate of MB colour change 69
4.5.2 Effect of MB concentration on rate of change in MB saturation 71
4.5.3 Effect of bacterial concentration on rate of change in MB saturation 73
4.6 Characterization of MB as optical metabolic indicator in PDMS nanowell device 77
4.6.1 Proof of Concept: Use of MB with Redesigned Rapid Culture Nanowell Device 77
4.6.2 Effect of bacterial concentration on rate of metabolism of MB in nanowells 80
4.7 Effect of Human Milk on MB metabolism 82
4.7.1 Testing of Bacterial Metabolism Detection in Milk Samples 82
4.8 Comparison of time required for detection of bacterial presence using Nanowell Device vs. Culture Plate 86
Chapter 5 – Conclusion & Future Work 88
5.1 Conclusion 88
5.2 Future Work 90
References 93
Appendix A Standard Operating Procedure for Preparation and Streaking of LB Agar Culture Dishes 102
Standard Operating Procedure for Preparation of LB Agar dishes 102
Standard Operating Procedure for Bacterial Streaking of Agar Dish 103
Appendix B Standard Operating Procedure for ImageJ Processing & Analysis 104
Appendix C Code for organizing ImageJ Data into columns for Excel 106
Appendix D Effect of bacterial concentration on rate of MB colour change using older stock of MB 107
Appendix E MB Concentration Comparison in Nanowell Devices 109
Appendix F Preliminary Experiment testing a higher MB Concentration in LB Nanowells 111

List of Figures

Figure 1: Breakdown of the median global number of A.) Foodborne Illnesses and B.) Foodborne Deaths, with 95% uncertainty intervals, based on the type of hazard (bacterial, virus, parasite, or chemical and toxin). Data extracted from [1]. 2
Figure 2: Anatomy of lactating breast. Modified from [27]. 8
Figure 3: Growth phases of bacteria. Reproduced from [61]. 16
Figure 4: Pasteurization of human milk in donor banks. A.) Typical pasteurization machine used to sterilize samples of milk. T30 Human Milk Pasteuriser pictured here. Subset i.) shows an image of loaded milk bottles. B.) Temperature cycle of the pasteurization process. Adapted from [49], [68]. 20
Figure 5: Standard plate count detection method used by Human Milk Donor Banks. A.) MacConkey's and B.) Blood Agar plates are used to differentiate and identify the bacterial species present. Adapted from [70]–[72]. 22
Figure 6: A.) Structure of MB in its oxidized and reduced forms. B.) Hypothesized mechanism of methylene blue redox reaction in vivo. Methylene blue is reduced through NAD(P)H-dependent reaction into its colourless form, then the leucomethylene form is oxidized by auto-oxidation. Adapted from [73]..... 25
Figure 7: UV-visible spectra comparing change in absorption peaks when methylene blue is converted into leucomethylene blue. There is a loss of peak at ~660 nm. Reproduced from [78]. 26
Figure 8: Segmentation of larger volumes into multiple cubes containing smaller amounts can artificially increase the concentration of bacteria, therefore decreasing the expected detection rates. Reproduced from [90]..... 31
Figure 9: Simplified representation of metabolism in bacteria that resides within a well in the nanowell device. Image of metabolism modified from [91]..... 31
Figure 10: Schematic illustration of the main photolithography steps. 38
Figure 11: Components involved in Multi Jet Modeling 3D printing. An inkjet head adds a layer of curable liquid photopolymer onto a tray which is rapidly polymerized by UV light. The inkjet head is also able to extrude a gel-like sacrificial material as support for overhanging or complex structures. Once the part has been fully printed, post-processing is required to dissolve the supports. Reproduced from [100] 39
Figure 12: PDMS nanowell device fabrication process flow. 41
Figure 13: Device Filling Schematic for MB staining method. The dye is added into the sample of bacteria and loaded into the prepared nanowell device. Once sealed, the device is imaged using the camera-based imaging system or microscope using brightfield setting. Imaging system images reproduced from [112], [113] 45
Figure 14: Schematic of the imaging set-up (front and side view) for the optical colorimetric DO concentration tests..... 47
Figure 15: Image of the imaging set-up for MB devices. This set-up could be adapted with the use of a light source and fluorescent filters for fluoroscopy. 48

Figure 16: Selection of areas of interest using ImageJ Processing. The dotted yellow rectangle or circle represents the region of interest for experiments done in A.) conical tubes, B.) Eppendorf tubes, C.) microwell plates, and D.) nanowell devices. 50
Figure 17: Relationship between the colouration state of Methylene Blue and DO concentration. Images of the varying conditions: air bubbled into solution for 1 minute, control, [1 mg/mL] Na2SO3, [5 mg/mL] Na2SO3, [25 mg/mL] Na2SO3, and [50 mg/mL] Na2SO3. n=3 for each . 52
Figure 18: Inverse relationship between the concentration of DO and the extracted mean gray value when using MB as the optical indicator. Data shown as mean ± SEM. 54
Figure 19: The effect of chemical and biological metabolism on MB colouration in Eppendorf Tubes. A.) Progression of images taken over a 17-hour period comparing the colour change of MB in the presence *E. coli* K12 MG1655 [10^8 CFU/mL] and Na_2S0_3 at 5 mg/mL. B.) Normalized MGV extracted from the images over the imaging period. C.) Effect of agitating the tubes on the saturation of MB indicator. The separate layers in the MB+LB control and *E. coli* tubes disappear, resulting in a homogenous darker colour and D.) MGV. 55
Figure 20: MB colour change due to chemical oxygen removal when loaded into PDMS nanowell device. 58
Figure 21: Comparison of methods for nanowell mould fabrication and its effects on the use of MB as an optical indicator within the rapid culture detection device. Photolithography (n=24) and 3D printed (n=12) fabricated moulds were tested to determine if the type of fabrication method impacts the time required to detect a change in oxygen concentration. Fabrication methods were contrasted when A.) inoculated with 10^8 CFU/mL bacteria and B.) without bacteria as a control. Lithography wells showed a significantly higher normalized MGV at t=24 hours ($p<0.0001$) than the 3D print wells in both bacteria and control devices. Data shown as mean ± SEM. 60
Figure 22: Images taken of a microwell plate to compare imaging modalities of cell phone camera (Google Pixel 2), DSLR camera (Nikon D810), and microscope (Olympus Inverted Microscope). Microscope images were taken with the lowest objective lens (4x) and a monochrome camera. 62
Figure 23: Time lapse of MB indicator with *E. coli* bacteria in wells using Tecan Plate Reader to measure the absorbance (λ=668 nm) change over 24 hours. Concentration of [10^8 CFU/mL] (n=6) were compared to control measurements of empty wells (n=6), LB only wells (n=6), and MB+LB wells (n=12). Difference in bacteria and MB+LB wells were significant ($p<0.0001$) after 8 hours, and significant at all time points when compared to LB and empty well controls. Data shown as mean ± SEM. 66
Figure 24: A.) Select images taken with the DSLR-Macroscope system of the effect of *E. coli* bacteria on the MB indicator colour change over 24 hours. Concentrations of [10^8 CFU/mL] (n=24) were compared to control measurements of empty wells (n=6), LB only wells (n=6), and MB+LB wells (n=24). B.) Normalized MGV were extracted to determine that bacteria could be differentiated from MB+LB wells after 5 hours ($p<0.0001$). Differences with LB and Empty well controls were also significant ($p<0.01$). Data shown as mean ± SEM. 67
Figure 25: Comparison of the DSLR-Macroscope camera system and the microscope in their ability to image the nanowells filled with MB within the redesigned Rapid Culture Nanowell Device. 68
Figure 26: Comparison of rate of colour change between fresh and older stock of MB when in the presence of bacteria. 70

Figure 27: Effect of MB freshness on rate of MB colour change due to metabolism. MGV were extracted from time-lapse images taken every hour for 24- hours. A.) Comparison of bacteria inoculated Old MB (n=24) and New MB (n=18) samples. B.) Comparison of Old MB (n=24) and New MB (n=24) samples without bacteria. The MGV of new MB samples were lower than that of the old MB, therefore indicating a darker blue colour. The steeper slope of the old MB bacteria samples also indicated a faster rate of colour change compared to the new MB. Data shown as mean ± SEM. 71
Figure 28: Normalized mean gray value of the colour change of the new and old MB. A.) Comparison of bacteria inoculated Old MB (n=24) and New MB (n=18) samples. B.) Comparison of Old MB (n=24) and New MB (n=24) samples without bacteria. Data shown as mean ± SEM. 71
Figure 29: Effect of MB concentration on rate of colour change over a 24-hour period. Reduction via *E. coli* [10^8 CFU/mL] metabolism was tracked in both concentrations. n=18 for each condition. 72
Figure 30: Comparison of rate of MB colour change dependent on the concentration of MB in wells without bacteria and those with. Concentrations of A.) 1.0 mg/mL and B.) 2.5 mg/mL were tested. Lower concentration of MB showed faster and greater degree of colour change than higher concentration of MB. n= 18 for each condition: 2.5 mg/mL MB control, 2.5 mg/mL MB+*E. coli* [10^8 CFU/mL], 1.0 mg/mL control, 1.0 mg/mL MB+*E. coli* [10^8 CFU/mL]. Data shown as mean ± SEM. 73
Figure 31: Effect of bacterial concentration on time of 1.0 mg/mL MB colour change due to bacterial metabolism. Selected images taken from the 48-hour imaging period that show the colour change progression of varying *E. coli* concentrations. [MB] = 2.5 mg/mL. 74
Figure 32: Extracted saturation of MB indicator for varying bacterial concentrations. Wells of *E. coli* [10^8 CFU/mL] (n=18) show increase in normalized MGV that differentiates from the control at 10 hours. Concentrations of [10^4 CFU/mL] (n=18) differentiate from the controls at 24 hours. Data shown as mean ± SEM. 75
Figure 33: End-point achieved with MB and [10^8 and 10^4 CFU/mL] bacteria in microwells. A.) Sequence of timed images at t=0, 2, and 5 days. B.) Comparison of the normalized MGV of 10^8 and 10^4 CFU/mL *E. coli* to quantify the saturation of MB at an end-point of 5 days. Data shown as mean ± SEM. MB+*E. coli* [10^8] n=18, MB+*E. coli* [10^4] n=18, MB+LB control n=18..... 77
Figure 34: Time-lapse comparison of 10^8 CFU/mL of *E. coli* (n=236) and sterile control (n=256) over 24-hour period, every 10 minutes. A.) Before and after images of filled lithography fabricated devices. B.) Extracted saturation change of the wells, showing a significant difference between bacterial and control wells after 4.83 hours ($p<0.01$). The control normalized mean gray value stayed fairly constant over the 24-hour period whereas the MGV for bacterial devices showed an increase, coinciding with the lightening of colour and indicating the presence of bacteria. Data shown as mean ± SEM..... 78
Figure 35: A.) Comparison of lithography mould nanowell devices with varying *E. coli* concentrations. After a period of 24-hours, the wells of 10^8 CFU/mL were visibly a different shade of blue compared to the control, whereas it is difficult to distinguish a difference in the lower concentration. LB *E. coli* [10^8 CFU/mL] n=817, LB *E. coli* [10^4 CFU/mL] n=685, and LB Control

n= 664. B.) Normalized MGV were extracted using image analysis and compared at 3, 6, and 24-hour time-points. Data shown as mean ± SEM..... 82
Figure 36: Time lapse measuring the MB colour change dependent on bacterial presence over 24 hours comparing the effect of different media. A.) Lithography nanowell devices filled with LB media and human milk as the nutrient media. Bacteria milk samples (n=635) were artificially inoculated with 10^8 CFU/mL of *E. coli*. Control milk n=266. LB *E. coli* [10^8] CFU n=817 and LB Control n= 664. B.) 96 well plate 300 µL wells filled with human milk and compared to LB as the nutrient media. Bacteria milk samples (n=9) were artificially inoculated with 10^8 CFU/mL of *E. coli*. Control n=3. LB control (n=9), LB bacteria (n=9). Data shown as mean ± SEM..... 83
Figure 4.37: Comparison of colour change due to bacterial metabolism in LB media or human milk in microwells over 24 hours. A.) DSLR images of the microtiter wells filled with either LB or human milk and [10^8 CFU/mL]. Bacteria LB samples (n=9) and milk samples (n=9) were artificially inoculated with 10^8 CFU/mL of *E. coli*. Control LB (n=9) and milk (n=3). 96 well plate 300 µL wells filled with human milk and compared to LB as the nutrient media. B.) Comparison of the different media on the normalized MGV of the controls were not significant, however the difference between Milk and LB bacteria wells were highly significant ($p<0.0001$) at 24 hours. Data shown as mean ± SEM. 85
Figure 38: Fluorescent images tracking the growth of bacteria via GFP fluorescence. The increase in GFP intensity indicating viable growth of bacteria within A.) a single nanowell and B.) a microwell filled with human milk. (n=3)..... 86
Figure 39: Images comparing appearance of bacterial colonies on LB Agar dish over time..... 87
Figure A40: Streaking pattern on LB agar plate. Adapted from [127]..... 103
Figure A41: Effect of bacterial concentration on time of MB colour change due to metabolism. A.) Selected images taken from the 48-hour imaging period that show the colour change progression of varying E. coli concentrations. [MB] = 2.5 mg/mL. B.) Wells of *E. coli* [10^8 CFU/mL] (n=36) show increase in normalized MGV that differentiates from the control at 8 hours. Concentrations of [10^4 CFU/mL] (n=36) differentiate from the controls at 24 hours, and for [10^2 CFU/mL] (n=36), 36 hours. Data shown as mean ± SEM. 108
Figure A42: Comparison of MB concentrations in nanowell devices to determine ideal concentration for use. A.) Time lapse images of devices with bacteria and those without. MB at B.) 1.0 mg/ml and C.) 1.5 mg/mL were chosen based on experiments in microwell volumes. Sample sizes for each of the conditions follow: 1.0 mg/mL MB no bacteria, n=187; 1.0 mg/mL MB bacteria, n=252; 1.5 mg/mL MB no bacteria, n=199; and 1.5 mg/mL MB bacteria, n=202. Data shown as mean ± SEM. D.) Comparison of the difference in colour based on concentration showing greater change in 1.0 mg/mL than 1.5 mg/mL. 110
Figure A43: Nanowells filled with 2.5 mg/mL MB as a preliminary test to increase saturation and colour change. A.) Images of wells filled with 10^8 CFU/mL bacteria (n=625) and those without (n=625) taken at t=0 and 46 hours. B.) The normalized saturation of the bacteria wells was not significantly different from the sterile wells. Data shown as mean ± SEM. 111

List of Tables

Table 1: Select major components of human milk and their functions. Reproduced with modifications from [29], [35]. 10
Table 2: Common bacterial contaminants in human milk categorized by pathogenicity. Accumulated from various sources noted in the table. 15
Table 3: Comparison of select nutrients available to baby through mother's milk and pasteurized donor milk. Reproduced with modifications from [35]. 20
Table 4: Bovine Milk Quality Classification of MBRT. Reproduced from [51] 25
Table 5: Measured DO concentrations of the various test conditions as measured with the Exstik II commercial sensor 53
Table 6: Comparison of imaging methods to be used in future characterizations of the Rapid Culture Device 64

Abbreviations

ATP	adenosine triphosphate
BSC	Biological scientific cabinet
CFU	Colony forming units
CAD	computer-aided design
DNA	deoxyribonucleic acid
DSLR	digital single-lens reflex
DO	dissolved oxygen
DPI	dots per inch
FFA	free fatty acids
GI system	gastrointestinal system
GFP	Green fluorescent protein
HDM	human donor milk
HIV	Human Immunodeficiency Virus
HMBANA	Human Milk Banking Associating of North America
HTLC	Human T cell Leukemia virus
IgG	immunoglobulin G
IgM	immunoglobulin M
ISO	International Organization of Standardization; standardizes sensitivity of camera sensors
LC-PUFA	long-chain polyunsaturated fatty acids
LB media	Luria-Bertani media
MGV	Mean Gray Value
MB	Methylene Blue
MBRT	Methylene Blue Reduction test
MJM	Multi Jet Modeling
MP	Mega-pixel
NEC	Necrotizing enterocolitis
NICU	Neonatal Intensive Care Unit
NADH	Nicotinamide Adenine Dinucleotide
NADPH	Nicotinamide Adenine Dinucleotide Phosphate
OD	optical density
PDMS	polydimethylsiloxane
PCR	Polymerase chain reaction
ROS	reactive oxygen series
RBC	Red blood cells
RGB	Red-green-blue
RNA	ribonucleic acid
sIgA	secretory immunoglobulin A
SASPs	small acid-soluble proteins
spp.	species
SPC	Standard Plate Count
STL	Stereolithography CAD format
3D	Three-dimensional
TNTC	Too numerous to count
TB	Tuberculosis
UV	ultraviolet
wa	water activity
WHO	World Health Organization

Nomenclature

$(c_2 - c_1)$	difference in concentration of gas across membrane in the direction of flow
µm	micrometers or microns (units)
a	absorbance
A	area of membrane
CH_4	methane
H_2O	water
H_2O_2	Peroxide
MB	Methylene Blue
MB_{ox}	oxidized state of MB
MB_{red}	reduced state of MB
Na_2SO_3	sodium sulphite
NH_3	ammonia
nL	nanoliters (units)
nm	nanometers (units)
O_2	oxygen
P	permeability
p_0	partial pressure of gas on lower side of membrane
p_1	partial pressure of gas on higher side of membrane
PtTPTBP	platinum (II) 5, 10, 15, 20-*meso*-tetraphenyltetrabenzoporphyrin
RTDP	ruthenium (II) tris(2,2'-bipyridyl) dichloride hexahydrate
t	time
T	transmittance
v	volume of gas
x_n/x_0	Relative saturation
δ	thickness of membrane

Chapter 1 – Motivation and Organization

1.1 Motivation

Foodborne diseases have been a worldwide issue since the beginning of humanity. Consumption of these contaminated foods can lead to symptoms ranging from mild and self-limiting (nausea, vomiting and diarrhea) to those that are debilitating and life-threatening (kidney and liver failure, brain and neural disorders, paralysis, potentially cancers, and premature death) [1]. An estimated 600 million people fall ill after ingesting contaminated foods each year. Of this statistic, 420,000 individuals succumb to their disease [1]. Approximately 60% of illnesses and deaths are caused by bacterial foodborne hazards (Figure 1). The other foodborne hazards include viruses (cause of 23% of foodborne illnesses and 14% of deaths), parasites (17% and 21%, respectively), and chemicals or toxins (0.03% and 4%, respectively). Foodborne pathogens particularly take advantage of weakened immune systems, targeting pregnant women, the elderly, the immuno-compromised, and especially malnourished infants and children. Children under five years old account for 40% of the foodborne disease burden [1]. Technology that can detect spoilage or contamination of foods before consumption is necessary to mitigate and prevent future incidences of food-related diseases.

In particular, donor human milk banks require a rapid detection system in order to ensure the distribution of safe pasteurized milk to immunocompromised neonates. Approximately 70% of preterm infants in Ontario hospitals do not have access to the full supply of their mother's own milk [2]. These banks remove the barriers to lifesaving milk particularly for prematurely-born children or those born with gastrointestinal sensitivities. With the incredible health and developmental benefits of human milk, research has shown that premature infants hospitalized in the neonatal intensive care unit (NICU) who received donor milk had a 13% lowered risk of death

for every 100 mL/ 100 g of milk consumed in the first 14 days of life [3]. However, quantities of human milk are limited with an estimated shortage of 6 million ounces a year, further stressing the need for quick distribution [4].

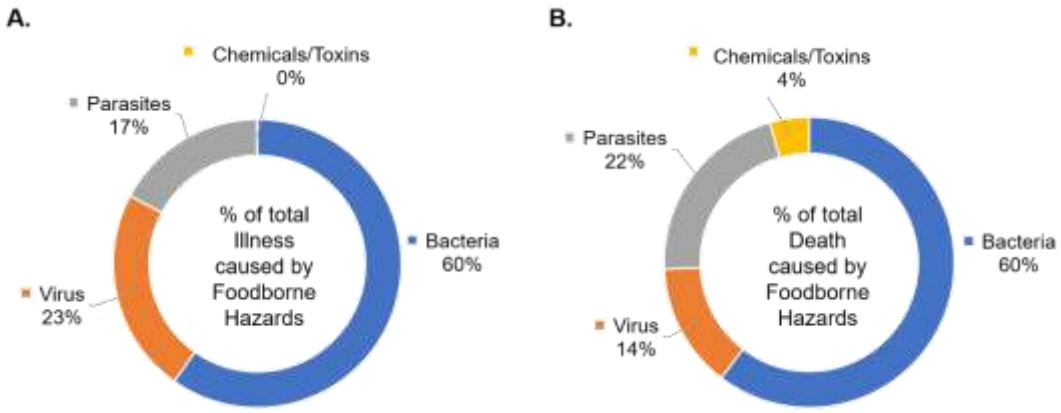

Figure 1: Breakdown of the median global number of A.) Foodborne Illnesses and B.) Foodborne Deaths, with 95% uncertainty intervals, based on the type of hazard (bacterial, virus, parasite, or chemical and toxin). Data extracted from [1].

The tools used by milk banks to ensure safe distribution rely heavily on the culture plate [4]–[9]. It is the golden standard in microbiological screening, however, the procedural time can last several days [6], [10], [11]. This delays the distribution of human milk to the infants who need it most. Advances in microfluidics, particularly in combination with the concept of monitoring metabolites to indicate bacterial viability, are promising in significantly reducing the long processing times of culture plates. Combining the concept of compartmentalized culture and a chromogenic optical dye typically used in the bovine dairy industry could be advantageous in updating the existing Rapid Culture Detection system. Milk banks require a tool that will quickly detect bacterial contamination in their limited donations to ensure efficient delegation of resources without compromising the health and safety of the already-sensitive babies [4].

1.2 Organization of Thesis

The structure of the thesis is organized into the following chapters:

Chapter 2 introduces the issue of foodborne illnesses, with a focus on the impact of contaminated breast milk on the society and economy. A comprehensive background is provided on human milk and the milk banking system to understand the necessity of developing a faster method of contamination detection than the conventional culture plate. Understanding the growth and metabolism of bacteria is essential to identifying a mechanism to indirectly detect and quantify its viability in human milk, as well as the potentially fatal consequences if not preventatively found. Parallels from the bovine dairy industry are also discussed as sources of inspiration for a mechanism to measure bacterial metabolism. Finally, an analysis of current microfluidic biomedical devices is conducted, highlighting the novelty of the Rapid Culture Nanowell Device.

Chapter 3 elaborates on the working principle of compartmentalization and its potential in detecting bacteria for human milk banking applications when combined with a metabolic monitoring system. Design criteria for the updated Rapid Culture Nanowell Device are discussed based on current Donor Milk Banking protocols. Method of microfluidic device fabrication, type of indicator material, and imaging platform are explored in this thesis. Additionally, the materials involved in the characterization of Methylene Blue (MB) intensity and dissolved oxygen concentration, fabrication of the microfluidic device and bacteria preparation are detailed. Lastly, the protocols involved in the testing and characterization of the updated Rapid Culture Nanowell Device and imaging platform are presented, from fabrication steps to imaging and analysis.

Chapter 4 reports the results obtained through the development of the complete system, including the classification of the optical indicator MB, the redesign of the Rapid Culture Nanowell Device, and the development of an affordable imaging platform. Once optimized, the nanowell

device and MB indicator are studied while comparing a variety of factors such as bacterial concentration, well volume, and media type to determine its viability as an alternative to the culture plate for Donor Milk Banks. The proof of concept indicates that the updated Rapid Culture Nanowell Device and DSLR-Macroscope system can detect concentrations of 10^3 *E. Coli* bacteria/well within 3.33 hours compared to 24 hours in the microwell liquid culture and the 16 hours necessary to visualize a single colony grown on a culture plate.

Chapter 5 summarizes the initial development of MB as a viable indicator of bacterial metabolism in the redesigned Rapid Culture Nanowell Device while suggesting areas of potential future work. The analysis of the RGB-breakdown of images may be a tool to be harnessed to identify bacterial presence faster than the average Mean Gray Value (MGV) that was calculated. Additionally, the testing of a smaller volume between the first and second iterations of the Rapid Culture Nanowell Device should be tested to determine if the detection time can be further decreased. Further developments such as the adaptation of the device to other bacterial species are also suggested.

1.3 Contributions

The innovation in this thesis is the adaptation of methylene blue as an optical indicator for the Rapid Culture Nanowell device as an alterative to the fluorophore RTDP. MB has been traditionally used in bovine milk applications to determine its quality by measuring the metabolism of bacteria. The viability of using MB to detect bacteria suspended in LB and human milk was tested through the image characterization with the DSLR-Macroscope system. The updated size of the Rapid Culture Nanowell Device of 75 nL (500x500x300 µm) was successful in shortening the detection time compared to a microwell volume of 300 µL, however, a volume between 1-75

nL will need to be explored to determine the ideal volume for detecting bacterial presence in the shortest amount of time.

Chapter 2 – Introduction

2.1 Foodborne Illnesses and Bacterial Contamination of Human Milk

Foodborne illnesses are one of the most common and widespread health burdens in the world. They are caused by bacteria, viruses, parasites or chemical substances that trigger infectious or toxic ailments after their consumption [1], [12]. Consumption of these contaminated foods can lead to symptoms ranging from mild and self-limiting (nausea, vomiting and diarrhea) to those that are debilitating and life-threatening (kidney and liver failure, brain and neural disorders, paralysis, potentially cancers, and premature death) [1]. An estimated 600 million people fall ill after ingesting contaminated foods and 420,000 individuals die each year [1]. Children under five years old account for 40% of this population. The World Health Organization (WHO) has identified 31 foodborne hazards, of which 12 are bacterial in nature [1]. Development of sensors that can determine spoilage or contamination of foods before consumption are required to prevent future incidences of food-related diseases.

One particular food source that has the potential to be fatal when consumed is breast milk inoculated with pathogenic bacteria. Human milk banks take the greatest precautions to protect their users, but some of these microorganisms manage to circumvent the employed methods. Consumption of milk inoculated with bacteria, such as *Bacillus cereus, Enterococcus* species (spp.), *Streptococcus* spp., and *Staphylococcus aureus*, can cause severe sickness especially in the critically ill and low-birth-weight neonates who rely on donor milk [6], [13]–[16]. Although no known reports of direct infectious disease transmissions from banked human milk to infants have been reported to date in North America, its safety cannot be absolutely and imminently assured [4], [17]. International case studies have documented infections in children who were given pasteurized donor pooled milk, although the exact vector of infection could not be confirmed [18].

Bacterial contamination can also indirectly affect the young by further stressing the shortage of available human milk. Without this lifesaving nutrition, infants do not receive a multitude of benefits from its consumption. These include lower risks to a wide range of diseases and infections [4], [6], [19]–[21]. In turn, short and long-term healthcare costs are reduced. Preterm infants who are given breast milk have shorter hospital stays compared to those who consume formula [22]–[24]. The American healthcare system is also estimated to incur an additional $1 billion per year on the treatment of common medical diagnoses in infants who were not given breast milk [23]. Finally, the establishment of donor human milk banks has been found to heighten the awareness of breastfeeding within the community, which could translate to substantial economic benefits for the whole society [4]. Researchers approximate that $4 billion can be saved annually if the majority of American women breastfeed their children [25]. For these reasons, a reliable means of detecting bacterial contamination of human milk before its distribution is beneficial for the population and economy.

2.2 Human Milk

Human milk is an important source of nutrition for babies, especially those who are born premature, immunocompromised, or with other serious congenital health concerns. It is produced by a female's mammary glands, specifically the milk secreting cells called lactocytes within the alveoli. The milk then travels down the ducts to the lactiferous sinuses in the areolar region (Figure 2) [26], [27]. This complex process occurs at the end of pregnancy via the hormonal interactions of the hormones prolactin and oxytocin, which are responsible for the production and secretion of milk [27], [28]. In this subsection, the composition and benefits of breast milk are detailed.

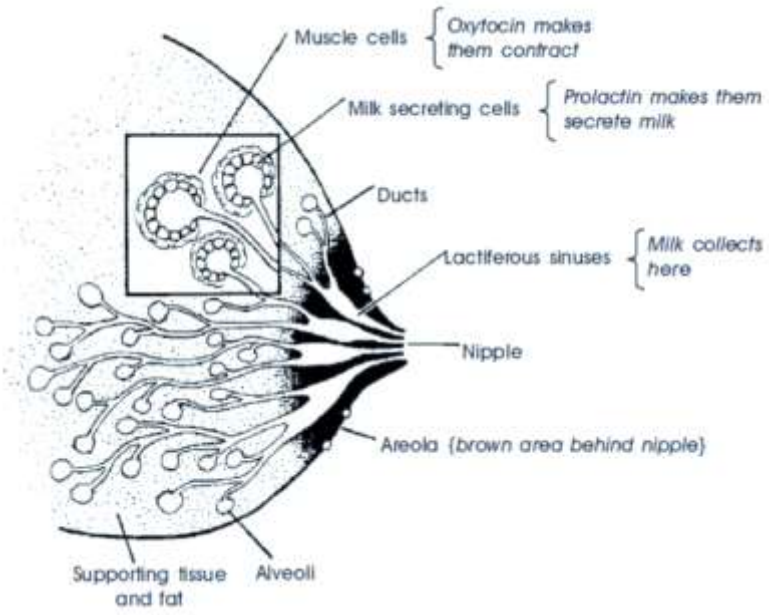

Figure 2: Anatomy of lactating breast. Modified from [27].

2.2.1 Composition of Human Milk

Human milk has been hailed as 'liquid gold' due to its reputation as the optimal source of nutrition for infants. It consists of a multitude of macronutrients, enzymes, hormones, immunological and anti-inflammatory properties, and beneficial bacteria that concurrently protect the child while aiding in their development [29], [30]. It has a general composition of 87% water, 3.8% fat, 1.0% protein, and 7% lactose [31]. Table 1 lists the major nutrient categories and specific examples of each, as well as their functions.

The composition of breast milk changes over time to meet the baby's requirements [29], [32], [33]. The initial sticky, yellow substance is referred to as colostrum. It largely contains bioactive proteins and properties that protect the infant from diseases. These include antibodies (the secretory form of immunoglobulin A (sIgA), immunoglobulin M (IgM), and immunoglobulin G (IgG)), immune competent cell types (macrophages, granulocytes, T and B lymphocytes), and anti-inflammatory cytokines [32], [34]. It also contains lactoferrin and lysozyme, which help to

inhibit pathogenic bacterial invasion. With time, the milk becomes thicker and creamier as it develops into transitional milk, then mature milk. These later stages are more concentrated in carbohydrates (lactose and oligosaccharides), fats (triglycerides, long-chain polyunsaturated fatty acids (LC-PUFA) and free fatty acids (FFA)), and enzymes that digest these macronutrients (amylase and lipase). The shift indicates a transfer of energy to helping the baby grow from its initial focus on the establishment of their immune system [29]. Finally, hormones such as prolactin, cortisol, thyroxine, insulin and growth factors help to regulate the child's gastrointestinal and overall health, as well as the mother's production of milk and return to pre-pregnancy state throughout the lactation process.

Human milk has also been found to contain natural microflora that helps populate the infant's intestines to protect against pathogenic bacteria [30], [34]. A specific list of species can be found in Table 2. These healthy bacteria are commonly isolated in breast milk at concentrations of 10^4-10^5 CFU/mL [30], [34]. The exact mechanism through which the probiotic bacteria mix with the milk is unknown, but has been hypothesized to be from the skin and nipple transmission, and the vertical transfer of intestinal bacteria from the mother's gut to her milk [34]. Human milk contains a myriad of protective components that makes it a crucial element in the establishment of the infant's immune system, modulation of the gastrointestinal tract, and development.

Table 1: Select major components of human milk and their functions. Reproduced with modifications from [29], [35].

Nutrients	Function
Protein	
sIgA antibody	Immune protection; binds microbes in baby's digestive tract to prevent their passage into other tissues
IgM antibody	Immune protection; targets pathogens to which mother has been exposed
IgG antibody	Immune protection; targets pathogens to which mother has been exposed
Lactoferrin	Anti-infective, iron carrier and slows down bacterial growth
Enzymes	
Lysozyme	Anti-infective; attacks bacterial cell wells
Amylase	Digestion of saccharides, specifically amylose
Lipase	Digestion of fats to release monoglycerides and FFA
Carbohydrate	
Lactose	Energy source
Oligosaccharides	Microbial ligands
Fat	
Triglycerides	Energy source
LC-PUFA	Essential for brain and retinal development and for infant growth
FFA	Anti-infective; disrupts membrane coating of viruses and protozoans
Cells	
Macrophages, granulocytes, and lymphocytes	Microbial phagocytosis, production of lymphokines and cytokines, interaction with and enhancement of other protective agents
Cytokines	Modulate functions and maturation of the immune system
Hormones	
Prolactin	Enhances the development of B and T lymphocytes, affects differentiation of intestinal lymphoid tissue
Cortisol, thyroxine, insulin and growth factors	Promote maturation of the newborn's intestine and development of intestinal host-defense mechanism

2.2.2 Benefits of Human Milk

The WHO has suggested that mothers exclusively breastfeed for the first six months of their baby's life, then incorporate it as part of their child's diet for the first two years and beyond [33]. Human milk has shown to reduce the risk of illnesses, as well as promoting optimal growth, immune function, and development [4], [36]. Studies have indicated a lower risk of ear infections, diabetes (type 2), gastrointestinal infections, obesity and the prevention of allergy, eczema, and asthma in infants who consumed breast milk from their mothers [37]–[40]. Lower susceptibility to these illnesses also translates to lower healthcare costs spent diagnosing and treating them. Riordan et al. estimated that the American healthcare system spent an additional $1 billion (1997 dollars) on four conditions in infants who were not breastfed [23]. The breakdown for the four diagnoses is as follows: infant diarrhea, $291.3 million; respiratory syncytial virus, $225 million; insulin-dependent diabetes mellitus, from $9.6-124.8 million; and otitis media, $660 million. Limited evidence also supports better cognitive development throughout childhood and early retinal and visual development in infants who consumed breast milk [41], [42].

Unfortunately, not all mothers are capable of providing adequate or any of this nutrition to their children. Possible reasons could include a poor latch onto the breast, birth of multiple babies at one time, adoption or surrogacy, low supply, breast anomaly or surgical history, maternal illness or hospitalization, and maternal death [43]. When a mother's milk is not available, the next best option is pasteurized and screened human donor milk (HDM) [44], [45].

Donor milk is considered to be breast milk that has been produced by someone other than the mother of the child. The generosity of these donors allows infants to access the many benefits of human milk. The most critical demand is for vulnerable babies who have been born before a gestational period of 37 weeks, also known as being born prematurely or preterm [4]. As of 2010, approximately 7% of the 350,000 children born in Canada each year fall under this category.

Preterm babies typically have more barriers to receiving their mother's milk compared to those born at full term (40 weeks). In addition to the aforementioned reasons why the maternal milk supply may be compromised, hospitalization away from their mothers inhibits a neonates' access to this lifesaving source of nutrition. Unfortunately, these children also have the greatest need for human milk due to their higher susceptibility to illness and health problems.

Research has universally shown that premature infants in the NICU do better on human milk feedings. Fewer instances of severe infections and feeding intolerance have been reported, including a decreased likelihood of developing necrotizing enterocolitis (NEC) by 79% [4]. Additionally, fewer days of intravenous nutrition were required when donor milk feedings were provided due to the ease and efficiency of digestion [46]. Breast milk also decreased sepsis, gastrointestinal issues, length of hospital stay and improved developmental outcomes in premature infants [4], [15], [24], [47], [48]. The risk of death decreased by 13% for every 100 mL/ 100 g increase in human milk received in the first 14 days of life [3]. As a whole, human milk is an invaluable source of nutrition that holds a myriad of benefits to the child, their family, and society.

2.3 Human Milk Banking

The first ever human milk bank was established in Vienna, Austria in 1909 [4]. The first North American location followed two years later in Boston, USA. The popularity of banking continued well into the 1980s until the fear of HIV (Human Immunodeficiency Virus) transmission forced many to shut down. In 1985, the Human Milk Banking Association of North America (HMBANA) was formed [49]. Their mission is to ensure the safety, accessibility, and affordability of milk as a non-profit organization. Currently, there are 27 HMBANA milk banks that have maintained a clean safety record for over thirty years [49].

With current screening and safety protocols, milk banks provide lifegiving nutrition to fragile infants who would otherwise not receive it. Therefore, their establishment has removed many of the barriers to the benefits that human milk consumption brings. Unfortunately, this valuable food source is in short supply. HMBANA locations distribute approximately 3 million ounces a year, but if all hospitals with NICUs utilized donor milk, 9 million ounces would be required [50]. Therefore, there is a shortage of 6 million ounces. This scarcity stresses the system to ensure quick processing and screening of donated supplies in order to facilitate efficient distribution to those in most need. The current safety protocols include screening for bacterial contaminants that may be detrimental if consumed by the immunocompromised and vulnerable premature infants.

2.3.1 Bacterial Contamination

With the pervasive prevalence of bacteria in the atmosphere and majority of the earth's surfaces, it is difficult to find substances without any microbial presence. A wide variety of both beneficial and pathogenic bacteria has been found to inhabit human milk from donor mothers. With a water activity (aw) level, otherwise known as the amount of water available, of 0.98 aw, milk is optimal for bacterial survival. Generally, bacteria dominate in foods that are between 0.90-1.0 aw [51]. Table 2 summarizes a list of specific species that have commonly been found in human milk, as well as their natural habitat and risk to infants. Non-pathogenic or 'natural microflora' strains commonly originate from a mother's skin, nipple ducts, or gastrointestinal (GI) system and have been deemed safe, if not beneficial, for healthy infant consumption. Although the exact threshold for microbiological safety has not been universally determined, counts of natural microflora in pre-pasteurized milk lower than 10^4-10^5 CFU/mL are considered safe for healthy infants [9], [30], [34]. The antimicrobial defences of human milk and their immune systems help

to contain the microbiota to the intestinal tract, preventing infection. Pasteurized donor milk, however, does not contain any non-pathogenic bacteria.

The presence of pathogenic bacteria is more strictly regulated due to its high potential of causing fatal consequences in infants. A concentration of any more than 10 pathogenic bacteria is considered unacceptable, although donor milk with the presence of a single bacterium post-pasteurization is discarded [4], [9], [17], [30], [52]. Strains such as *B. cereus, Enterobacter* spp., and *E. coli* can cause infection, sepsis or death in infants. These dangerous microorganisms can be introduced during collection, storage or processing of the donated human milk [5]. Additionally, researchers have indicated that the location where milk was pumped could more accurately indicate potential contamination [5]. Milk that was expressed at a donor's home had significantly higher rates of pathogenic bacteria contamination compared to the hospital. The increased likelihood is attributed to the inadequate cleaning and reuse of pumping and or storage equipment at home compared to the NICU setting. Access to sterile equipment and nursing support who reinforce proper pumping techniques encourage better hygiene. Further, these pathogenic bacteria can be transferred by vectors such as contaminated food, surfaces, and improperly washed hands.

Table 2: Common bacterial contaminants in human milk categorized by pathogenicity. Accumulated from various sources noted in the table.

	Bacteria	Natural Environment	Risk to Infants
Non-pathogens	Coagulase-negative *Staphylococcus* spp. (*S. epidermidis, S. hominis* and *S. capitis)*	Human skin, may be found in breast milk	Low risk [34]
	Bifidobacterium spp.	Human GI tract	Low risk [34]
	Lactobacillus spp. (*L. gasseri, L. rhamnosus, L. acidophilus, L. plantarum* and *L. fermentum*)	Human GI tract	Low risk [34]
	Streptococcus spp. *(S. salivarius, S. mitis, S. parasanguis, and S. peroris)*	Human mouth and upper respiratory tract	Low risk [34]
Opportunistic pathogens	*Enterococcus faecalis*	Human GI tract	Low-medium risk [53]
	Escherichia coli	Human GI tract, contaminated water supply	High risk [54]
	Staphylococcus aureus	Human skin, milk ducts in cases of mastitis, may be found in breast milk	High risk [34]
	α-hemolytic Streptococcus viridans	Human mouth and upper respiratory tract, may be found on skin	Low risk [55]
	Group B streptococcus (GBS)	Human GI tract and female genital tract, may be found in breast milk	High risk [54]
Pathogens	*Acinetobacter* spp.	Moist and dry environments	High risk [56]
	Bacillus spp. *(B. cereus)*	Soil and spoiled food	High risk [5]
	Clostridium perfringens	Raw meat and poultry	High risk [57]
	Enterobacteriaceae family *(Enterobacter, Klebsiella, Proteus, Salmonella, Shigella)*	Human GI tract, particularly in patients with diarrhea, contaminated water supply	High to Very high risk [58]
	Pseudomonas aeruginosa	Moist environments	High risk [59]

2.3.1.1 Growth Phases of Bacteria

To study and diagnose bacterial infections, a foundational understanding of the growth of bacteria is required. A single bacterium propagates by splitting into two identical daughter cells through a process called binary fission [60]. As it replicates, the bacteria form a single colony

consisting of genetically identical cells. A bacterial colony undergoes four main phases throughout its lifetime: lag, log, stationary, death (Figure 3) [61].

During the lag phase, the cells prepare for division. Ribonucleic acid (RNA) and proteins are synthesized from carbon sources. This phase occurs slowly compared to the following stages. Next, the bacteria begin to divide. As the rate of division increases to its maximum rate, the colony enters the log or exponential phase. The bacterial concentration rapidly increases. The time it takes for the concentration to double in size is termed the "doubling time", which can vary from a matter of minutes to hours, depending on the species. In ideal conditions with sufficient nutrients and oxygen, the doubling time of *E. coli* is 20 minutes [62]. Once the essential nutrients (carbon and nitrogen sources) required for propagation are limited due to the increased competition, the stationary phase begins. The rate of replication now equals the rate at which cells are dying. This phase can last from a day to a few weeks, depending on the bacterial species. Finally, the death phase occurs when the number of dying cells outnumber those that are replicating. The cycle restarts when the cells are placed in a new environment where the nutrient source is plentiful again [61]. The shape of the curve varies depending on the impact of the available growth factors like temperature and quantity of available nutrition.

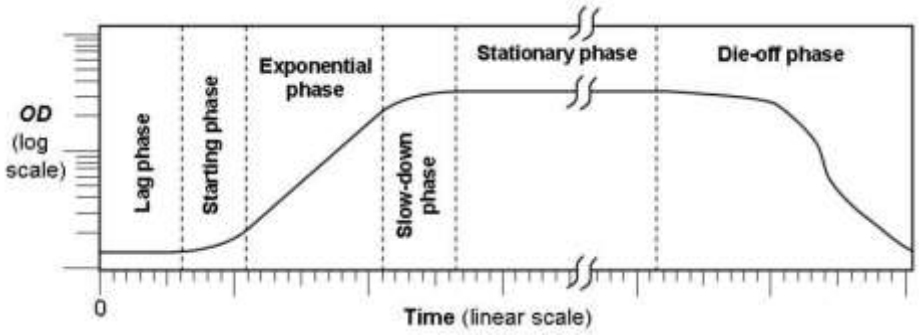

Figure 3: Growth phases of bacteria. Reproduced from [61].

2.3.1.2 Bacterial Metabolism

Bacteria have evolved to metabolize and survive in a variety of environmental conditions. Metabolism describes the chemical processes taken by the organism to obtain sufficient energy to survive. They can be classified based on the mechanisms through which they attain chemical energy and carbon sources [63]. Chemical energy can be harnessed via three methods: light energy, oxidization of organic molecules, or oxidization of inorganic molecules. Bacteria that use photons are called phototrophs and use photosynthesis to generate enough energy for survival. Microorganisms that break down organic molecules, such as sugars, are referred to as chemoorganotrophs. Finally, organisms that oxidize inorganic molecules, such as ammonia (NH_3) or methane (CH_4), are chemolithotrophs. The classification criterion of attaining carbon sources is based on the method of obtaining these building blocks [63]. Organisms that are able to synthesize their own building block compounds are called autotrophs, while those that rely on other organisms as their source of carbon are heterotrophs. These two classifications can be combined to describe the unique metabolic processes of each species. The bacteria of interest for this thesis, *E. coli*, is considered a chemo-organo-heterotroph as it procures its energy source through the break down of sugar molecules from other organisms.

For optimal growth, bacteria require a unique set of ideal conditions. These include extrinsic factors such as oxygen levels and environmental temperature. Bacteria can be categorized based on the amount of oxygen (O_2) required for metabolism. Those that depend on oxygen to produce the energy molecule ATP (adenosine triphosphate) are aerobes, whereas those who use processes without oxygen are called anaerobes [64]. Facultative anaerobes are able to make ATP when oxygen is present and are able to switch to fermentative or anaerobic processes in environments lacking oxygen. Additionally, bacteria can be categorized based on the temperature at which their optimal growth occurs. Thermophiles and psychrophiles are species that are capable

of surviving in respective hot (55-65+°C) and cool (0-15°C) temperatures [64]. Mesophiles thrive in 20-45°C and include almost all pathogens that infect humans. The limitation of these factors impacts the growth rate of bacteria, thereby being a potential way of indirectly measuring bacterial viability.

2.3.2 Milk Banking Safety Protocols

Due to the vulnerable population that they serve, donor milk banks must take the greatest precautions to ensure their supply is free of microbiological dangers [9]. Each milk bank follows safety protocols that include an initial screening to separate out milk that has potential contaminants which cannot be easily extracted or destroyed. Donors are asked to fill out lifestyle and health questionnaires to screen for the use of illegal drugs, alcohol, certain medications, herbal supplements, and foreign travel to specific areas of the world. Serological tests are also conducted to scan for HIV, Hepatitis B and C, Human T cell Leukemia virus (HTLV), and syphilis [4]. Once accepted, donors are educated on techniques for safe collection and storage of milk. Milk banks then employ pasteurization protocols to eradicate any remaining contaminants. Finally, bacteriological screening tests are conducted to confirm the safety of DHM prior to distribution. Only when the cultures have satisfied all applicable regulations, including dairy food inspection standards, is it distributed under a physician's prescription. Although the acceptable limit for bovine dairy is $1x10^5$-$4x10^5$ CFU/mL post-pasteurization, human milk samples that show any indication of bacterial presence, whether beneficial or pathogenic, are discarded [4], [9], [65], [66]. The following sections will elaborate on the pasteurization and bacterial screening process.

2.3.2.1 Pasteurization and its Effects

Pasteurization is used to eradicate the majority of the biological contaminants via the Holder Technique. Milk is placed in a water bath and the temperature is slowly raised to 62.5°C,

held for 30 minutes, then cooled to 4°C before storage [9]. Figure 4 shows the typical set-up and pasteurization cycle. This practice has been rigorously studied and found to be effective on bacteria and viruses. Unfortunately, some beneficial immunological properties unique to human milk are compromised with the exposure to this level of heat. Table 3 outlines the effect of the Holder pasteurization technique on select components of human milk compared to raw breast milk.

Pasteurization has the greatest effect on the bioactive properties involving the immune and metabolic systems compared to the macro- and micronutrient elements. Carbohydrates such as lactose and oligosaccharides are largely unaffected [4]. Protein and fat content, however, are present at 50-90% of their original levels [67]. Vitamins and minerals are minimally altered after the procedure. White blood cells and the digestive enzyme bile salt-activated lipase are completely inactivated. The anti-infective lactoferrin and lysozyme properties are decreased by 25-60% of their original amounts. Lastly, the secreted immunoglobulin A (sIgA) antibody is maintained, preventing microbes from escaping into other tissues. Despite the inactivation or dampening effects of pasteurization on certain bioactive components, HDM still provides many of the nutritious and protective benefits as milk directly from the mother.

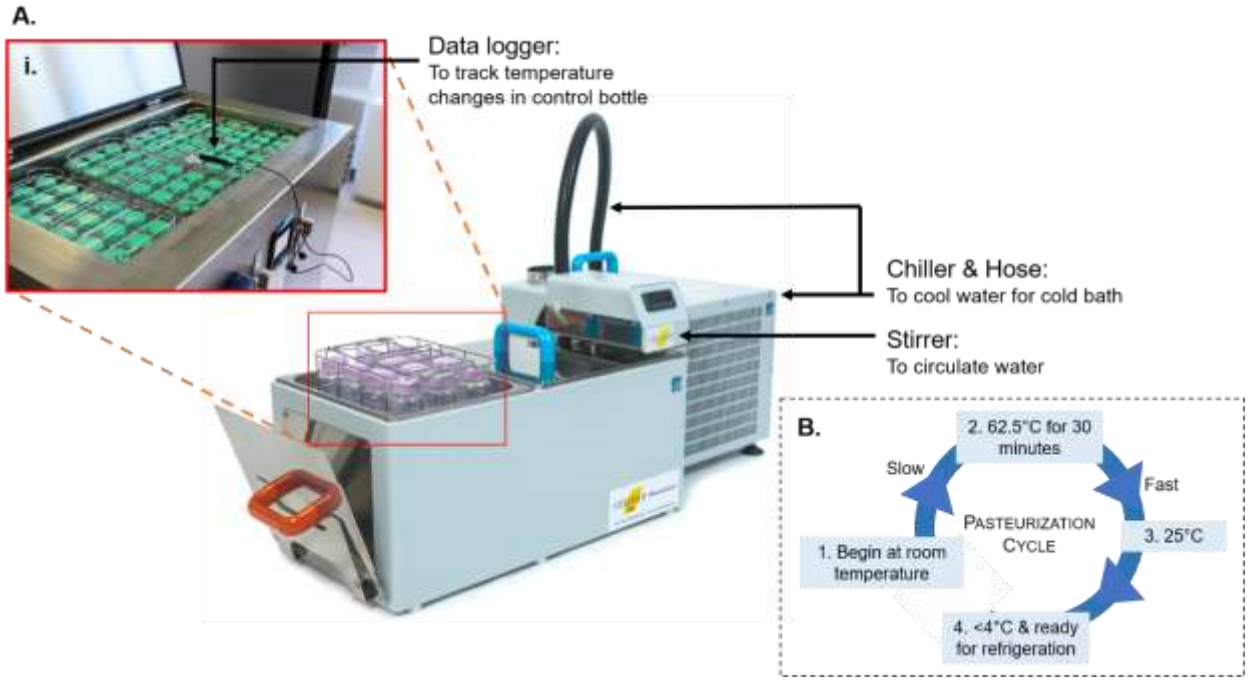

Figure 4: Pasteurization of human milk in donor banks. A.) Typical pasteurization machine used to sterilize samples of milk. T30 Human Milk Pasteuriser pictured here. Subset i.) shows an image of loaded milk bottles. B.) Temperature cycle of the pasteurization process. Adapted from [49], [68].

Table 3: Comparison of select nutrients available to baby through mother's milk and pasteurized donor milk. Reproduced with modifications from [35].

Components	Mother's Milk	Pasteurized Donor Milk
Human Milk oligosaccharides	100%	100%
sIgA antibody	100%	70%
Lysozyme	100%	75%
Lactoferrin	100%	40%
Bile salt stimulated lipase	100%	0%
White blood cells	100%	0%

Although the efficacy of pasteurization on most biological organisms, some have developed mechanisms such as sporulation to protect them in suboptimal conditions. Bacteria, such as *B. cereus*, become dormant and form endospores when stressed by high temperatures. They are capable of survival due to the small acid-soluble proteins (SASPs) that saturate its DNA

(deoxyribonucleic acid) and activate self-dehydration, protecting it from the intense heat [69]. Once the environment has become favourable once again, the endospore can hydrate and reactivate, returning to its original cell form and multiplying. The high temperatures of the Holder technique are not able to kill the *B. cereus* spores nor other bacteria present at pre-pasteurization at more than 10^6 CFU/mL. For this reason, preventative bacteriological screening is crucial to protecting donor milk users from infection and illness.

2.3.2.2 Standard plate count using culture plates

Due to the vulnerability of the preterm infants who consume donor milk, it is imperative for milk banks to preventatively screen for the presence of microorganisms. Banks typically outsource their bacteriological screening to external labs that determine if the milk meets public health and food regulatory standards. These laboratories follow protocols that parallel those used on bovine milk in the dairy industry. Since the purpose of these screens is for preventative and not specific diagnostic identification, labs employ the non-molecular method of Standard Plate Count (SPC) using culture plates.

SPC involves counting the number of colonies that grow on a non-specific solid nutrient agar plate post-incubation. For milk banking applications, a sample volume of 1 mL is taken from a container of pooled milk and streaked onto a variety of culture plates. Typically, MacConkey's and Blood agar plates are used to identify the most common mix of infectious bacterial species present in donor milk. MacConkey's agar selectively isolates for i.) *Escherichia* spp., *ii.) Enterobacter* spp., *iii.) Proteus* spp., *iv.) Salmonella* spp., and *v.) Staphylococcus* spp. (Figure 5.A) by differentiating their ability to ferment the lactose present in the nutrient agar and their morphologies (Figure 5.A.vi). Examples of lactose fermenting species include *Escherichia coli* and *Enterobacter aerogenes.* For more fastidious species, such as the Streptococci family, *B.*

cereus, *Pseudomonas*, and *C. perfringens*, blood agar dishes are employed (Figure 5.B.i). The method of hemolyzing or the breaking down of, red blood cells (RBC) within the agar due to extracellular enzymes helps to further identify the species. Alpha (α) hemolysis is defined as the partial lysis of RBC to produce a green-gray or brown discoloration around the colony (Figure 5.B.ii). Beta (β) hemolysis is the complete lysis of RBC, resulting in clear regions surrounding the colony (Figure 5.B.iii). Finally, Gamma (γ) or non-hemolysis indicates no breakdown of RBC (Figure 5.B.iv). After an incubation period of 48 hours, individual colonies are counted. Depending on the size of the colonies, this process can be done with the naked eye and manual counters, while others may require the magnifying help of microscopes. The legal maximum SPC for pasteurized milk is $1x10^5$-$4x10^5$ CFU/mL, however, milk banks dispose of any samples where there is the presence of even a single bacterium [4], [9], [65], [66].

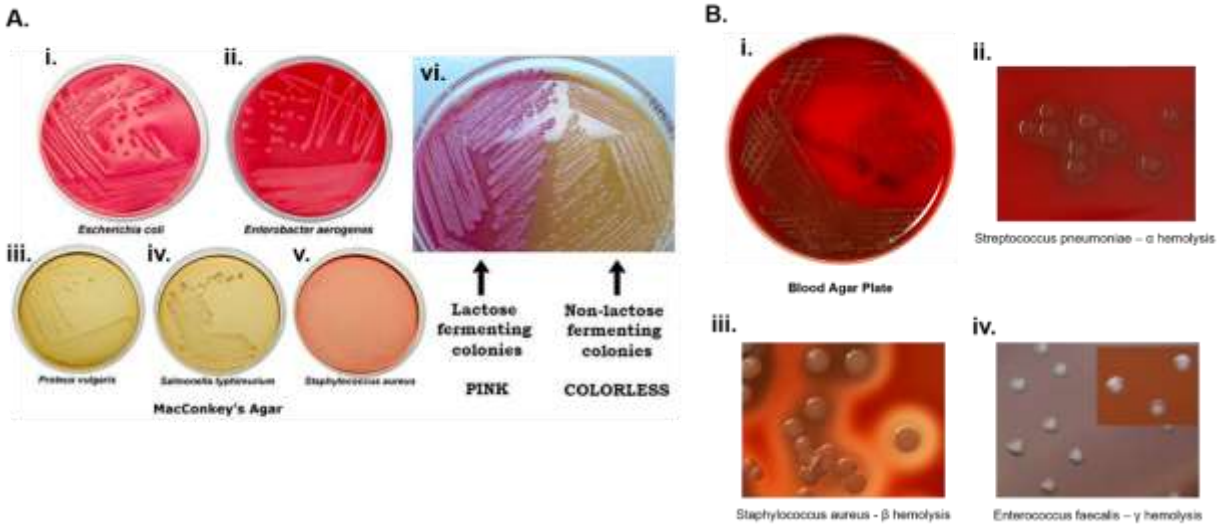

Figure 5: Standard plate count detection method used by Human Milk Donor Banks. A.) MacConkey's and B.) Blood Agar plates are used to differentiate and identify the bacterial species present. Adapted from [70]–[72].

SPC using culture plates has been the "gold standard" in screening for microbiological specimens due to its many advantages. It involves a low cost, is widely available, requires minimal sample preparation and expertise level to use, able to directly measure the growth of the bacteria, and is trusted [10], [65]. However, there are drawbacks to this system, including the lack of sensitivity at lower concentrations, its tedious nature, and long procedural times. Culture plates have a detection limit of 25-100 colonies due to the exaggerated inaccuracy caused by the dilution processing step. Samples need to be appropriately diluted so that the concentration on a single plate will result in isolated colonies that aren't inhibited due to overcrowding. Plates with more than 300 colonies are considered too numerous to count (TNTC) and need to be repeated after further dilution. Another drawback of the system is the requirement for trained technicians to manually count each of the colonies, making the process laborious, tedious, and error-prone. In some instances, colonies are too small to be seen without the aid of a microscope, further lengthening the overall process and introducing potential sources of error. Finally, the main drawback of this system is the long procedural times for bacterial culture plates that last several days [6], [10], [11]. Although microbiological cultures of donor milk are incubated at 32-35°C for 48 hours, it can take 3-7 days for the labs to determine final quantitative bacteriologic analysis for the donor banks [5], [6], [9]. This process is the rate-limiting step to providing lifesaving nutrition to preterm infants. Despite the problems with the culture plate, the fundamental concept of the simple visualization of colony growth with the naked eye could be leveraged by monitoring its metabolism as an indicator of its viability. Therefore, by monitoring a material that is consumed or excreted during metabolism, one can notice the viability of bacteria faster than waiting for a colony to grow. The development of a faster bacterial detection device that could be used

independently of external labs and within the donor milk bank facilities itself would streamline and expedite the distribution of safe human milk to the hospitalized premature infants.

2.4 Bovine Dairy Industry Methods of Detection: Dye Reduction

Donor milk banks have often times adapted their safe consumption standards and protocols from the bovine dairy industry. A common quality test that screens for microbial contaminants is called the dye reduction method. This technique is used to measure bacterial presence and concentration based on the time it takes for the sample of interest to change colour. The dye of choice is added into a 10 mL volume of milk, then incubated at 36°C until the solution decolorizes [51]. The removal of oxygen from milk and the formation of reducing substances during bacterial metabolism causes the colour to change. Thus, the time of reduction is a measure of the total metabolic reactions due to the number of viable organisms in the milk. The greater the bacterial load in the sample, the shorter the amount of time required to detect a change in colour.

Methylene blue (MB; methylthioninium chloride or 3,7-bis(dimethylamino)-phenothiazine-5-ium chloride) is one of the most common dyes used for dye reduction in bovine milk. It is used as a redox indicator where it presents as blue in oxidizing environments and colourless when reduced (Figure 6.A). The exact mechanism through which it changes colour *in vivo* from blue to colourless is not known, but it is believed to involve enzyme-catalyzed reduction from reductants, such as Nicotinamide Adenine Dinucleotide (NADH) or Nicotinamide Adenine Dinucleotide Phosphate (NADPH) (Figure 6.B) [73]. Transmembrane reductase enzymes present on the cell surface of the bacteria are hypothesized as the location of the redox reactions [74], [75]. When oxygen is present in the system, the reaction reverses. Oxygen transfers electrons back to MB, changing it back to its blue form, and binds to available water molecules (H_2O) to form reactive oxygen species (ROS) such as hydrogen peroxide (H_2O_2). H_2O_2, a destructive molecule,

is later broken down by catalase enzymes into harmless H_2O molecules. Therefore, when there are large concentrations of bacteria present, the requirement for oxygen is greater, which lowers the dissolved concentration in the solution, resulting in the faster disappearance of the colour. Table 4 outlines the Methylene Blue Reduction test (MBRT) suggested classification of bovine milk quality based on the decolorization time of 10 mL volumes.

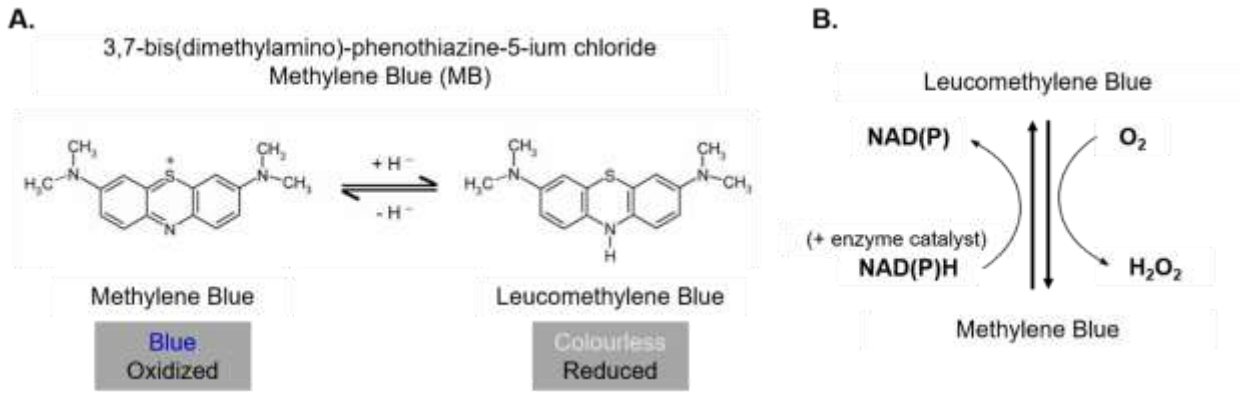

Figure 6: A.) Structure of MB in its oxidized and reduced forms. B.) Hypothesized mechanism of methylene blue redox reaction in vivo. Methylene blue is reduced through NAD(P)H-dependent reaction into its colourless form, then the leucomethylene form is oxidized by auto-oxidation. Adapted from [73].

Table 4: Bovine Milk Quality Classification of MBRT. Reproduced from [51]

Quality of Milk	Time until decolorization
Class 1: Excellent	8 hours +
Class 2: Good	Less than 8 hours but not less than 6 hours
Class 3: Fair	Less than 6 hours but not less than 2 hours
Class 4: Poor	Less than 2 hours

The popularity of this technique was largely due to its simple, rapid, and inexpensive use, as well as the potential for automation. However, the sensitivity of this test has not been correlated to a specific quantity of viable cells [75]. One reason for this is due to the greater distribution of bacteria with the fat globules that rise to the surface over time [76]. External interferences to ensure

homogeneity has shortened reduction times and therefore impacted its accuracy. The legal threshold of bacteria in bovine milk post-pasteurization is $1x10^5$ CFU/mL or $4x10^5$ CFU/mL, depending on the dairy product to be manufactured from it [65], [66]. For donor milk banking applications, the presence of a single bacterium is sufficient to discard the supply [4], [9]. Additionally, it has been reported that the exact end-point can be difficult to establish and is dependent on the sensitivity of the observer's eye to blue light [77]. The automation and precise quantitative analysis that is associated with modern cameras and image processing would help to accurately detect the end-point. Methylene blue has an absorption peak at a wavelength around 660 nm, within the red visible light spectrum. This peak disappears when it is converted into its reduced leucomethylene blue state (Figure 7). By harnessing methylene blue's ability to optically indicate the presence of bacteria through monitoring its metabolite oxygen, its fundamental concept could be applied to the detection of microorganisms in human milk.

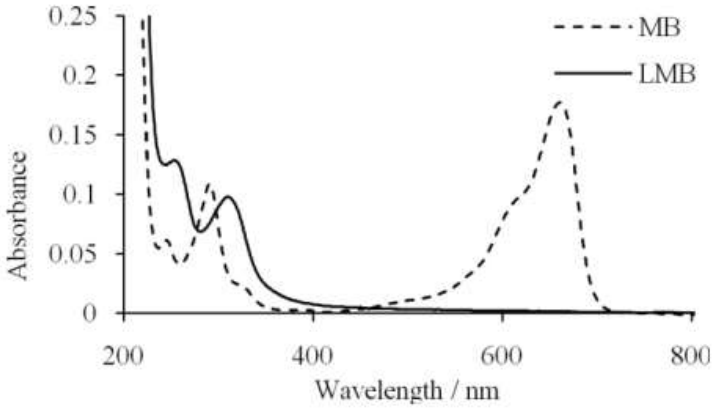

Figure 7: UV-visible spectra comparing change in absorption peaks when methylene blue is converted into leucomethylene blue. There is a loss of peak at ~660 nm. Reproduced from [78].

2.4 Current Microfluidic Biomedical Devices

The advent of microfluidics and the miniaturization of technologies have addressed many of the concerns of traditional diagnostic protocols. Microfluidic devices have been fabricated using

photolithography and 3D printing to create miniaturized platforms for rapid detection of bacteria. Several systems that do not rely on cultivation methods include the use of combinatory ligand detection using specific bacteria-targeted particles [79]–[81] or antibody binding [82], polymerase chain reaction (PCR)-based technologies [83], or flow cytometry [84]–[86] to name a few. These systems have been successful in decreasing the detection times and are very sensitive, however, all of these systems still required additional complicated and expensive post-processing to be able to visualize and quantify the level of bacterial contamination. Moreover, these systems, with the exception of flow cytometry, have difficulties in distinguishing between live and dead cells.

Monitoring bacterial metabolism has been leveraged by many microfluidic devices to succeed in detecting its presence quickly and be able to achieve this affordably. Kaushik et al. were able to accelerate the detection of a single bacterium in 20 picolitre (pL) drops using resazurin-based fluorescence [87]. Resazurin is an indicator that functions similarly to MB, changing from blue to pink when it interacts with bacteria. Cao et al. also demonstrated a microfluidic drop-based system for non-invasive optical monitoring of oxygen, however, they utilized the near-infrared (NIR)- emitting phosphorescent probe PtTPTBP (platinum (II) 5, 10, 15, 20-*meso*-tetraphenyltetrabenzoporphyrin) [88]. Gómez-Sjöberg et al. demonstrated the ability to concentrate bacterial cells from a dilute sample by a factor of 10^4-10^5, then detect their metabolic activity by leveraging the concept of "Impedance Microbiology" [89]. This is a concept where a change in electrical current measured by electrodes in contact with the medium can indicate bacterial growth. Despite their success, these systems require the additional processing step of droplet generation, fluorescent-based imaging, or a source of electrical current. A simpler system that uses colorimetric sensing while providing rapid, high-throughput screening would allow for greater adaptability and accessibility of the technology.

Ayyash et al. had developed the initial iteration of the Rapid Culture Nanowell device to monitor the metabolite oxygen in a microarray of 1 nL well volumes to screen for infectious bacterial diseases like tuberculosis (TB) [90]. However, their use of the fluorescent oxygen sensor RTDP (ruthenium (II) tris(2,2'-bipyridyl) dichloride hexahydrate) meant requiring the use of expensive equipment and limited the use of the whole system to laboratory environments to allow for accurate readings of the luminescent readings. By replacing the fluorescent sensor with the optical chromogenic indicator Methylene Blue, a dye commonly used in the bovine milk industry, the presence of bacteria could be detected with commercial cameras and even the naked eye. Further, the concept of compartmentalization can be used to shorten the time required to process the larger sample volume used by the donor milk industry compared to the TB sputum specimen.

2.5 Summary

With approximately 24,500 preterm children born annually in Canada and an estimated shortage of 6 million ounces of breast milk, the distribution of donor milk must be time-sensitive to efficiently meet this demand with the limited supplies [4], [50]. The tools used by milk banks to ensure safe distribution rely heavily on the culture plate [4]–[9]. It has been the "gold standard" in screening for microbiological specimens due to its wide availability, low cost, and simplicity [10], [65]. However, the procedural times for bacterial culture plates are long, lasting several days [6], [10], [11]. This delays the distribution of human milk to the infants who need it most. Advances in microfluidics, particularly in combination with the concept of monitoring metabolites to indicate bacterial viability, hold much promise to significantly reduce the long processing times of culture plates. Combining the concept of compartmentalized culture and a chromogenic optical dye for the detection of metabolic changes as a new diagnostic sensor could be advantageous in updating the existing Rapid Culture Detection system that initially used a fluorophore sensor. The

device would be intended for use in the donor milk bank facilities, removing the need to rely on external laboratories to conduct the tests (except in the case of emergency) and allowing for the expedition of the detection of microbial contamination. Staff will be able to directly test each bottle for bacterial presence post-pasteurization and obtain readings faster than the 3-7 days that the labs spend analyzing and processing the culture plates. This thesis will focus on the development of a quick, low-cost, easy-to-use bacterial detection system with Methylene Blue so to protect infants from foodborne infectious diseases and shorten the access time to the lifesaving nutrition.

Chapter 3 – Working Principle, Device Design, Materials, and Methods

This chapter details the working principle on which the device is based and the various components involved in the design of the complete detection system, including the microfluidic device, sensing method, and imaging modality. The chapter goes on to cover the materials and methods involved in the characterization and use of Methylene Blue as a redox indicator in detecting bacterial metabolism in the microfluidic device. This includes the fabrication methods of the nanowell devices, preparation of samples, experimental set-ups, imaging, and analysis.

3. 1 Working Principle

The fundamental concept applied to the design of the diagnostic device is the principle of segmentation. When large volumes of a sample containing few bacteria are sectioned into smaller units, the concentration in some of those units can be artificially increased. To illustrate this idea, Figure 8 shows a 1 mL volume with 10 bacteria in it as one large volume on the left and the same volume divided into 1000 portions holding 1 µL each to the right. The sample to the left has a concentration of 10 bacteria/ mL whereas the sample on the right has a range of concentrations. Most of the smaller units have a concentration of 0 bacteria/mL while some of the smaller units have a much higher number of 1 bacteria/µL or ~1000 bacteria/mL. By segmenting the larger volume, the concentration of bacteria is artificially increased by 100 times in some of the smaller volumes. This change can thus be detected by an imaging system quicker than in its larger scale if an assay based on metabolic activity was used.

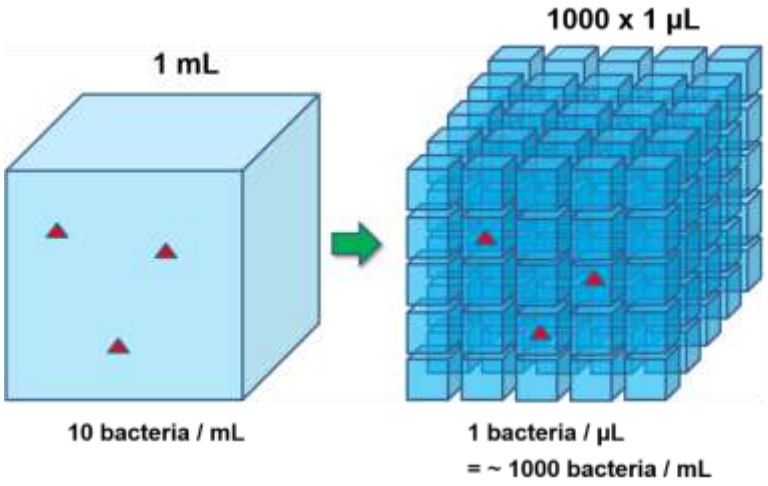

Figure 8: Segmentation of larger volumes into multiple cubes containing smaller amounts can artificially increase the concentration of bacteria, therefore decreasing the expected detection rates. Reproduced from [90]

Within each of these wells, the bacteria are expected to undergo normal processes like the catabolism of nutrients into building blocks that are later used in anabolism to repair and grow (Figure 9). Aerobic bacteria specifically require oxygen for metabolism and ultimate survival. Therefore, when bacteria are present and thriving in the well, the concentration of available oxygen decreases as they continue to grow and multiply.

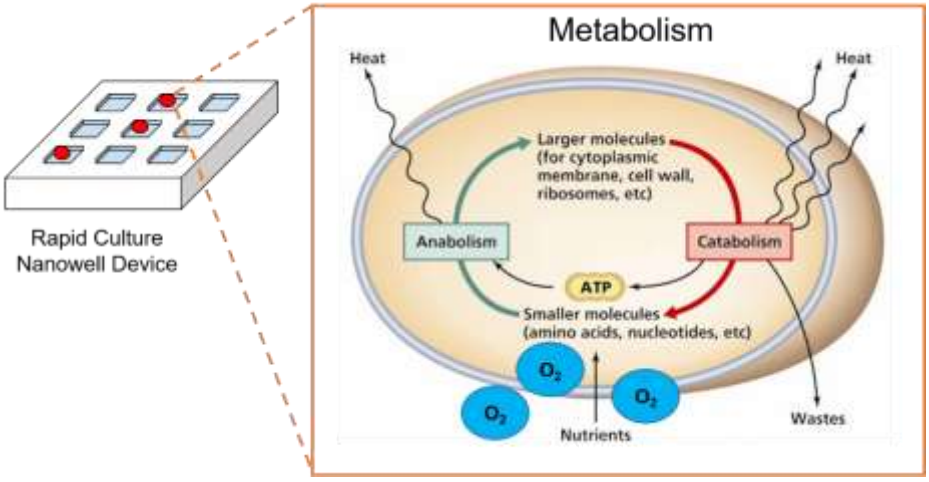

Figure 9: Simplified representation of metabolism in bacteria that resides within a well in the nanowell device. Image of metabolism modified from [91]

The oxygen consumption of aerobic bacteria could, therefore, be used as a metabolic indicator of bacterial presence and growth. By combining this assay with the sample segmentation principle, the change in oxygen level due to bacterial metabolism within the smaller volume can be larger and more evident than the difference within the larger system. One can, therefore, obtain a faster detection of bacterial growth in the smaller units with artificially increased concentration of bacteria.

3.2 Device Design

The aim of this thesis is to modify the prior version of the Rapid Culture Nanowell Device to encapsulate a large sample volume as required in conventional human milk diagnostic methods while balancing the ability to quickly detect bacterial presence. In the following section, the criteria involved in the overall design is outlined, as well as the exploration of the ideal method of device fabrication, type of indicator dye, and image capturing system.

3.2.1 Device Criteria

Conventional methods of bacterial detection for human milk banking applications are reliant on culture dishes that test 1 mL volumes of human milk over a 48-hour incubation period [6], [9], [17], [92]. Despite being the gold standard of bacterial screening, the culture dishes are limited by their ability to accurately detect growth below 100 CFU/mL and their slow turnaround times [6], [93]. Any level of bacterial contamination can be detrimental to the immunocompromised premature infants who rely on donor human milk. Therefore, the development of a system that can quickly and accurately detect bacteria would allow for faster and safer distributions of the life-benefiting source of nutrition. The redesigned Rapid Culture Nanowell Device must be able to match, if not supersede, the capabilities of the culture dish, in addition to addressing its limitations.

It must, therefore:

- Provide information on the presence and viability of bacteria in human milk samples,
- Deliver a response faster than 48-hours to allow for quicker turn-around times [6], [9], [17], [92]
- Detect any positive culture after pasteurization [4], [9], [17], and
- Process a total of 1 mL sample volumes [17], [94].

The updated Rapid Culture Nanowell device must ultimately be easy to use for maximum accessibility of the technology. The sample preparation, loading process, and interpretation of the results must be straightforward and uncomplicated. The simplicity of the system would also minimize the time and costs required to be spent on training users. A detection device that can address these criteria would be beneficial in both lab and resource-limited field settings.

3.2.1 Device fabrication method: 3D Print vs Lithography

Photolithography is commonly used in the process of fabricating microfluidic devices due to its ability to process photoresists that capture precise nanoscale patterns [95]. Previous success in detecting bacteria with the Rapid Culture Nanowell Device was accomplished with a master mould fabricated using photolithography [90]. However, in order to accommodate an increase in sample volume from 4.9 µL to 1 mL without sacrificing the portability of the overall device, the volume of a single well was adjusted. A limiting factor to the photolithographic fabrication is the maximum thickness of photoresist that can be achieved on a silicon wafer, and therefore, is a constraint on the depth of a single well. Photolithography is a multi-step fabrication process that can produce heights of a few tens of nanometers to hundreds of microns, depending on the photo-resist used [96], [97]. In the case of SU-8 3035, a single layer is limited to a thickness of ~120 µm [98]. With the explosive development of additive manufacturing, these 3D printers could provide an

alternative method of fabrication without compromising the resolution and fine detail required for microfluidic work. 3D printing advances have come so far as to achieve resolutions as small as 50-300 µm with certain forms of additive manufacturing technologies [99]. The Multi-Jet Modeling (MJM) type of 3D printing is one of the most attractive technologies for microfluidic applications due to its high resolution and capability of printing multiple materials at a time [100]. Dimensions down to ~200 µm have been achieved. However, the layer-by-layer printing approach may result in rough surfaces that interfere with the filling or sealing of the microfluidic device. In this thesis, the suitability of MJM 3D printing was compared to the typical photolithographic method in the fabrication of moulds for the Rapid Culture Nanowell device.

3.2.2 Device indicator material: Fluorescent vs Optical Dyes

Previous works have reported success with the use of ruthenium (II) tris(2,2'-bipyridyl) dichloride hexahydrate (RTDP) as a way to monitor oxygen concentration in biological systems [90], [101]–[104]. RTDP is a fluorescent dye that has been shown to detect bacterial presence through the sensing of metabolic oxygen. Although highly sensitive, the detection of its luminescent properties is reliant on the use of expensive imaging systems in specific limiting lighting conditions. To simplify the use of the Rapid Culture Device, MB was explored as the indicator of choice because it would allow for optical visualization instead of fluoroscopy. MB begins as a blue-coloured dye that later changes to its colourless counterpart leucomethylene blue when it is reduced metabolically by bacteria. With the change in reporting dye to MB, commercially available systems such as digital single-lens reflex (DSLR) or cell phone cameras may be used, making this detection system more accessible and affordable than conventional entities. The characterization and use of methylene blue for the detection of bacteria in the redesigned Rapid Culture Nanowell Device will be explored in this thesis.

3.2.3 Device imaging system

The typical imaging modalities used to determine bacterial viability in microfluidic devices rely on the fluorescent microscope or microarray scanner. Despite the high degree of sensitivity and reliability that these systems provide, this technology is expensive, bulky, time-consuming to use, and requires high levels of expertise to use. An alternative platform for imaging the Rapid Culture Nanowell Device that will be widely accessible, affordable, and easy to use is required. The use of an affordable camera-based imaging system will be explored, as well as the possibility of adapting it to cell phones cameras. However, the use of the camera macroscope must first be characterized and calibrated. This thesis will explore the use of a fluorescent microscope, DSLR-camera imaging system, and a cell phone camera as part of the initial exploration of the imaging of MB within the nanowell and microwell devices.

3.3 Materials

The materials used in this thesis are summarized in sections detailing the consumable reagents, items used to characterize Methylene Blue and dissolved oxygen levels, components involved in the fabrication of the Rapid Culture Nanowell device, and the elements associated with bacterial culture and incorporation.

3.3.1 Consumable Reagents

Methylene Blue (MB; M9140) is a common redox indicator that switches between its blue and colourless states. It was purchased from Sigma-Aldrich (St. Louis, MO). Sodium sulphite (Na_2SO_3; 71988) is a common oxygen scavenger. It was used to remove the oxygen dissolved from a given solution. It was purchased from Sigma-Aldrich (St. Louis, MO). Human milk was purchased through the Roger Hixon Toronto Milk Bank. Pasteurized term-milk from pooled donors who may have been on medications were provided.

3.3.2 Characterization Elements

The commercially available Extech DO600 Exstik II Dissolved Oxygen Meter (Extech Instruments) was used to measure the level of dissolved oxygen within a solution (Boston, MA). Air from the Chemical Hoods vent was bubbled into solutions through a piece of Tygon S3 E-3603 NSF 5 tubing. Solutions in Falcon 50 mL conical tubes were mounted on a stand fixed with Fisher clamps.

3.3.3 Microfluidic Device

The mechanical grade silicon wafers used as the photolithography substrate were purchased from University Wafer Co (South Boston, MA). Two sizes were used (3 inches and 5 inches) with a wafer thickness of 500 µm. The SU-8 3035 negative photoresist and developer used in the photolithography process were acquired from Microchem Co. (Westborough, MA). VisiJet EX200, the UV curable acrylic plastic used as the 3D printer substrate, was purchased through the McMaster University Machine Shop (Hamilton, ON). The Sylgard 184 Silicone Elastomer Kit used to prepare the PDMS device was purchased from the Dow Corning Corporation (Midland, MA). Microseal B PCR Plate Sealing Film (MSB1001) was used to seal the sample wells was purchased from Bio-Rad (Hercules, CA).

3.3.4 Bacteria

Escherichia coli K12 MG1655 wildtype was generously provided by the Schellhorn lab (McMaster University, Hamilton, ON) and used as an initial bacterial species of study. The GFP-tagged E. coli strain (pMS201) was generously provided by the Brennan lab (McMaster University, Hamilton, ON) [105]. The culture broth used was Luria-Bertani (LB) broth, subtype “Miller” (Fluka Analytical L3152), and was purchased from Sigma-Aldrich (St. Louis, MO). The antibiotic Kanamycin sulphate (Kn; #60615) was purchased from Sigma-Aldrich (St. Louis, MO).

3.4 Methods

3.4.1 Fabrication of Nanowell Device

The nanowell master mould was fabricated using photolithography and 3D printing techniques to determine if one procedure was better suited over the other. Both methods of fabrication are detailed in this subsection.

3.4.1.1 Master Mould Fabrication of Photolithography Device Mould

A grid pattern of 500 x 500 µm (pitch = 1000 µm) squares was designed using a solid modelling computer-aided design (CAD) program, such as Solidworks (Dassault Systèmes, Vélizy-Villacoublay, France). The file was then converted into a photomask by CAD/Art Services Inc. Figure 10 illustrates the subsequent photolithography steps. In Step 1, the silicon wafer substrate was covered with a layer of SU-8 3035 photo-resist. In Step 2, the covered wafer was baked on an even hot plate at 95°C for 45 minutes. In Step 3, an ultraviolet (UV) light was used to project the design onto the photoresist. The regions that were not blocked by the photomask were polymerized. In Step 4, the wafer was then baked again over a hot plate at 65°C for 1 minute, then at 95°C for 5 minutes. Steps 1 through 4 were repeated for the additional layers of photoresist. Since a single layer of SU-8 3035 is limited by its maximum thickness of ~120 µm, extreme precision needs to be taken to accurately layer multiple applications to achieve the final 300 µm thickness [98]. Finally, in Step 5, the wafer was submerged in a “developer” solution to remove the unpolarized photoresist [96].

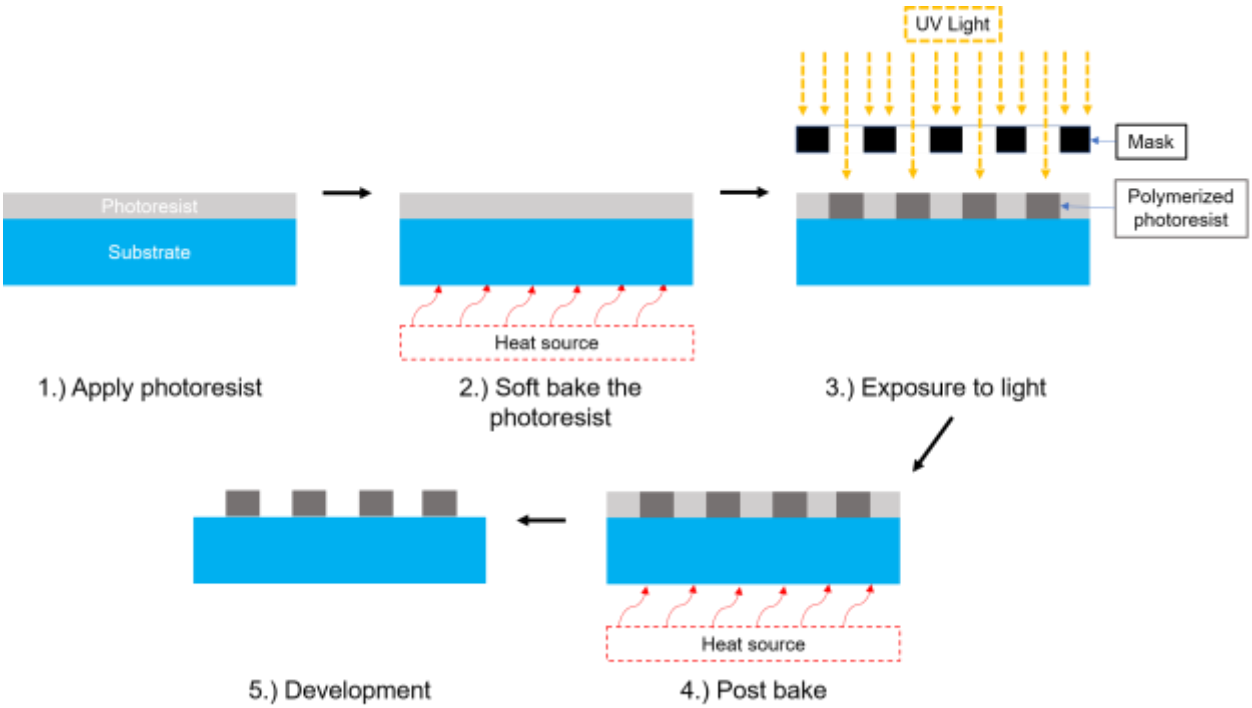

Figure 10: Schematic illustration of the main photolithography steps.

3.4.1.2 Master Mould Fabrication of 3D Printed Mould

The microfluidic chip mould was first designed using Solidworks or similar design software. The array consisted of a grid of squares (500 x 500 µm; pitch = 1000 µm). The file was then saved in an STL format (stereolithography CAD) and transferred into the computer program specific to the 3D printer (ProJet Accelerator Software). The ProJet 3000 printer prints the piece via Multi-Jet Modeling 3D Printing or photopolymer inkjet printing. As Figure 11 illustrates, this type of 3D printing involves an inkjet print head that is able to extrude a UV-curable build material and a sacrificial support material [100]. First, the materials were heated to 30-60°C to achieve optimal viscosity. As each layer of tiny photopolymer droplets was added onto the platform, a UV lamp quickly set it before the platform lowered and another layer was deposited on top. The resolution of the ProJet 3000 is 656 x 656 x 800 DPI (dots per inch; XYZ) with an accuracy of 0.025-0.05 mm per inch of part dimension [106]. Once the system finished printing, the piece was removed

from the printer and underwent post-processing to remove the supporting wax material. Before the mould was cast with PDMS, it was treated with silane to prevent excessive adhesion. After this step, the soft lithography can be used to produce the microfluidic device.

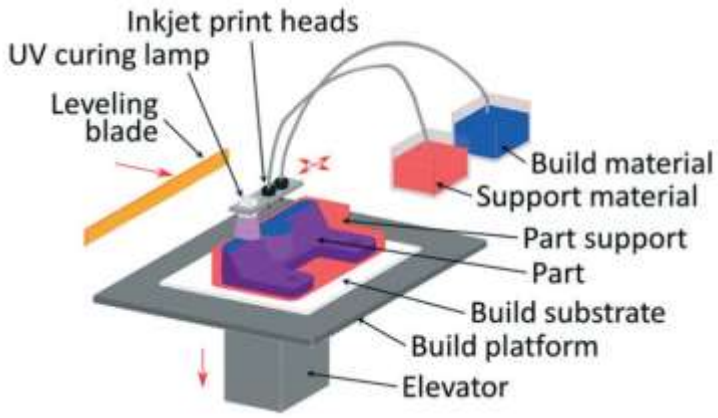

Figure 11: Components involved in Multi Jet Modeling 3D printing. An inkjet head adds a layer of curable liquid photopolymer onto a tray which is rapidly polymerized by UV light. The inkjet head is also able to extrude a gel-like sacrificial material as support for overhanging or complex structures. Once the part has been fully printed, post-processing is required to dissolve the supports. Reproduced from [100]

3.4.1.3 Nanowell casting

A soft-lithography technique was used to form the nanowell devices. Polydimethylsiloxane (PDMS) base and crosslinker were mixed in a 10:1 ratio. Then the solution was placed into a desiccator and vacuum system to remove any air bubbles. The final mixture was poured into either the master mould constructed via photolithography or 3D printing. Great care was taken to ensure no bubbles remain in the body of the device, as it would compromise the nanowell structure and imaging. The device moulds were placed on a level hot plate at 80°C for 12 hours. When the PDMS was fully cured, the devices were cut with a scalpel and carefully removed from the master mould (Figure 12). Submicron features were kept clean and free of debris by protecting it with a layer of scotch tape.

3.4.1.4 Surface treatment

Once the PDMS device was cured and removed from the mould, it must be treated to alter the surface properties. PDMS is naturally hydrophobic, therefore, surface modification is necessary to render the walls of the well to be hydrophilic. This would allow for easy filling of the samples being tested. Otherwise, it would be near impossible to fully fill such tiny volumes without interfering air bubbles. A plasma cleaner machine was used to treat the surface. The basic concept involves the use of plasma (partially ionized gas) to energize the neutral atoms found on the surface of the PDMS to break apart the molecules, forming reactive radicals [107]. These radicals break the air molecules apart, which then interact with the surface polymer groups to create reactive chemical functional groups. The exposed areas of the PDMS are now charged, rendering the surface hydrophilic. This process also sterilized the devices before use by removing any chemical or biological contaminations [108].

Figure 12 illustrates the steps taken to modify the surface of the PDMS devices. The PDMS pieces were placed into the Plasma Cleaner (Harrick Plasma, PDC-001 and PDC-FMG) chamber and exposed for 1.5 minutes at an ambient air flow of 30 mL/min. A piece of scotch tape was placed on top of the device after plasma treatment then lifted to remove the top-most layer. The PDMS below this top region had remained naturally hydrophobic. This property aids in the isolation of each individual well and prevents cross-contamination. Finally, the devices were submerged in water to maintain the hydrophilicity of the wells until use [109].

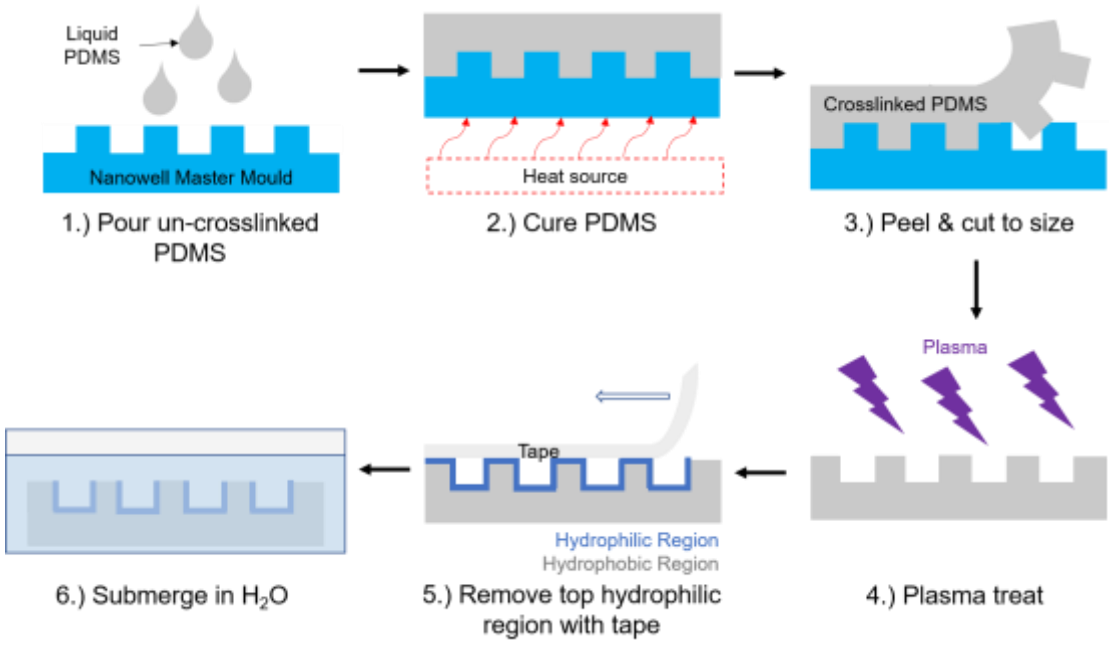

Figure 12: PDMS nanowell device fabrication process flow.

3.4.2 Sample Preparation

3.4.2.1 Bacteria preparation

To maximize user safety and minimize contamination of unwanted microorganisms, the inoculation of bacteria was done in a sterile ESBE Scientific biological scientific cabinet (BSC; Model SG403A-HE, Markham, ON). A pure culture of kanamycin resistant *E. coli K12* GFP bacteria was proliferated by selecting a single isolated colony from the culture dish and mixing it into a 4 mL tube of LB media. The antibiotic kanamycin (50 mg/mL) was added in 1:1000 ratio. The tube of bacteria was left to grow overnight for 16-18 hours at 37°C in a shaker. After the incubation time, a 200-300 µL sample was pipetted into a microwell plate and scanned by the Tecan Plate Reader infinite M200 Pro (#1406000155) to determine the turbidity or optical density (OD). An OD_{600} of 1 is equivalent to a *E. coli* concentration of 10^9 CFU/mL [110].

The solution then underwent serial dilution to obtain the required concentration. For example, to obtain a concentration of 10^7 CFU/mL, 100 µL of 10^9 CFU/mL is taken and added

into 900 µL of LB media. When sufficiently mixed, the solution has an evenly distributed concentration of 10^8 CFU/mL. The same process is repeated using 100 µL of the 10^8 CFU/mL mixture to make a final concentration of 10^7 CFU/mL.

3.4.2.2 Indicator Media Preparation

Test samples were prepared using the following protocol:

1.) Indicator samples with chemically augmented oxygen levels

To quantify the relationship between the MB colour its redox state, containers of different levels of dissolved oxygen were tested. To remove oxygen, the scavenger sodium sulphite (Na_2SO_3) was used at varying concentrations between 1-50 mg/mL. To increase DO levels, compressed air was bubbled into the solutions using the air vents in the chemical hoods at the lowest flow rate possible. Solutions were mixed in Falcon 50 mL conical tubes with a total volume of 10 mL. They consisted of 2.5 mg/mL Methylene Blue and LB media. Each container was tightly sealed to ensure minimal gaseous exchange with the environment. Na_2SO_3 testing solutions were left overnight to equilibrate, while the high O_2 condition is treated half-an-hour before being imaged.

2.) Sterile indicator samples

A stock solution of MB was prepared at a 10x greater concentration in LB media. MB concentrations of 1.0-2.5 mg/mL were tested to balance the darkness of the dye and the degree of colour change. Visibility of the dye was determined using optical images taken via cell phone and DSLR cameras. Stock solutions of the dye were sterilized in a water bath (72-80°C) for 30 minutes, then cooled before use. All tubes were wrapped in aluminum foil to avoid light desiccation of the dyes and vortexed to ensure homogeneity. To additionally prevent for unwanted bacterial contamination, the mixture was filtered using a 0.2 µm pore size membrane (Acrodisc Syringe Filters, Pall Corporation) and kanamycin was added. The behaviour of these samples acted as a

baseline measure. Final experiments were conducted with 2.5 mg/mL and 1.0 mg/mL in the microwells and 1.0 mg/mL concentrations in the nanowells. For quality assurance testing, culture plates were streaked with the test solutions to monitor for colony growth. No visible colonies indicated a sterile solution. The detailed protocol on the preparation and streaking of LB agar culture plates is provided in Appendix A.

3.) Indicator samples inoculated with bacteria

To mimic actual medical test samples, bacteria were added into MB indicator solutions. Bacteria at different concentrations ranging from 10^2-10^9 CFU/mL were added into MB solutions to detect different rates of oxygen uptake. Inoculated solutions were also streaked onto culture dishes to determine the bacterial presence and rough counts. Colony numbers were considered "TNTC" (Too numerous to count) if there were greater than approximately 300 colonies per dish [111]. The detailed protocol on the preparation and streaking of LB agar culture plates is provided in Appendix A.

3.4.2.3 Human Milk Preparation

Initial amounts of human milk were delivered in a frozen state from the Rogers Hixon Toronto Milk Bank. Upon arrival, samples were placed in a 37°C water bath and removed the moment the whole bottle was visually defrosted. Milk was then aliquoted into 5-10 mL quantities and refrozen for future experiments. It was critical that the number of freeze-thaw cycles was minimized to keep the integrity of the milk intact. The freeze-thaw process can degrade the milk proteins and enzymes, leading to inaccurate results. When required for experiments, an aliquot of milk was defrosted in a water bath set to 37°C until the total volume had melted. Each tube was then vortexed to ensure even distribution of the milk components. Samples were used up within 24 hours of being thawed as per HMBANA guidelines [9].

3.4.3 Sample Loading and Experimental Set-up in Nanowell device

3.4.3.1 Sample Loading

When solutions had been prepared, the sample was deposited on top of the PDMS device with a 1 mL syringe. A microscope slide was used to "squeegee" the solution to fill the wells evenly [90]. Once fully filled, the wells were sealed with the Microseal B adhesive tape. A microscope slide was used again as a squeegee over the adhesive to remove any excess solution from around the wells. This step also helped to firmly adhere the tape to the PDMS device. Then, the devices were sandwiched between two microscope slides with enough pressure to ensure sealing of the individual wells. Devices are ready to be imaged.

3.4.3.2 Experimental Set-up

A schematic of the loading process is outlined in Figure 13. Prepared solutions consisting of bacteria and the MB indicator were dispensed onto the treated nanowell devices. Next, the test sample was spread and compartmentalized into the individual wells. The device was sealed, then imaged with either the custom-built DSLR-camera imaging system, microscope, or cell phone camera. Images of the empty and loaded nanowell device are included in the figure.

Due to the optical qualities of MB, the colour change could be tracked using the inverted Olympus Microscope (IX51S1F-3), the camera-based imaging system created by Reza Ghaemi from the Selvaganapathy Lab called the DSLR-Macroscope, as well as any cell phone camera. Photos from the three imaging modalities were then collected and computer analyzed. The Tecan Plate Reader infinite M200 Pro (1406000155) was used as a confirmatory baseline to compare the trends amassed from the three imaging modalities. More details about this process can be found in Section 3.4.8.

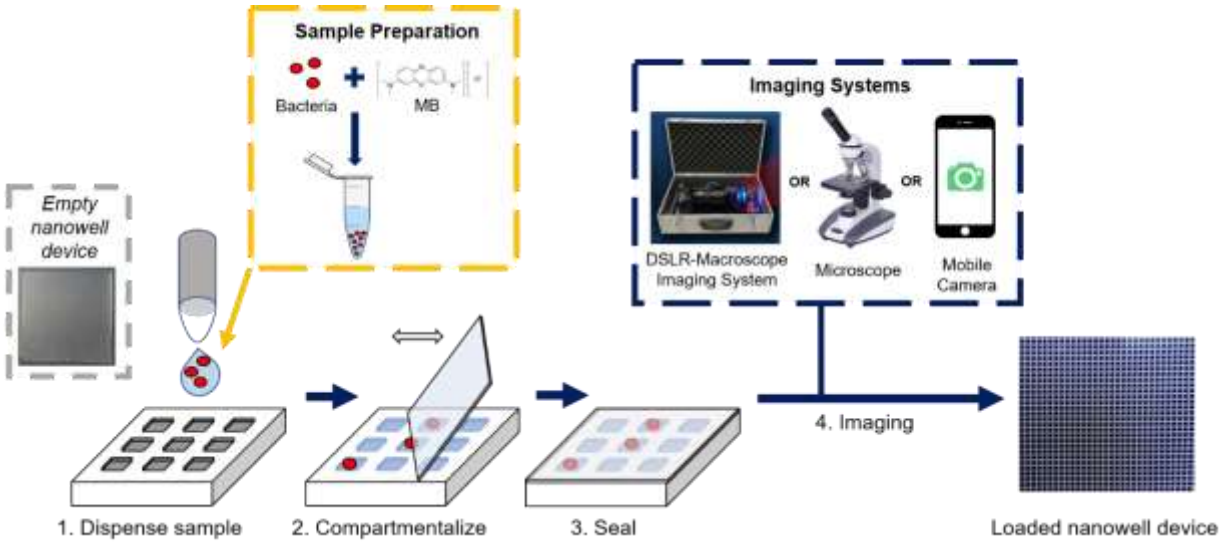

Figure 13: Device Filling Schematic for MB staining method. The dye is added into the sample of bacteria and loaded into the prepared nanowell device. Once sealed, the device is imaged using the camera-based imaging system or microscope using brightfield setting. Imaging system images reproduced from [112], [113]

3.4.4 Dissolved Oxygen Measurement

Concentrations of dissolved oxygen (DO) were measured in different solutions using the Extech DO600 Exstik II Dissolved Oxygen Meter. After waiting for the handheld device to self-calibrate, the tip of the ExStik II was fully submerged into the test sample. A period of 4 minutes per sample was required for the DO reading to stabilize. Each reading is provided in mg/mL. After the measurement was noted, the probe was rinsed with water than 70% ethanol and dried before placement into the next sample.

3.4.5 Imaging

Several types of imagers were explored in this thesis including the Tecan Plate Reader, cell phone camera, fluorescent microscope, and DSLR camera. Each of the systems and their experimental set-ups is highlighted in this section.

3.4.5.1 Imaging in Tecan Plate Reader

Samples of interest were filled into a 96-well plate, sealed with adhesive, and inserted into the Tecan Plate Reader. Using Tecan's Magellan Microplate Reader software, a script was written to identify the correct brand and size of microplate used, as well as the type of imaging to be conducted. To measure the absorbance of the MB over time, a wavelength of 668 nm was set. As the plate was being read, the data was transferred to a Microsoft Excel document for efficient data analysis. More details on the methods of data analysis can be found in section 3.4.9.

3.4.5.2 Imaging with Cell Phone

To quantify the relationship between the MB colour its redox state, containers of different levels of dissolved oxygen were tested and imaged with the Google Pixel 2 camera. Key specifications of the Google Pixel 2 camera include 12.2 MP (mega-pixel) dual pixel rear camera (resolution of 1080x1920 pixels), CMOS image sensor, optical and electronic image stabilization, and f/1.8 aperture [114]. Each conical or Eppendorf tube was placed into the set-up shown in Figure 14. The camera was placed at the same distance to ensure consistency in lighting. For tests using conical tubes, the camera was 5 inches away from the sample. For tests using Eppendorf tubes, the camera was 7 inches away to accommodate all the tubes in one frame. Flash was not used. Images were collected and analyzed using ImageJ. For more details about the image analysis process, see section 3.4.6.

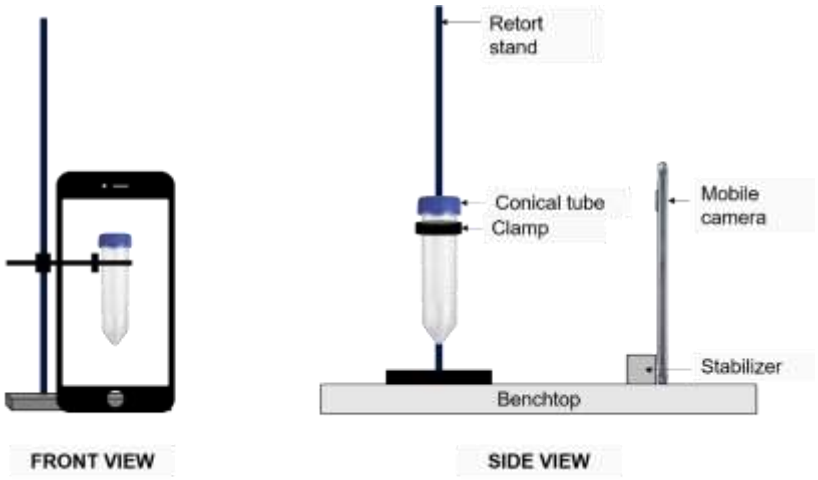

Figure 14: Schematic of the imaging set-up (front and side view) for the optical colorimetric DO concentration tests.

3.4.5.3 Imaging with Fluorescent Microscope

The fluorescent microscope has been the typical imaging tool used in microfluidics. With its flexibility to monitor samples using either brightfield or fluorescent modes, luminescent or optical indicators can be used. For the purposes of this thesis, the inverted Olympus microscope was used in parallel with the DSLR-Macroscope to verify the validity of the new system. Images were collected via the greyscale monochromatic Retiga-2000R camera (High Sensitivity IEEE 1394 FireWire Digital CCD Camera) and the cellSens Life Science Imaging software (Olympus, Germany). Images were saved in both .tiff and .jpeg formats.

The following settings were used with the Olympus microscope. In the brightfield mode, the light source dial was set to the second notch. When measuring the fluorescence of the GFP-tagged *E. coli* K12, the FITC filter was used (EX filter range: 475-485 nm, EM filter range: 485-536 nm). The fluorescent light source was set to the second level of intensity.

3.4.5.4 Imaging with DSLR-Macroscope system

The benefits of the camera-based imaging system are its ability to act as a "macroscope", is more affordable than an equally powered fluorescent microscope, and is capable of clearly imaging the microfluidic devices without being limited to fluorescent lighting conditions. This system consisted of a digital single-lens reflex (DSLR) camera, the Nikon D810, that was fixed to a rig holding it perpendicular to the imaging surface. The key specifications of the Nikon D810 include: 36.3 MP full-frame CMOS sensor (max resolution of 7360x4912 pixels), no anti-aliasing or optical low pass filters, ISO range of 64-12,800 (expands to ISO 32-51,200), Multi-CAM 350FX 51-Point AF Sensor, and 91,000-pixel RGB metering sensor for advanced subject tracking and metering [115]. It was housed in a black box to mitigate interfering ambient light, along with a sample stage and a white backlight (LED-SP Lamp). The camera was connected to a laptop that runs the open source digiCamControl program (Duka Istvan, Massachusetts Institute of Technology) (Figure 15). This program interfaced with the camera to easily visualize and control the settings externally.

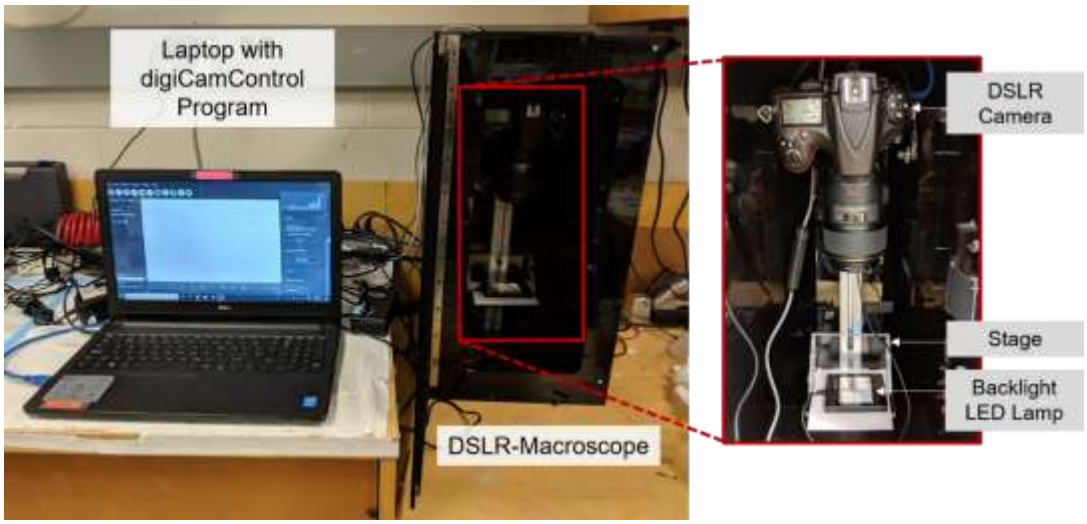

Figure 15: Image of the imaging set-up for MB devices. This set-up could be adapted with the use of a light source and fluorescent filters for fluoroscopy.

To image the devices, the sample of interest was placed below the camera lens. For microwell experiments, 96-well plates were placed at the bottom of the box to visualize a 10x6 well region. For nanowell experiments, devices were placed on top of the backlight LED lamp, which subsequently was raised on the stage to a distance of 10 inches from the lens. The combination of ISO, aperture, and shutter speed were chosen to obtain a balanced exposure: ISO-200, f/3.3 aperture, ¼ second shutter speed, and with flash. Once all factors are set and the devices positioned, the box door was closed and digiCamControl was set to take images according to the time-lapse frequency settings. Images were saved in a .tiff format to retain as much information as possible for image processing and data extraction.

3.4.6 Image Processing and Data Extraction

The colour saturation of the different DO conditions needed to be quantified to determine its relationship. Appendix B details the complete image processing and analysis protocol. Images from all three imaging modalities (microscope, DSLR-Macroscope, and cell phone camera) were collected and analyzed with the open source imaging processing program called ImageJ (Wayne Rasband, National Institutes of Health). Time-lapse images were collected into a stack and the wells were aligned using the StackReg plugin. An area of interest, as indicated in Figure 16 was selected in ImageJ, depending on the experiment. With the samples of larger volume, each sample was selected manually as shown in Figure 16.A-B. Due to the number of wells to be processed in the micro- and nanoarrays, individual wells were selected via the Microarray Profile Plug-in as per Figure 16.C-D. The mean gray value was then measured.

Once the data was collected from ImageJ, it was then transferred to Microsoft Excel and R (Ross Ihaka and Robert Gentleman) for organization and primary analysis. The short code written in R efficiently clumps the time point sequences for an individual well together, in addition to

performing normalization and standard deviation calculations (Appendix C). These numbers were then inputted into Microsoft Excel to be graphed and statistically analyzed.

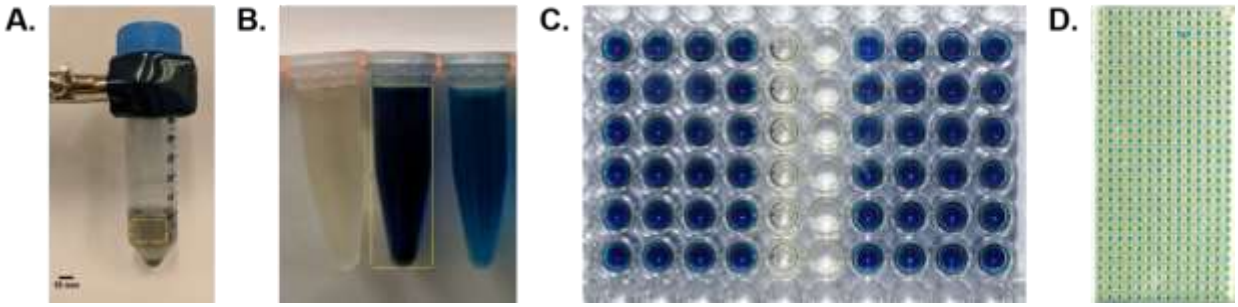

Figure 16: Selection of areas of interest using ImageJ Processing. The dotted yellow rectangle or circle represents the region of interest for experiments done in A.) conical tubes, B.) Eppendorf tubes, C.) microwell plates, and D.) nanowell devices.

3.4.7 Data Analysis

3.4.7.1 Relative Grey Scale Measurement

To measure the change in dye intensity within a specific well, the readings from image number n (x_n) were compared to its initial state (x_0). To do this, the intensity value at subsequent time points was divided by the initial intensity value ($relative\ saturation\ =\ x_n/x_0$) so that the data was normalized to a value of 1. Therefore, each well's intensity was converted into a value that directly compares it to its initial presentation. This measurement allows for a means to compare the colour change of multiple wells across experiments and the conditions tested in the thesis. n can be related to a specific time based on the imaging frequency set for each experimental design.

3.4.7.2 Statistical Analysis

Data analysis consisting of t-tests and two-way repeated measures ANOVA was performed in Microsoft Excel 2016 using the Data Analysis ToolPak and GraphPad Prism.

Chapter 4 – Results & Discussion

In this chapter, a series of experiments were conducted to study the use of Methylene Blue as an optical dissolved oxygen indicator of metabolism. With an understanding of the relationship between redox states, DO concentration, and quantification via an image analysis software, the detection of bacteria using MB was characterized to be used in conjunction with the re-designed Rapid Culture Nanowell Device. The effects of MB concentration, miniaturization of well volume from the micro- to nanoscale, and different nutrient media for the application to human milk banking was also explored and discussed.

4.1 Characterization of the use of Methylene Blue as an optical dissolved oxygen indicator for metabolism

4.1.1 Relationship between the colouration of Methylene Blue redox states and Mean Gray Value extracted from images

In order to determine the efficacy of using Methylene Blue as an indicator of bacterial metabolism, the relationship between a solution's colour after the addition of MB and its concentration of dissolved oxygen (DO) needed to be explored. To simulate a gradient of DO concentrations, six solutions of MB and LB media were subjected to various conditions that either artificially increased or decreased the level of oxygen: 1. Air bubbled into the solution for 1 minute to increase [DO], 2. Control equilibrium within the container, 3. Addition of the oxygen scavenger sodium sulphite (Na_2SO_3) at 1 mg/mL concentration, 4. Na_2SO_3 at 5 mg/mL, 5. Na_2SO_3 at 25 mg/mL, and 6. Na_2SO_3 at 50 mg/mL. All tubes were tightly sealed and allowed to sit for 24-hours. Tubes for condition 1. were bubbled with air then sealed half an hour before being measured. Refer to section 3.4.4 for the experimental procedure and set-up. Each condition was repeated in triplicate.

The effect of various conditions that alter the DO concentration of the solution is shown in Figure 17. Over the 24-hour reaction period, the solutions with a higher concentration of Na_2SO_3 became paler, compared to the control and solution where the air was bubbled into. Both of the latter conditions remained dark blue in colour. This indicates that a larger presence of the oxygen scavenger Na_2SO_3 led to a lower concentration of oxygen, therefore, resulting in a greater reduction of MB in the solution. These findings aligned with the expected redox chemical reactions of methylene blue, classically demonstrated in what is called the Blue Bottle Test where MB undergoes a colour change from blue to colourless when it is reduced [116]. In the characterization experiment, the solutions with higher concentrations of Na_2SO_3 were expected to be paler due to the reduction of MB by the sulphite reducing agent [117].

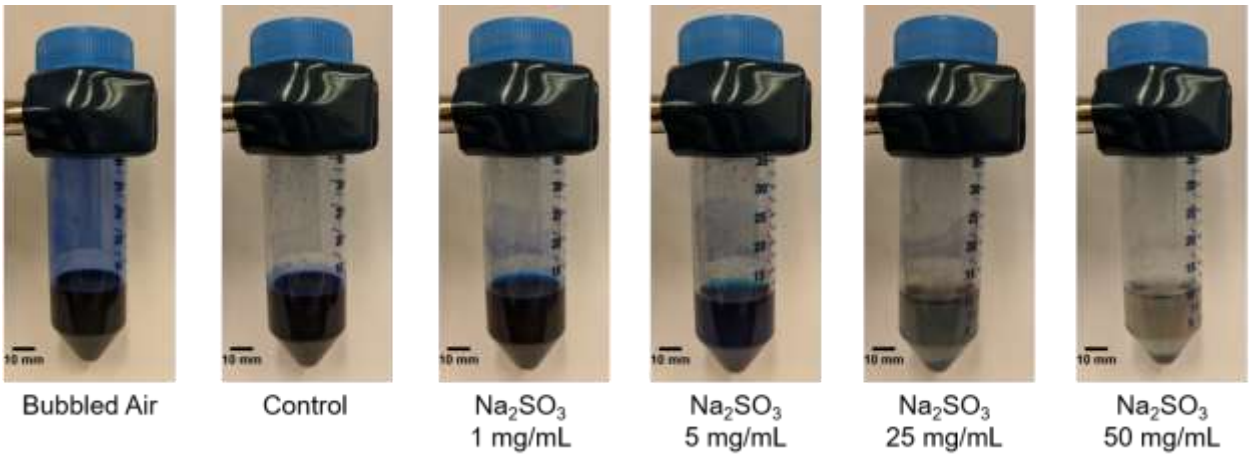

Figure 17: Relationship between the colouration state of Methylene Blue and DO concentration. Images of the varying conditions: air bubbled into solution for 1 minute, control, [1 mg/mL] Na2SO3, [5 mg/mL] Na2SO3, [25 mg/mL] Na2SO3, and [50 mg/mL] Na2SO3. n=3 for each

To confirm the level of oxygen in each condition, a commercial DO sensor was used. The DO concentrations of each condition were measured as the following: Bubbled O_2 air, 3.44 mg/mL; Control solution, 3.41 mg/mL; Na_2SO_3 [1 mg/mL], 2.32 mg/mL; Na_2SO_3 [5 mg/mL], 1.08 mg/mL; Na_2SO_3 [25 mg/mL], 0.59 mg/mL; Na_2SO_3 [50 mg/mL], 0.45 mg/mL (Table 5). The

decrease in DO concentration was expected due to the ability of Na_2SO_3 to remove the oxygen from the solution to form sodium sulphate [118].

Table 5: Measured DO concentrations of the various test conditions as measured with the Exstik II commercial sensor

Condition	[DO] (mg/mL)
Bubbled Air	3.44
Control	3.41
Na_2SO_3 1 mg/mL	2.32
Na_2SO_3 5 mg/mL	1.08
Na_2SO_3 25 mg/mL	0.59
Na_2SO_3 50 mg/mL	0.45

The colour saturation or intensity of the paler solutions matched with the lower DO concentration readings obtained from the commercial sensor. The change in colour, as measured via the extracted mean gray value (MGV) from the image, was inversely proportional to the DO concentration (Figure 18). However, the sample that was bubbled with air remained at a similar saturation level and colour to the control. The tubes in which air was bubbled should have been more saturated, becoming a darker blue colour. The similarity between the two conditions is likely due to being in equilibrium with the air, which is why bubbling more air into the solution did not cause a change or that an insufficient amount of air bubbled into the solution to significantly increase the dissolved oxygen content. Despite the difference in the DO concentrations of the control tube, Na_2SO_3 [1 mg/mL] and Na_2SO_3 [5 mg/mL], the MGV are all approximately the same. This could indicate that the sensitivity of MB as a DO sensor is limited to a DO concentration of 0-1 mg/L.

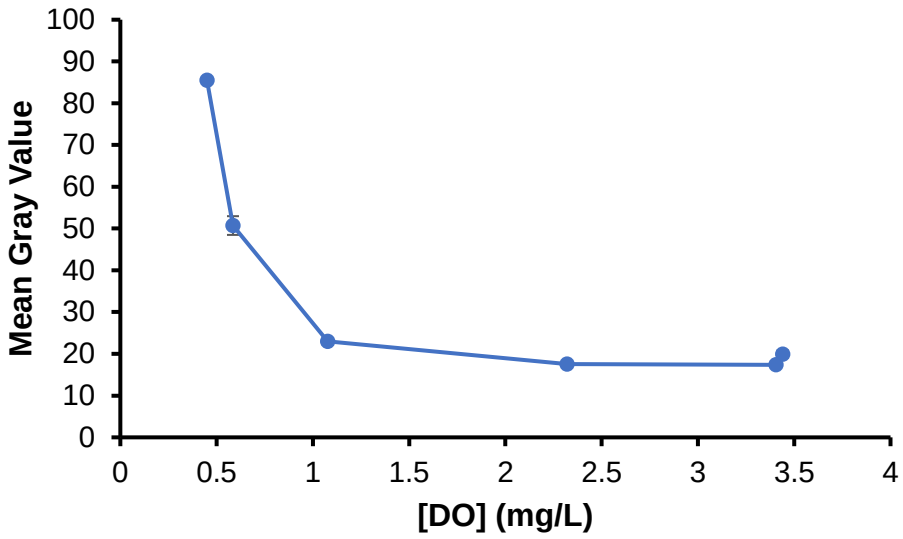

Figure 18: Inverse relationship between the concentration of DO and the extracted mean gray value when using MB as the optical indicator. Data shown as mean ± SEM.

The various Na_2SO_3 concentrations along with the control and bubbled air conditions, therefore, provide an inverse relationship between the intensity and DO concentration. When the solution is blue, there is a higher oxygen concentration than when the solution is colourless. In summary, blue solutions were confirmed as having a higher dissolved oxygen concentration and a lower MGV, whereas clear solutions contained low DO levels and a higher MGV. This relationship will be the basis to determine the oxygen concentration within the wells of the Rapid Culture Nanowell Device.

4.1.2 Effect of metabolism on Methylene Blue saturation

In order to determine if the oxygen consumption by bacteria can be detected with MB as the reported dye, the effect of metabolism was explored by testing the biological removal of oxygen through a large concentration of *Escherichia coli* K12 MG1655 (10^8 CFU/mL) and compared to Na_2SO_3 (Figure 19). The goal was to identify the quantitative end-point of a fully reduced MB solution in a smaller volume than what was tested in the prior characterization test.

Four conditions were tested: 1. LB media, 2. MB+LB media control, 3. MB+Na_2SO_3 [5 mg/mL], and 4. MB+*E. coli* [10^8 CFU/mL]. LB media was the control for the expected end-point reduced colouration and MB+LB tube allowed for comparison to the oxidized state. An MB concentration of 2.5 mg/mL was tested. Eppendorf tubes were used due to their small volume requirement of a 1.5 mL. After 24-hours, the tubes were agitated to mix the distinct layers, creating a homogenous colour throughout (Figure 19.C). Refer to methods section for complete experimental protocol and set-up.

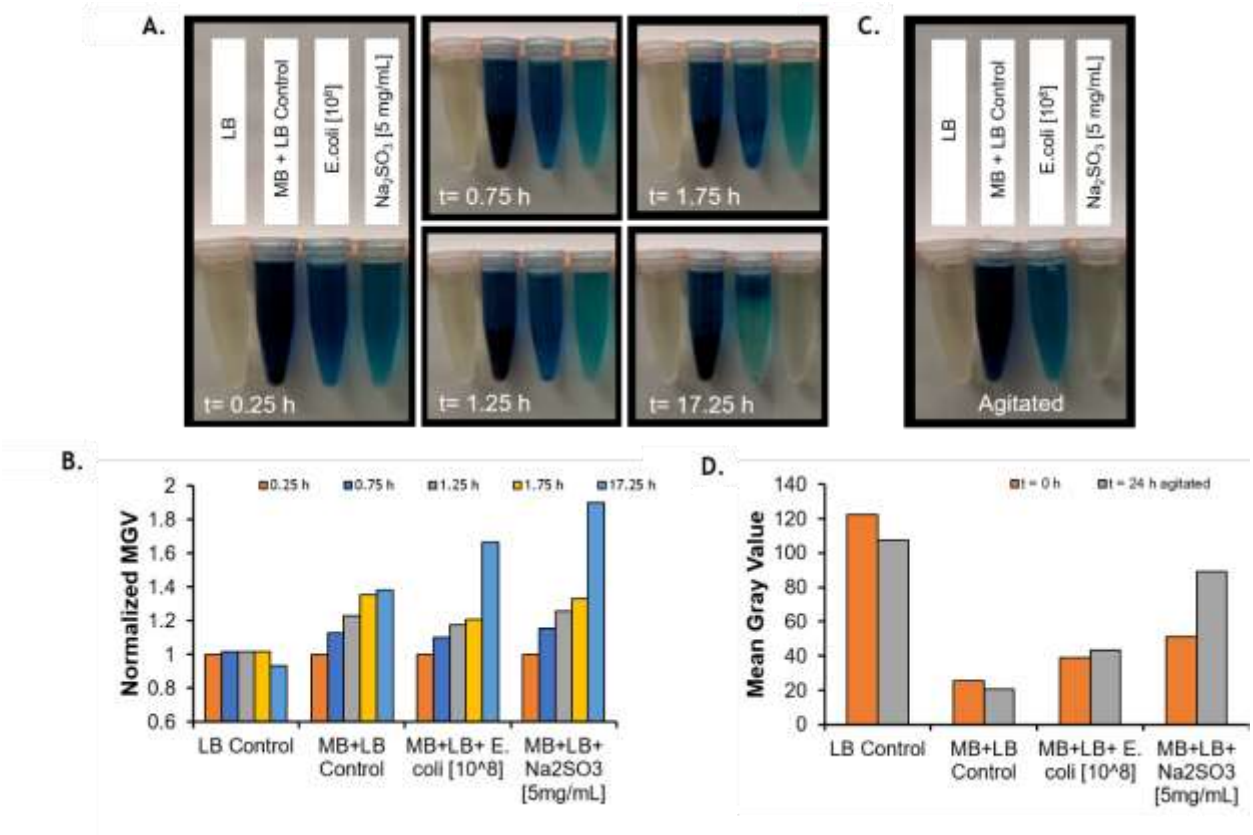

Figure 19: The effect of chemical and biological metabolism on MB colouration in Eppendorf Tubes. A.) Progression of images taken over a 17-hour period comparing the colour change of MB in the presence *E. coli* K12 MG1655 [10^8 CFU/mL] and Na_2S0_3 at 5 mg/mL. B.) Normalized MGV extracted from the images over the imaging period. C.) Effect of agitating the tubes on the saturation of MB indicator. The separate layers in the MB+LB control and *E. coli* tubes disappear, resulting in a homogenous darker colour and D.) MGV.

Over the imaging period, the LB control tubes showed a slightly decreasing intensity trend compared to the MB+LB control, Na_2SO_3, and *E. coli* tubes, which all increased (Figure 19.A-B). The MGV of the LB control was between 114.0 – 124.6 units throughout this time period, a decrease of 6%. The slight variance could be due to interference from ambient light or variable brightness of the captured images by the cell phone camera. A tube containing only LB media should not change colour over a span of 17-hours. The effect of the imaging system in collecting and analyzing the colouration of MB will be studied in a later section of this thesis. The MB+LB control tube, however, was initially measured to be 25.6 MGV units, increasing +38% to 35.4 units by the end of the imaging period. The unexpected increase in MGV could be explained by the layer of MB precipitate at the bottom of the tube. Once the tube was agitated, the MGV was measured to be 20.7 units, which was closer to its initial value. It was expected that the MGV of the MB+LB control would remain constant without a biological or chemical method of removing oxygen in the system.

The Na_2SO_3 tubes were initially measured to be 51.3 MGV units. These tubes were paler than the others due to the quick removal of oxygen. Over time, the MGV increased by 89.9% to 97.4 units. These tubes were colourless at t=17 hours. This was expected as all the oxygen would bond to the Na_2SO_3, removing it from the solution and reducing MB. The chemical removal of oxygen resulted in a colourless solution, whereas the tube with bacteria remained blue. The tube with bacteria was initially measured to have an MGV of 38.9 units. Over time, the MGV increased to 64.8 units (+66.4%). Compared to the MB+LB control at 35.4 MGV units, the bacteria tube was paler in colour. The expectation was that both chemical and biological means of oxygen removal would lead to a colourless MB_{red} state. Based on the final colouration of the bacteria tube, the bacteria were not as effective in completely reducing the MB within the solution as Na_2SO_3 within

24 hours. A potential explanation could be due to an unequal distribution of bacteria within the high aspect container. Support for this hypothesis comes from the gradation in colour observed in bacterial tubes. The tips of the tubes were lighter than the upper portion. This phenomenon seems to be explained by the settling of bacteria near the bottom of the tube due to gravity. The area of great bacterial accumulation was lighter in colour, therefore more MB was converted to its leucomethylene blue state. A well with a lower aspect ratio may be ideal in obtaining a homogenous and equal metabolism of MB via bacteria. Another possibility could be that more time is required for the bacteria to reduce the MB at the same rate as the chemical oxygen scavenger. The method of reduction differs such that it is believed a specific reductase enzyme located on the membrane of the bacteria is responsible for reducing MB [74], [75]. The specific kinetics of this enzyme needs to be further studied, but it is out of scope for this particular thesis.

Based on these results, the MGV of the colourless tubes were measured to be between 90-120+ units and the coloured tubes had a value between 20-90 units. Specifically, the lower the value within this latter range, the darker the shade of blue. Subsequently, the opposite held true – the higher the MGV in the blue range was visualized as a lighter shade of blue. The inverse relationship between DO concentration and MGV that was explored in section 4.1.1 was still observed, even with the smaller volume. Therefore, the use of MB as an indicator for bacterial metabolism may be an ideal complement to the revised nanowell device design with the caveat that the final colourless state may not be achieved within a period of 24 hours.

4.2 Colour change of MB in PDMS nanowell

To determine if MB could be used as an indirect indicator of bacterial metabolism, a colour change must be visualized and detectable when in the nanowell PDMS device. Na_2SO_3 at a concentration of 15 mg/mL was used to quickly remove the oxygen in the solution. MB at a

concentration of 2.5 mg/mL was used to fill the 3D fabricated PDMS nanowells, as per the Methods section. Images of the device were taken both with the Google Pixel 2 and the Olympus microscope. After 24 hours, a visible difference in colour was seen between the MB+LB control and MB+LB+ Na_2SO_3 device (Figure 20). This was quantified as an average MGV of 139.51 ± 1.55 units for the control wells and 150.86 ± 6.55 units for the Na_2SO_3 wells, a difference of 8%. Therefore, the colour change of MB in the absence of oxygen could be detected within the PDMS nanowell device.

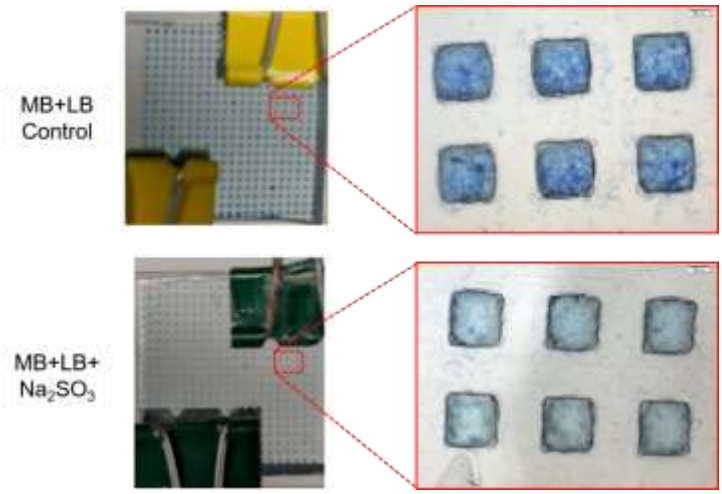

Figure 20: MB colour change due to chemical oxygen removal when loaded into PDMS nanowell device.

4.3 Effect of the Method of Mould Fabrication on the effectiveness of MB as an optical sensor within the re-designed Rapid Culture Nanowell Device

Based on the design criteria discussed prior, the individual well size of the original Rapid Culture Nanowell Device needed to be increased to process larger quantities of test samples at one time [90]. The dimension of 500x500x500 µm was chosen to better accommodate a total device volume of 1 mL compared to the original 100x100x100 µm design [119]. In order to achieve this

size, the mould fabrication via 3D printing was explored, as an alternative to photolithography. A 3D printed 500x500x500 µm nanowell mould was compared to a photolithography 500x500x300 µm nanowell mould. Both moulds were treated with silane (SiH_4) post-processing to allow for easier release of the casted device. PDMS, the polymer of choice for this microfluidic device, was poured into each of the moulds and prepared following the protocol in Chapter 3. Devices were filled with MB (2.5 mg/mL) mixed with LB media and imaged with the Inverted Olympus Fluorescence Microscope at t=1 and 24 hours (Figure 21). All devices were sealed with PCR adhesive tape and sandwiched between microscope slides to ensure a firm sealing. For each fabrication method, devices were tested with bacteria (*E. coli* K12 MG1655 at 10^8 CFU/mL) and without bacteria (control). The images were later analyzed with ImageJ to quantify the change in MGV within each individual sealed well as per the methods outlined in Chapter 3.

A clear difference in the texture of each well was observed between the two fabrication methods. Images of the lithography devices under the microscope showed smoother and more precise well walls compared to the 3D print devices. However, it was difficult to visually identify a detectable difference in the colours of each well between the two fabrication methods. Using ImageJ analysis, the lithographically fabricated wells containing bacteria showed a significantly ($p<0.0001$) higher normalized MGV at t=24 hours (1.02 ± 0.01 units) compared to the 3D-print fabricated wells containing bacteria (0.86 ± 0.02 units) (Figure 21.A). Similarly, the lithographically fabricated control wells without bacteria at 24 hours had a higher normalized MGV of 0.91 ± 0.01 compared to the 3D-printed fabricated wells at 0.80 ± 0.02 units (Figure 21.B). These differences are also significant ($p<0.0001$). When comparing the wells inoculated with *E. coli* bacteria to the sterile controls, the photolithography wells showed a 10.9% change in 24 hours compared to the 6.4% change in 3D printed wells.

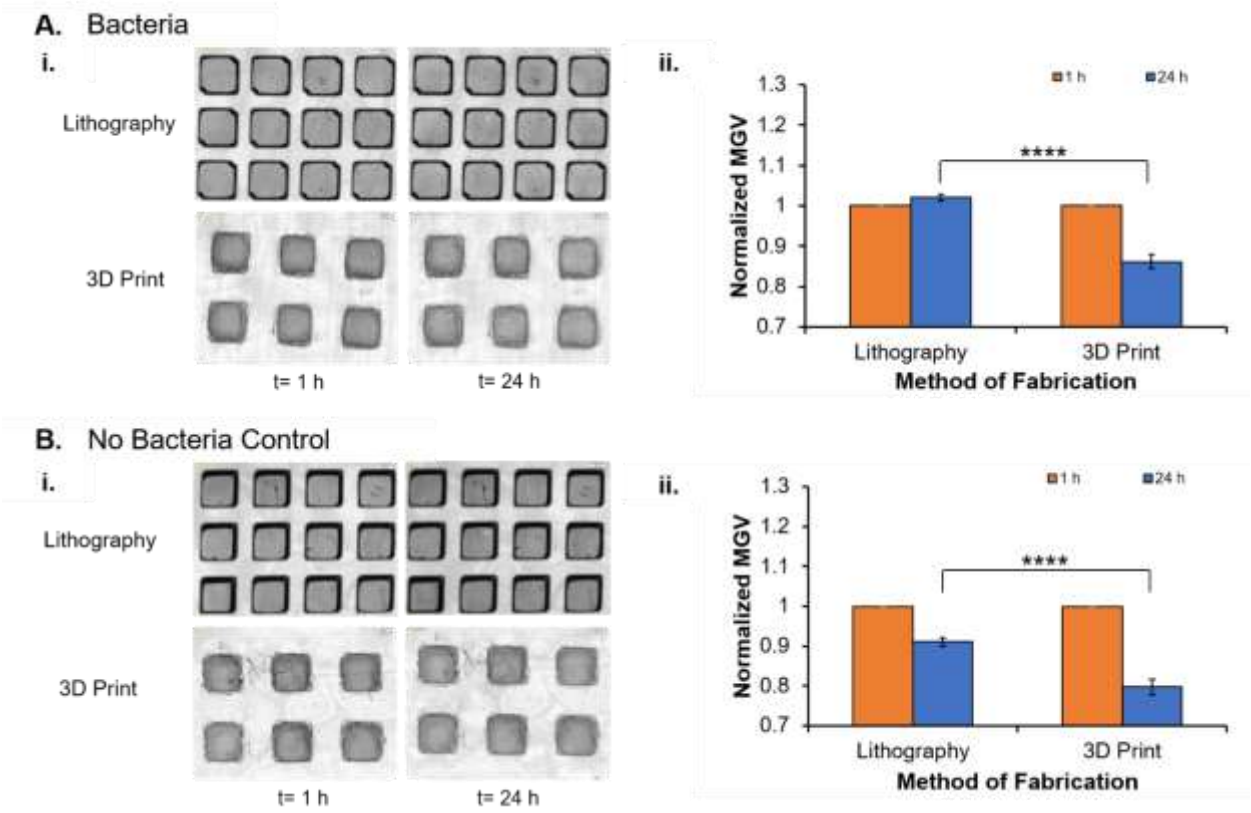

Figure 21: Comparison of methods for nanowell mould fabrication and its effects on the use of MB as an optical indicator within the rapid culture detection device. Photolithography (n=24) and 3D printed (n=12) fabricated moulds were tested to determine if the type of fabrication method impacts the time required to detect a change in oxygen concentration. Fabrication methods were contrasted when A.) inoculated with 10^8 CFU/mL bacteria and B.) without bacteria as a control. Lithography wells showed a significantly higher normalized MGV at t=24 hours ($p<0.0001$) than the 3D print wells in both bacteria and control devices. Data shown as mean ± SEM.

Based on prior characterization studies, a lower MGV reading indicated a more saturated colour which contained more MB_{ox}, and, therefore, was indicative of a higher [DO]. The lower normalized MGV of the 3D print wells compared to the photolithography wells could, therefore, indicate a greater [DO] concentration. In the presence of bacteria, the normalized MGV should continually increase due to the consumption of oxygen within the well via bacterial metabolic functions. Therefore, the observed lower normalized MGV could indicate that the seal of the device had been compromised, allowing external air to diffuse into the well, and affecting the

solution's colouration. This hypothesis is also supported by the lower normalized MGV of the sterile control devices. When there are no bacteria present, a decrease in normalized MGV is expected due to the permeability of oxygen in PDMS (diffusion coefficient of $D_{PDMS} = 3.25\text{x}10^{-9}$ m^2/s) and the gaseous equilibrium phenomenon as per Fick's law, which states that the flux will travel from regions of high concentration to regions of low concentration [120]. The concentration of oxygen available in atmospheric air will permeate through the PDMS and diffuse into the nanowell to reach equilibrium. However, the decrease in 3D printed wells was 4.5% more than the photolithography ones. Therefore, the method of fabrication impacted the degree of indicator colour change due to the surface roughness within 24 hours. The photolithographic mould for the nanowell device was used with MB to detect the bacterial presence in the following experiments.

4.4 Development of Imaging Set-up

The key to detecting the colour change of MB as an indicator of metabolism within the nanowell device lay in the development of an imaging set-up that would be able to track the device as a whole, be accurate, affordable, and control for variances in optic noise. As part of the proof of concept to test the viability of MB as an optical indicator for metabolism, the Tecan M200 Infinite Pro Plate Reader was used to determine a baseline to compare alternative imaging systems. Despite the accuracy of the Tecan M200, it is limited by its ability to only provide a single point measurement. Therefore, three optical capture systems: a microscope, cell phone camera, and DSLR-Macroscope system, were explored to determine the ideal platform for imaging the future MB characterizations in micro- and nanowells.

4.4.1 Exploration of imaging modalities for MB characterization in microwells

To develop the ideal imaging set-up for the characterization of MB as an optical indicator in microwells, the image taking capabilities and environments of the Olympus Inverted Bright Field and Fluorescence Microscope (Model IX51S1F-3), Google Pixel 2 camera, and the Nikon D810 DSLR camera were compared. The microscope was operated in the Biointerfaces Institute (BI) facility at McMaster University. Images taken with the cell phone camera were taken in the open lab space of the BI facility's Bacterial Suite. Finally, the DSLR-camera was mounted within the dark box system as described in Chapter 3. A 96-microwell plate was filled with a 2.5 mg/mL MB and LB media solution and imaged with the three different modalities and their respective systems (Figure 22).

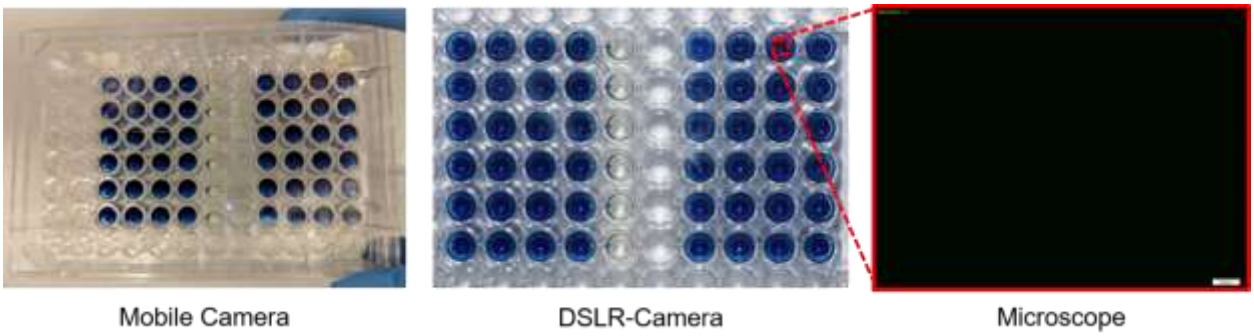

Figure 22: Images taken of a microwell plate to compare imaging modalities of cell phone camera (Google Pixel 2), DSLR camera (Nikon D810), and microscope (Olympus Inverted Microscope). Microscope images were taken with the lowest objective lens (4x) and a monochrome camera.

Compared to the other imaging systems, the DSLR-Macroscope system was able to take clear images of the full microwell plate with minimal reflection interference from external sources. Having a large area of focus allows for the ease of monitoring multiple wells at a glance and efficiency in the analysis of wells. This system also has the added benefit of an automated computerized interface which would be able to take time-lapse images over a specified time period. Development of this system could be well-suited to the use in Donor Milk Bank facilities in

developed nations. The cell phone camera was also able to capture the full 96-well plate, however, its advantageous flexibility and spontaneity in being able to take a quick picture in any environment is also its detriment as the changing light environment and reflections impact the ability to collect accurate baseline data. Although the cell phone camera is our ultimate goal in user accessibility and usability in areas that require an affordable imaging system, it is not an adequate system to be used in the initial characterization and baseline tests for our updated device design. Lastly, the microscope was limited to imaging one microwell at a time, as compared to the other two systems. Having to manually position each individual well in large assays would be an inefficient task and hinder the parallelization of high-throughput monitoring. This system would not be ideal in observing behaviours in the micro-scale or larger due to its magnification limit. However, it could be promising for smaller systems, particularly individual nanowells. Table 6 summarizes the advantages and disadvantages of each of the imaging modalities. In conclusion, of the three imaging systems explored, future experiments for the characterization of MB will be conducted using the DSLR-Macroscope system. This will provide a better baseline measure of the usability of the DSLR-Macroscope due to its capability of capturing higher quality and greater resolution images compared to the cell phone camera.

Table 6: Comparison of imaging methods to be used in future characterizations of the Rapid Culture Device

Imaging Method	Advantages	Disadvantages
Microscope	- Highly accurate and reliable - Versatile due to various available filters: i.e. FITC to image for *E. coli* GFP growth, brightfield for overall MB colour saturation - Ability to track individual bacterium within each well - Provides quantitative and qualitative result	- Magnification scale too large, requiring manual manipulation to image whole device - Cannot monitor all parts of microarray in parallel - Difficult to automatized - Expensive - Requires training to use
Tecan Plate Reader	- Accurate and reliable - Versatile due to measuring absorbance and fluoresce: i.e. Ability to track absorbance of MB and GFP signal of *E. coli* growth	- Quantitative value can only be provided - Expensive - Requires training to use
DSLR Camera System	- High imaging quality - Higher resolution than mobile cameras & larger sensors - Able to image the full device quickly and fully - Allow for parallelization of imaging large arrays - Provides quantitative and qualitative result - Cheaper alternative than microscope and plate reader - Easy to use	- New system that has not been widely proven to be accurate and beneficial in scientific studies - More expensive than certain mobile cameras
Mobile camera	- High imaging quality - Allow for parallelization of imaging large arrays - Provides quantitative and qualitative result - Affordable system due to wide availability - Easy to use	- Quality is not as good as DSLR due to smaller sensor (also variance in model of phone & associated camera) - Lack of an environment that would control for variability in light pollution in sub-optimal conditions

4.4.2 Comparison of DSLR-Macroscope system to Tecan Plate Reader system

To test the accuracy of the DSLR-camera imaging set-up, microwells in a 96-plate were imaged with both the Tecan Plate Reader and the DSLR-Macroscope system over a 24-hour period. Solutions of 2.5 mg/mL MB were mixed into LB media. Wells containing bacteria were inoculated with 10^8 CFU/mL of *E. coli*. Microwells were read by the Plate reader once every for 24 hours at an absorbance wavelength of 668 nm. With the DSLR-Macroscope system, an image was taken every half an hour for 24 hours. Refer to methods section for complete experimental protocol and set-up. The point at which the bacterial wells changed colour compared to the control MB+LB media wells should be similar with both systems.

As shown in Figure 23, the point at which the bacterial wells were significantly different from the MB+LB controls was at 8 hours with an absorbance measurement of 3.85 ± 0.02 units compared to the control absorbance of 3.96 ± 0.01 units ($p<0.0001$). After this point, the trend for the inoculated wells continues to decrease by 80% to 0.77 ± 0.02 absorbance units at 24 hours. This result was as expected since the presence of bacteria should reduce the concentration of MB present, thereby increasing the amount of transmitted light that reached the light detector. The MB+LB control wells remained steady at 3.9 units. The LB and empty well controls remain constant at around an absorbance value of 0 throughout the imaging period and were significantly different from both MB+LB and MB+LB+bacteria wells ($p<0.0001$). This was expected as no MB was available to be excited by the light source at the specified wavelength.

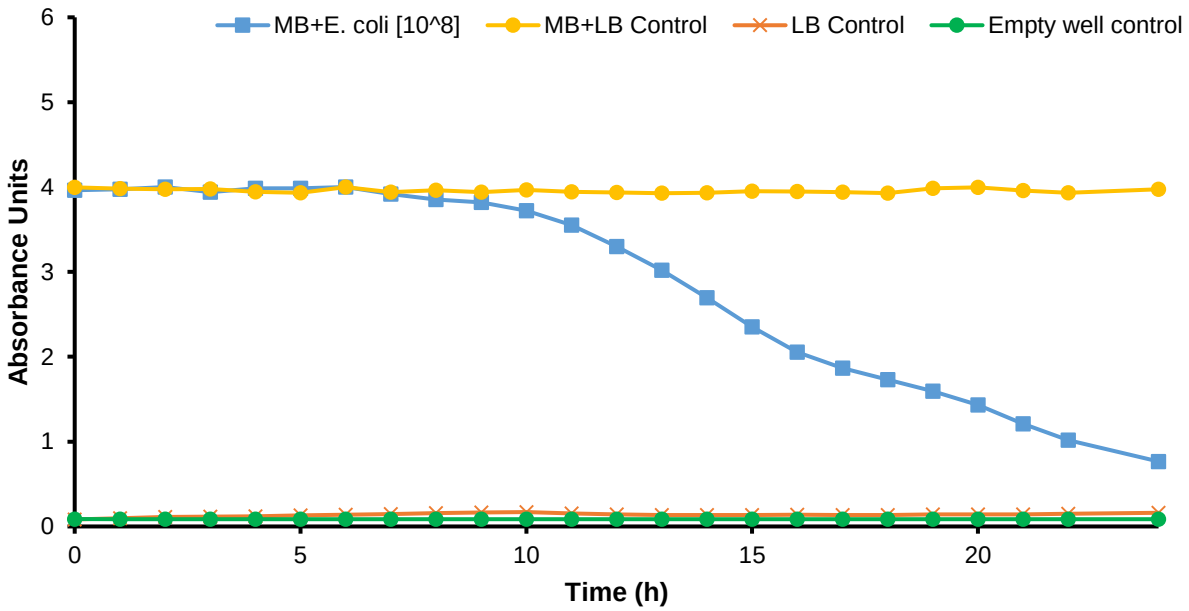

Figure 23: Time lapse of MB indicator with *E. coli* bacteria in wells using Tecan Plate Reader to measure the absorbance (λ=668 nm) change over 24 hours. Concentration of [10^8 CFU/mL] (n=6) were compared to control measurements of empty wells (n=6), LB only wells (n=6), and MB+LB wells (n=12). Difference in bacteria and MB+LB wells were significant ($p<0.0001$) after 8 hours, and significant at all time points when compared to LB and empty well controls. Data shown as mean ± SEM.

In comparison, the DSLR system showed that it detected a significant difference between inoculated and control wells starting at 7.5 hours ($p<0.0001$) (Figure 24). The average of the normalized MGV of *E. coli* wells was 1.02 ± 0.01 units compared to the control (0.95 ± 0.01 units). After this point in time, the normalized MGV trend in bacterial wells continues to increase by 160% to 2.60 ± 0.05 normalized MGV units at t=24 hours. All of the controls (empty well, LB media, and MB+LB control) remained around the normalized value of 1 (1.00 ± 0.01 units, 1.03 ± 0.01 units, and 0.93 ± 0.01 units, respectively). A comparison of the two different imaging systems confirmed that the DSLR-Macroscope system was a viable and reliable means to characterize the use of MB as an optical indicator for bacterial presence in microwell volumes.

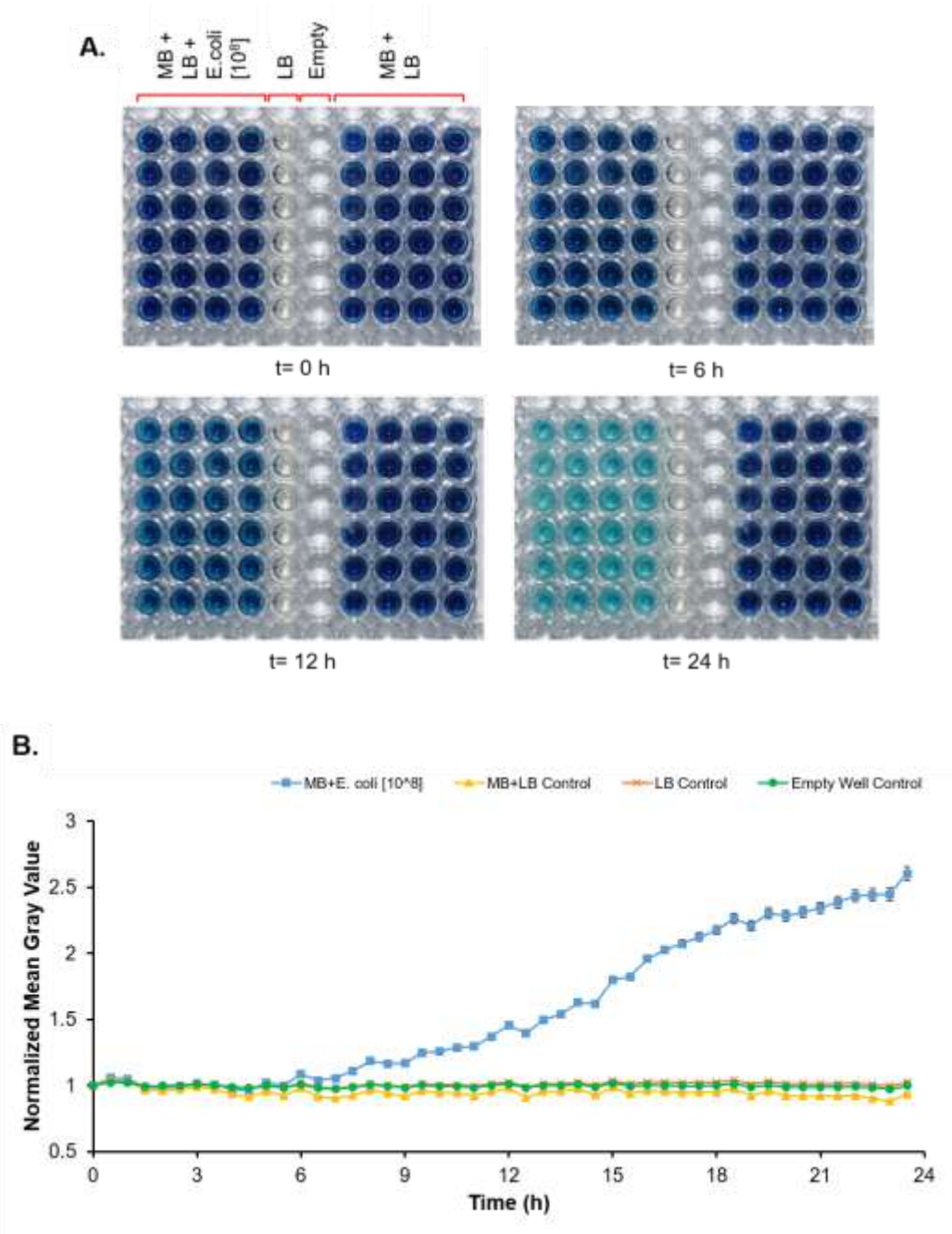

Figure 24: A.) Select images taken with the DSLR-Macroscope system of the effect of *E. coli* bacteria on the MB indicator colour change over 24 hours. Concentrations of [10^8 CFU/mL] (n=24) were compared to control measurements of empty wells (n=6), LB only wells (n=6), and MB+LB wells (n=24). B.) Normalized MGV were extracted to determine that bacteria could be differentiated from MB+LB wells after 5 hours ($p<0.0001$). Differences with LB and Empty well controls were also significant ($p<0.01$). Data shown as mean ± SEM.

4.4.2 Exploration of imaging modalities for MB characterization in nanowells

When imaging the nanowell devices, it was imperative to develop a data collection system for each individual well within the device. To test if the DSLR-Macroscope was transferable in imaging the nanowell devices, a comparison was conducted between it and the Olympus Inverted Bright Field and Fluorescence Microscope. PDMS devices made from the photolithography mould were imaged with both systems and compared in Figure 25.

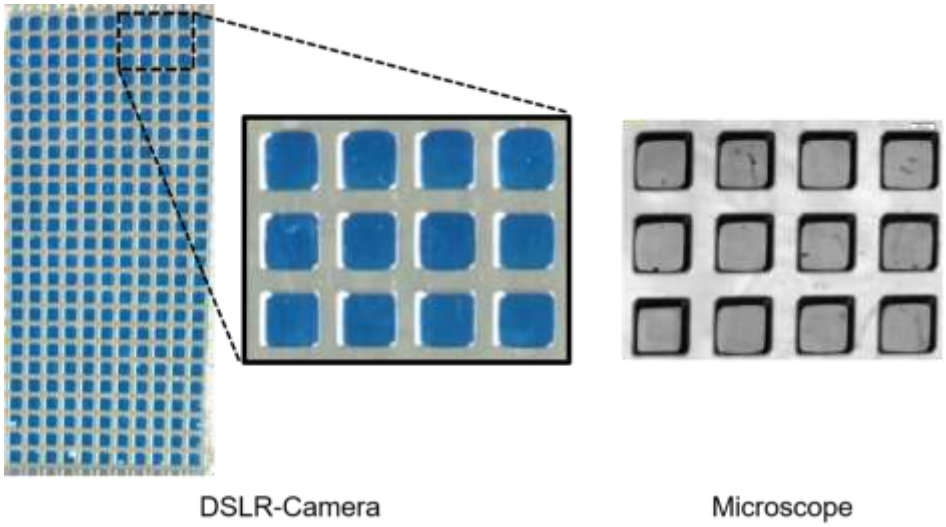

Figure 25: Comparison of the DSLR-Macroscope camera system and the microscope in their ability to image the nanowells filled with MB within the redesigned Rapid Culture Nanowell Device.

Both imaging systems allowed for clear imaging of the individual nanowells when filled with methylene blue. However, the DSLR-Macroscope was able to capture more than 12 wells at a time compared to the microscope. As for the microscope, under the lowest objective lens (4x), only 12 nanowells could be observed at any one point of time. In comparison, a device containing 275 wells can be easily imaged at one time when using the DSLR camera. Additionally, the resolution of the Nikon D810 delivers a high-quality image when the photo was zoomed to focus

match the as seen through the microscope. Therefore, the DSLR-Macroscope proved to be the ideal imaging platform for the nanowell device.

4.5 Characterization of MB as optical metabolic indicator in microwells

4.5.1 Effect of MB quality on rate of MB colour change

Before the hypothesis that the nanowell device can detect bacterial presence with MB as the optical indicator of choice faster than the microwell liquid culture, the baseline for detection in microwells must first be characterized. To determine if the quality of the MB would impact the rate of colour change, an experiment was conducted to compare newly purchased stock of MB powder in June 2018 with MB that was purchased prior to 2015. *E. coli* at 10^8 CFU/mL were added to solutions of MB [2.5 mg/mL] and LB media. This solution was added into microwells of 300 µL volumes and imaged with the DSLR-Macroscope as per the to imaging protocol in the methods section. A visual comparison of the two states of MB at t=0, 12 and 24 hours are presented in Figure 26.

Visual observation of the images taken of the two conditions showed that the bacteria wells mixed with old MB became paler at a faster rate when compared to the wells stained with new MB over time. Figure 27 shows the MGV that was extracted from the time-lapse images taken every hour for 24 hours. The old MB resulted in wells with a consistently higher MGV (range of 48.6 ± 1.3 – 124.9 ± 1.3 units) than the new MB samples (range of 20.1 ± 1.2 – 48.7 ± 1.9 units). The lesser saturation could be explained by the degradation of the old MB caused by prolonged light due to improper storage methods [121]. This indicates that the older MB is more sensitive than the newer MB. However, the overall change in colour was similar between the two samples of MB after 24-hours (Figure 28). This suggests that despite being less sensitive, the new MB was still capable of measuring the same overall colour change due to bacterial metabolism.

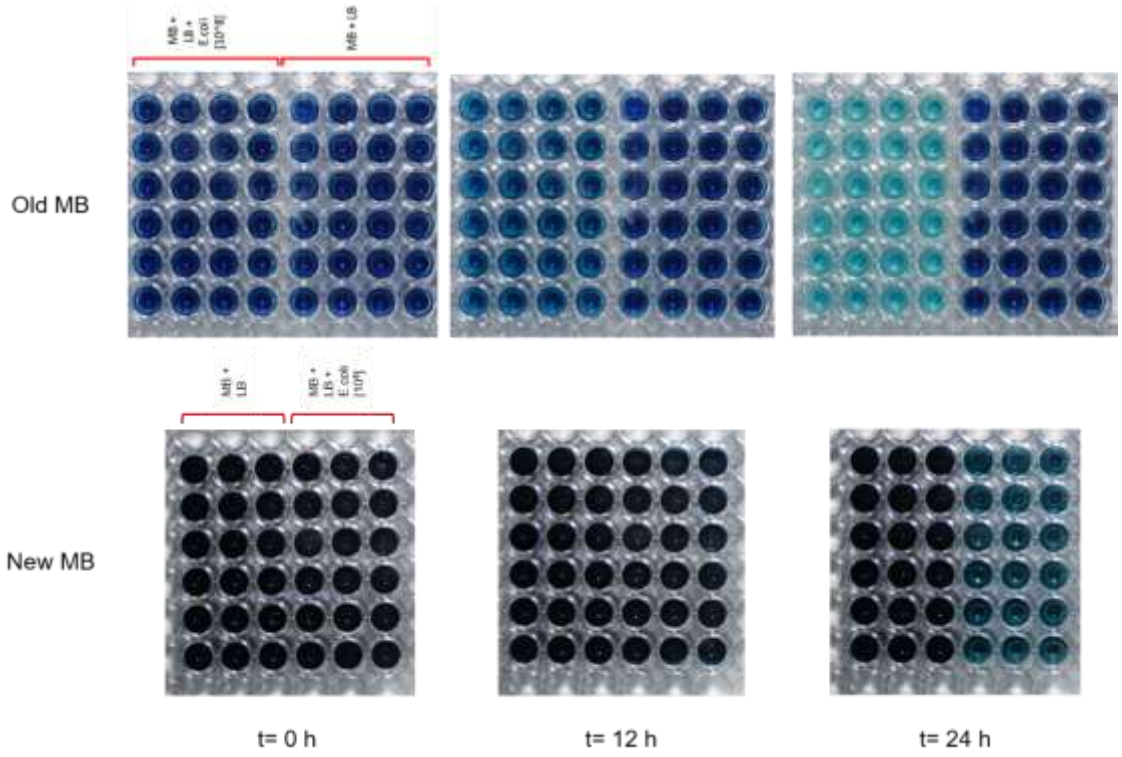

Figure 26: Comparison of rate of colour change between fresh and older stock of MB when in the presence of bacteria.

A similar trend was also noticed with the wells where no bacteria were added. The normalized rate of colour change was similar despite the old MB being paler with an MGV between 40-60 units compared to the new MB at 10-15 MGV units. This indicates that the new MB presented as a more saturated blue colour than the new MB. When the MGVs were normalized, the rate of colour change was also similar between the two samples. Therefore, to maintain an accurate characterization of the rate for MB metabolic colour change, the normalized data should be used to determine the point of colour change instead of the raw MGVs. Despite the increased sensitivity to reduction by bacteria, fresh MB had to be used in the future experiments due to its availability and for repeatability.

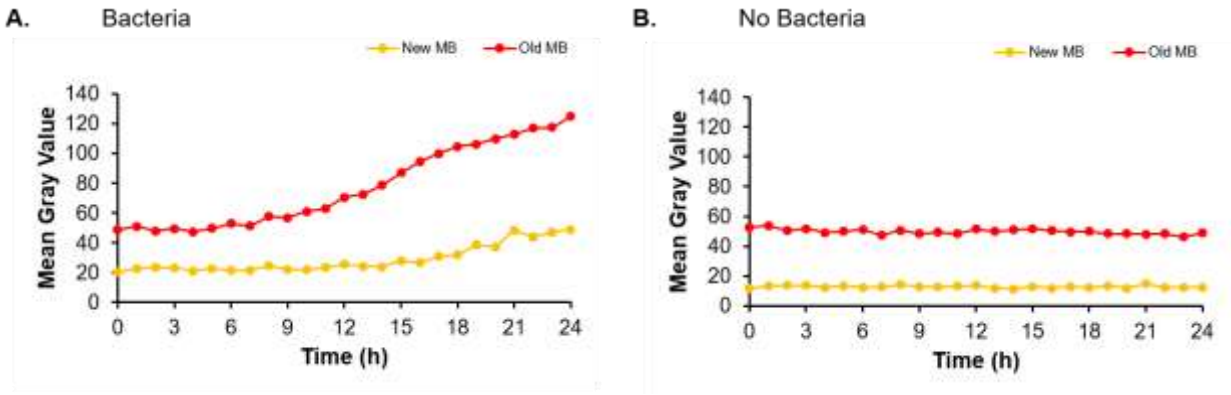

Figure 27: Effect of MB freshness on rate of MB colour change due to metabolism. MGV were extracted from time-lapse images taken every hour for 24- hours. A.) Comparison of bacteria inoculated Old MB (n=24) and New MB (n=18) samples. B.) Comparison of Old MB (n=24) and New MB (n=24) samples without bacteria. The MGV of new MB samples were lower than that of the old MB, therefore indicating a darker blue colour. The steeper slope of the old MB bacteria samples also indicated a faster rate of colour change compared to the new MB. Data shown as mean ± SEM.

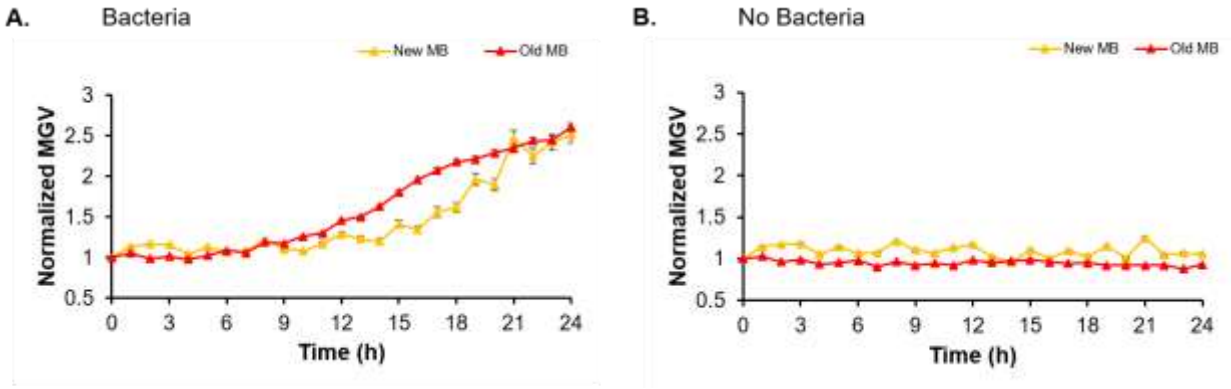

Figure 28: Normalized mean gray value of the colour change of the new and old MB. A.) Comparison of bacteria inoculated Old MB (n=24) and New MB (n=18) samples. B.) Comparison of Old MB (n=24) and New MB (n=24) samples without bacteria. Data shown as mean ± SEM.

4.5.2 Effect of MB concentration on rate of change in MB saturation

To determine the effect of MB concentration on the rate of change in MB saturation, bacteria were added to wells with 2.5 mg/mL and 1.0 mg/mL as the concentration of MB. This characterization is important in order to find the optimal concentration for rapid detection of the bacterial presence, as the change in saturation indirectly measures bacterial metabolism. For both

concentrations of MB, *E. coli* at a concentration of 10^8 CFU/mL were tested as the method of reduction. The experiment was repeated in triplicate and imaged with the DSLR-Macroscope system. Images at t=0, 12, and 24 hours for both MB concentrations are observed in Figure 29.

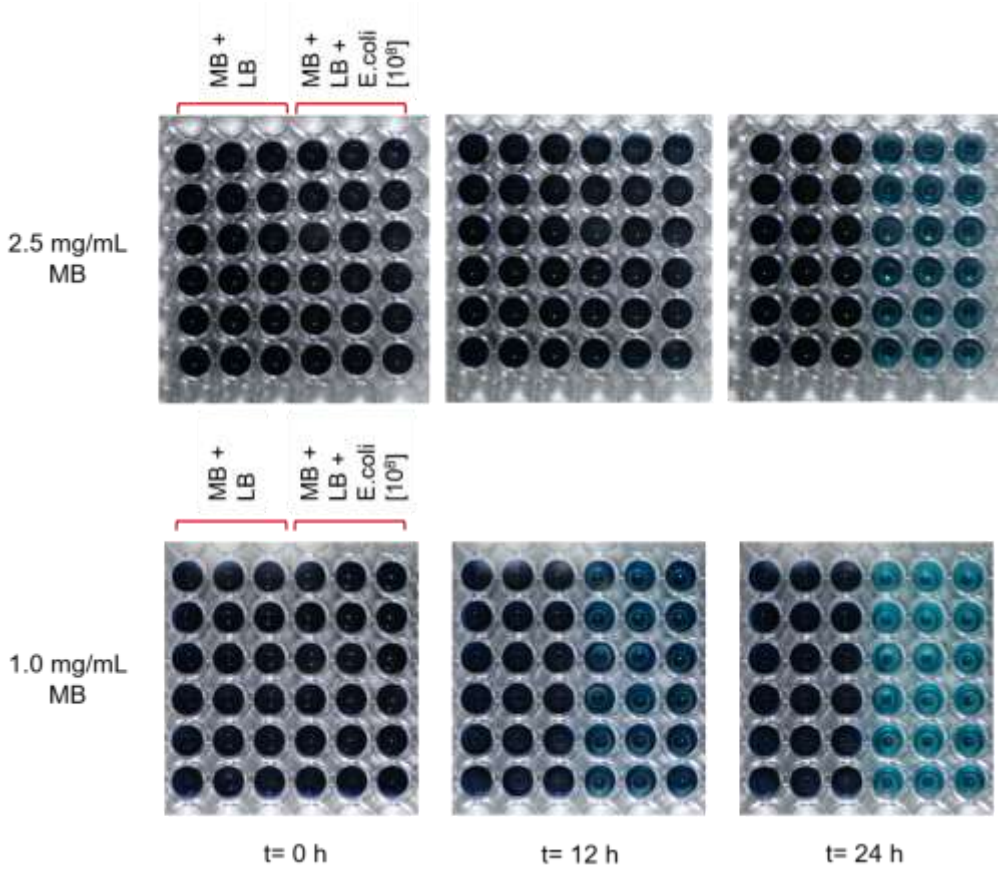

Figure 29: Effect of MB concentration on rate of colour change over a 24-hour period. Reduction via *E. coli* [10^8 CFU/mL] metabolism was tracked in both concentrations. n=18 for each condition.

When comparing the chosen two concentrations, the time at which wells with bacteria could be significantly differentiated from those without was faster in 1.0 mg/mL than in 2.5 mg/mL concentration. The rate of the colour change of the 1.0 mg/mL concentration increases at 10 hours ($p<0.0001$) (Figure 30.A) compared to the 13 hours ($p<0.01$) (Figure 30.B) for the higher concentration. At 24 hours, the MGV of 1.0 mg/mL MB is 261% higher than the initial reading (21.4 ± 1.0 units) to a final value of 77.2 ± 1.3 units. This percent change can be compared to the

143% change from 20.1 ± 1.2 units to 44.8 ± 1.9 units for 2.5 mg/mL MB. This is expected since the bacteria would be able to reduce a smaller amount of MB faster than a larger amount, resulting in a sooner change in colour. When analyzing the wells without bacteria, no significant difference was detected between the two concentrations. Both concentrations remained constant at a normalized value of approximately 1 unit throughout, as expected (Figure 30.A-B). Based on the faster rate of MB metabolism in the lesser concentration of 1.0 mg/mL, this concentration was used within the nanowells to quicken detect bacterial presence.

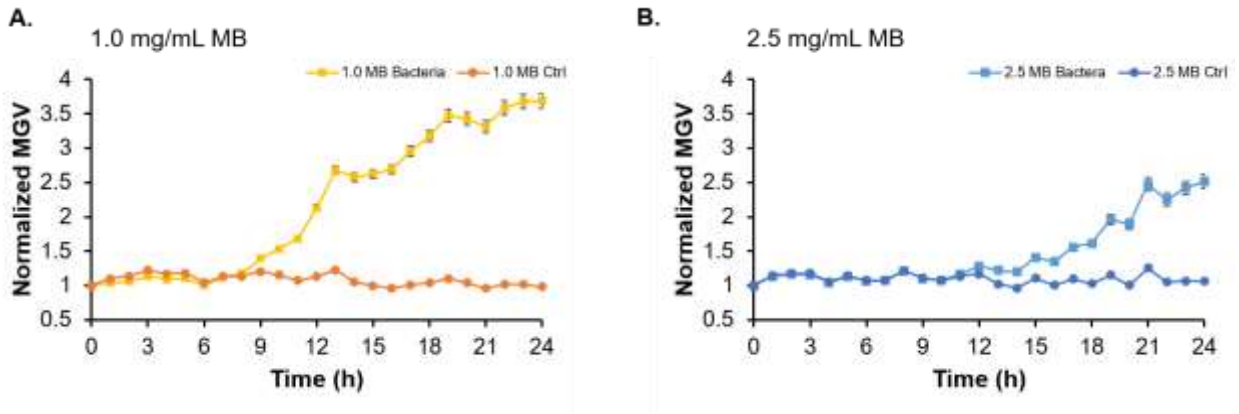

Figure 30: Comparison of rate of MB colour change dependent on the concentration of MB in wells without bacteria and those with. Concentrations of A.) 1.0 mg/mL and B.) 2.5 mg/mL were tested. Lower concentration of MB showed faster and greater degree of colour change than higher concentration of MB. n= 18 for each condition: 2.5 mg/mL MB control, 2.5 mg/mL MB+*E. coli* [10^8 CFU/mL], 1.0 mg/mL control, 1.0 mg/mL MB+*E. coli* [10^8 CFU/mL]. Data shown as mean ± SEM.

4.5.3 Effect of bacterial concentration on rate of change in MB saturation

To study the effect of bacterial concentration on the rate of MB metabolism, samples of MB+LB solutions inoculated with 10^8 CFU/mL and 10^4 CFU/mL were compared to MB+LB media, LB media, and empty well controls. Microwells with volumes of 300 µL were imaged every two hours for 48 hours. These experiments were repeated in triplicate and imaged with the DSLR-Macroscope system as per the Methods chapter. The results are shown in Figure 31.

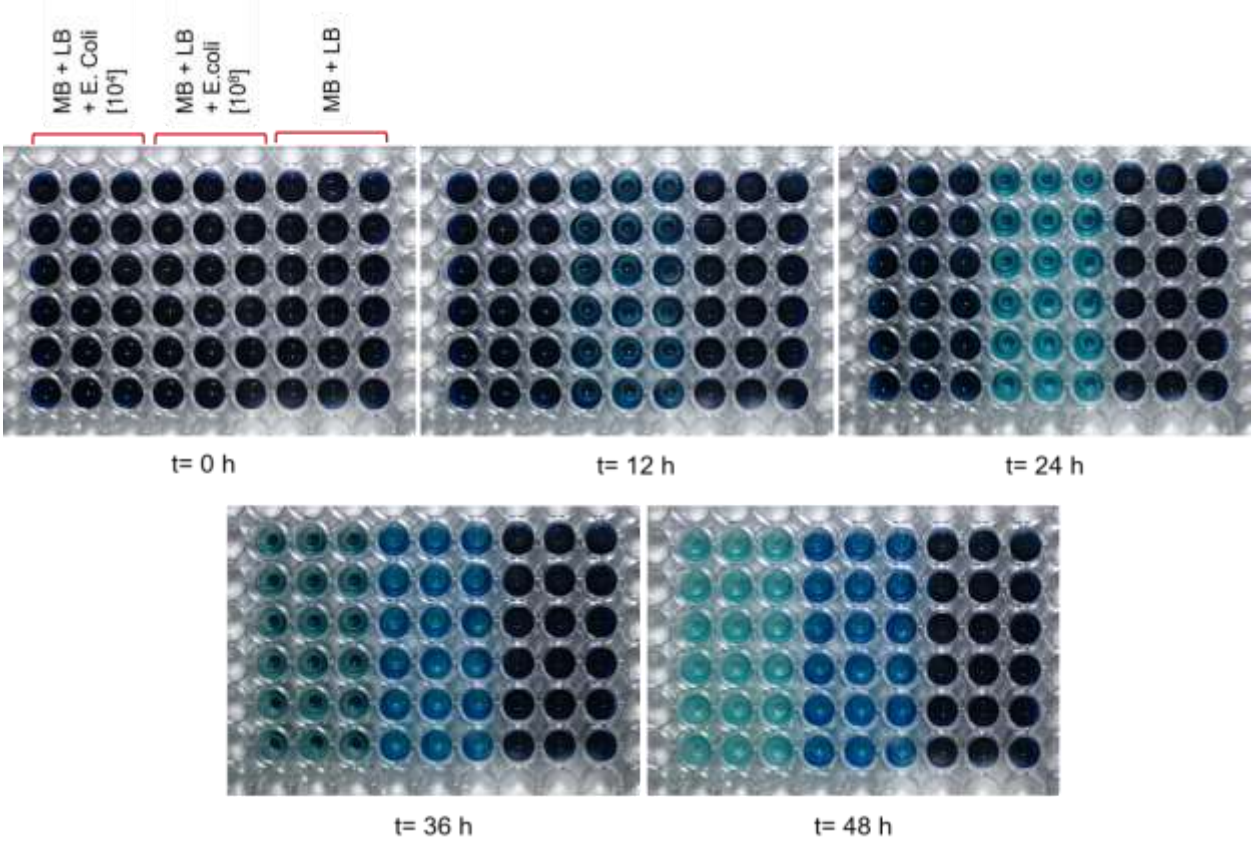

Figure 31: Effect of bacterial concentration on time of 1.0 mg/mL MB colour change due to bacterial metabolism. Selected images taken from the 48-hour imaging period that show the colour change progression of varying *E. coli* concentrations. [MB] = 2.5 mg/mL.

Wells of *E. coli* 10^8 CFU/mL or 10^7 bacteria/well showed the fastest colour change over time, with the point of detectable difference compared to the controls at 10 hours ($p<0.01$) (Figure 32). The normalized MGV at this point was 1.53 ± 0.03 units. Concentrations of 10^4 CFU/mL or 10^3 bacteria/well were subsequently differentiated from the control wells without bacteria at 24 hours, at a normalized MGV of 1.33 ± 0.02 units ($p<0.01$). As expected, the colour change was observed sooner in wells with higher concentrations of bacteria. This could be explained by the presence of more bacteria that reduce the same concentration of MB available in the two different bacterial solutions. Therefore, resulting in a faster rate of reduction. This characterization may help to identify the concentration of bacteria in a contaminated sample. Factoring in the error bars, the

threshold to distinguish bacterial presence from empty wells seems to be a normalized MGV of approximately 1.3 units. Therefore, this threshold can be used as a baseline detection to determine the presence of bacteria in future experiments.

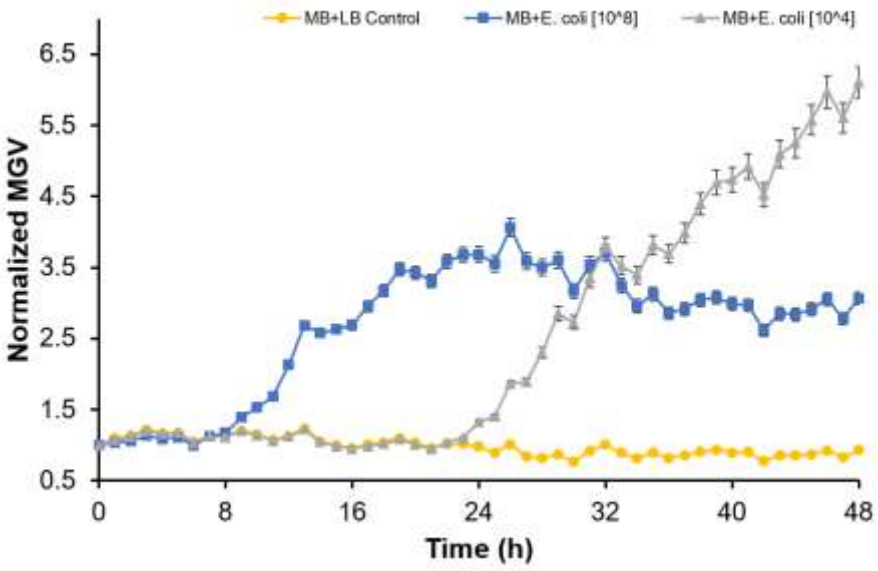

Figure 32: Extracted saturation of MB indicator for varying bacterial concentrations. Wells of *E. coli* [10^8 CFU/mL] (n=18) show increase in normalized MGV that differentiates from the control at 10 hours. Concentrations of [10^4 CFU/mL] (n=18) differentiate from the controls at 24 hours. Data shown as mean ± SEM.

However, the maximum colour change of each concentration differed. The normalized levels for 10^7 bacteria/well reached a maximum value after 26 hours at 4.06 ± 0.13 units. The 10^3 bacteria/well volumes were measured to have a maximum normalized MGV of 6.10 ± 0.23 units at 48 hours (Figure 32). This variance could be explained by the potential overcrowding of bacteria in the larger concentration, increasing competition for nutrients, which hinder the growth of bacteria and therefore the rate of MB reduction. Similar results were observed with the use of an older stock of MB, such that the maximum level of normalized MGV observed for 10^3

bacteria/well concentrations were higher than that of 10^7 bacteria/ well concentration (3.22 ± 0.12 units and 3.01 ± 0.10 units, respectively; Appendix D).

When the wells were imaged after 5 days (120 hours), both concentrations had similar normalized MGV levels of 4.18 ± 0.14 units for 10^7 bacteria/well and 4.71 ± 0.17 units for 10^3 bacteria/well (Figure 33.A-B). This could result from an overall depletion of nutrients available in 120 hours, in addition to an increased pH past optimal conditions due to the metabolism of amino acids [122]. Despite the extended period of observation, none of the bacterial concentrations were able to completely reduce the MB in solution to its colourless leucomethylene blue state. The control conditions – empty wells, LB media only, and mixtures of LB and MB – remain around a normalized value of 1, with a slight decrease near the end of the imaging period, as expected with the gas equilibrium homeostasis that occurs. Without the presence of bacteria, the sterile wells contain less oxygen than the ambient environment, causing a shift and slow diffusion into the well, thereby increasing the saturation of MB and resulting in a lower normalized MGV.

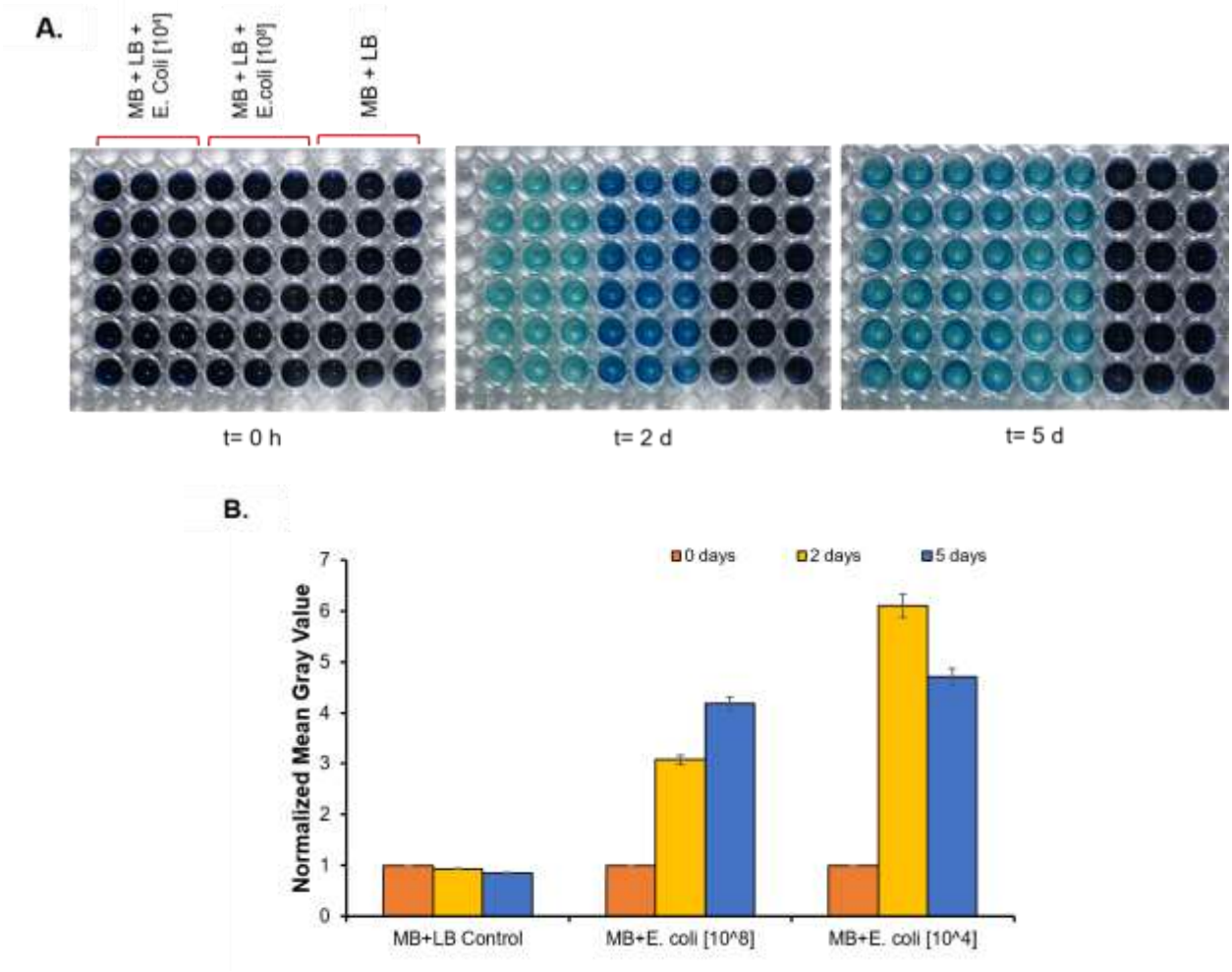

Figure 33: End-point achieved with MB and [10^8 and 10^4 CFU/mL] bacteria in microwells. A.) Sequence of timed images at t=0, 2, and 5 days. B.) Comparison of the normalized MGV of 10^8 and 10^4 CFU/mL *E. coli* to quantify the saturation of MB at an end-point of 5 days. Data shown as mean ± SEM. MB+*E. coli* [10^8] n=18, MB+*E. coli* [10^4] n=18, MB+LB control n=18.

4.6 Characterization of MB as optical metabolic indicator in PDMS nanowell device

4.6.1 Proof of Concept: Use of MB with Redesigned Rapid Culture Nanowell Device

In order to develop an effective and accurate diagnostic device for bacterial presence, the redesigned Rapid Culture Nanowell Device must be able to distinguish between wells with and without bacteria faster than the conventional culture plate. An MB concentration of 1.0 mg/mL

was used in the nanowells based on the preliminary MB concentrations tests in Appendix E. A high concentration of *E. coli* MG1655 [10^8 CFU/mL] was used to arrive at a final number of 10^3 bacteria/well. These conditions were repeated in triplicate and the devices were imaged using the DSLR-Macroscope system every ten minutes for 24 hours (Figure 34).

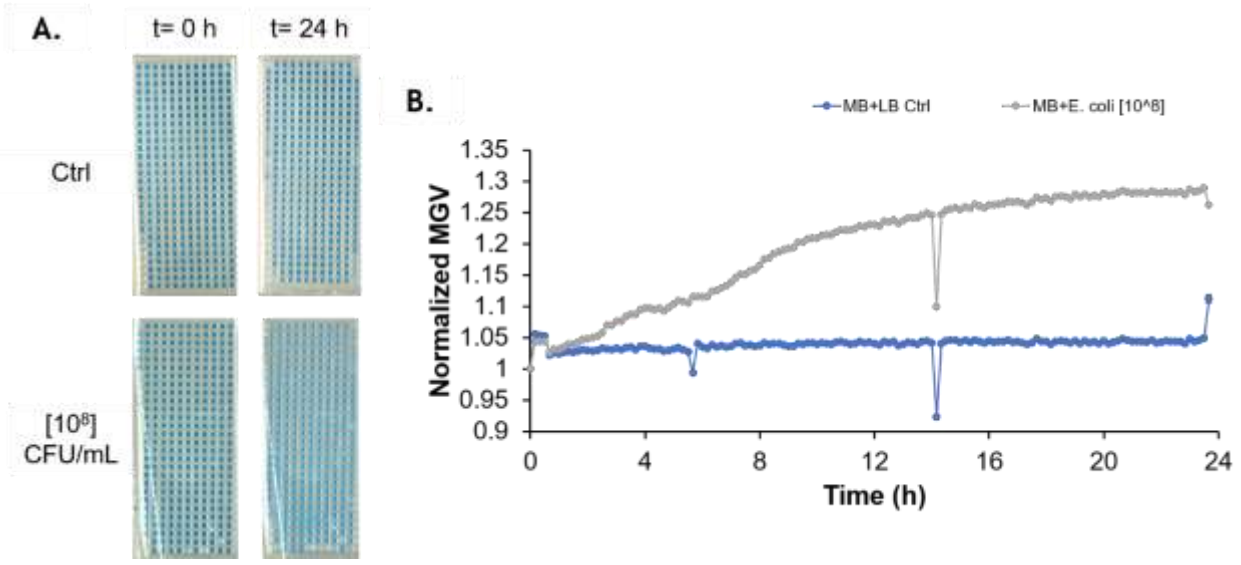

Figure 34: Time-lapse comparison of 10^8 CFU/mL of *E. coli* (n=236) and sterile control (n=256) over 24-hour period, every 10 minutes. A.) Before and after images of filled lithography fabricated devices. B.) Extracted saturation change of the wells, showing a significant difference between bacterial and control wells after 4.83 hours ($p<0.01$). The control normalized mean gray value stayed fairly constant over the 24-hour period whereas the MGV for bacterial devices showed an increase, coinciding with the lightening of colour and indicating the presence of bacteria. Data shown as mean ± SEM.

An obvious visible difference between the sterile wells and those with bacteria was difficult to detect until a comparison at the 24-hour mark (Figure 34.A). The first point at which MB + *E. coli* [10^8 CFU/mL] wells were significantly different from the control wells was observed at 3.33 hours ($p<0.05$) (Figure 34.B). The normalized MGV at this point was 1.08 ± 0.01 units compared to the control at 1.03 ± 0.01 units. When comparing to the microwells at the same distribution of 10^3 bacteria per well, the change in colour was 620% faster in the nanowells (3.33 hours) compared

to the microwells (24 hours). This was as expected as per the concept of segmentation to shorten the detection time.

However, the threshold of 1.08 units in the nanowells is lower than that of the microwells at 1.3 normalized MGV units. This could be explained by the difference in permeability of the two materials, leading to an increased rate of diffusion in the PDMS wells. Fick's First Law states that a solute will move from region of high concentration to region of low concentration across a concentration gradient. It can give rise to Equation 1 [123]:

$$\text{flux} = -P(c_2 - c_1) \tag{1}$$

where permeability (P) is proportional to the difference in concentration of gas across a membrane in the direction of flow ($c_2 - c_1$). Permeability (P) is an experimentally determined membrane "conductance" for given gas at a given temperature. It can be calculated using Equation 2:

$$P = \frac{v\delta}{At(p_1 - p_0)} \tag{2}$$

where v is the volume of gas that penetrates through the membrane, δ is the thickness of the membrane, A is the area of the membrane, t is time, p_1 is partial pressure of gas on the higher side of the membrane, and p_0 is the partial pressure on the lower side of the membrane [124]. PDMS is known for its superior gas permeability compared to polystyrene [125]–[128]. A greater permeability would allow for atmospheric oxygen to penetrate and diffuse through the device and into the well samples, augmenting the oxygen levels and therefore resulting in a more saturated colour.

The overall colour change in the nanowells also reached a lower maximum of 1.29 ± 0.06 units compared to the 6.10 ± 0.97 units in the microwells. This could be explained by the Beer-Lambert Law (Equation 3):

$$T = e^{-a\delta} \quad (3)$$

where T is the proportion of light transmitted at a given wavelength, a is the absorbance at that wavelength, and δ is the thickness of the material. This law correlates the absorbance of a material is directly proportional to the concentration of the attenuating species and its thickness or path length. Therefore, a solution's hue is dependent on the concentration of the solution and the depth or thickness of the medium. The depth of the microwell was approximately 35 times greater than the nanowell. This difference, therefore, influences the saturation of the colour. Then when the MB is reduced, the difference in colour change would be exponentially more evident.

From this conclusion, one can assume that a higher concentration of MB would be required in the nanowells in order to increase the saturation of the wells. However, the preliminary test with an MB concentration of 2.5 mg/mL in the nanowells was also not able to fully reduce MB into its colourless state, despite showing a significantly detectable difference between the sterile and inoculated wells after an hour (Appendix F). A significant difference was seen when comparing the wells with 10^3 bacteria/well and the sterile control wells over the 46-hour imaging period ($p<0.0001$). Further tests with extended imaging periods need to be conducted to determine the final end-point colour in the nanowell assay.

4.6.2 Effect of bacterial concentration on rate of metabolism of MB in nanowells

To be able to correctly identify an unknown level of contamination in real medical test samples, the effect of bacterial concentration needed to be characterized in the nanowell system. Concentrations of 10^8 CFU/mL and 10^4 CFU/mL were filled into three devices and monitored over 24 hours to determine the effect of bacterial concentration on the rate of colour change. These concentrations were chosen to represent the distribution of 10^3 bacteria/ well and 1 bacterium/well, respectively. Refer to Methods chapter for specific experimental design and imaging parameters.

It was difficult to see an obvious visual difference in colour between the inoculated wells compared to their controls with the DSLR images (Figure 35.A). Using ImageJ analysis, the highest degree of change in colour was seen with 10^8 CFU/mL concentration (10^3 bacteria/well) at 20.6%, as expected with the greater number of bacteria present (Figure 35.B). This change was significantly different from the sterile wells after 1 hour ($p<0.0001$). Control wells stayed fairly constant, with a 3.3% increase over the 24 hours. The MGV of 10^4 CFU/mL (approximately 1 bacterium/well) wells only changed by 2.3% and was significantly different from the control at 24 hours ($p<0.0001$). This was expected as the rate of metabolism of an individual bacterium in each well would be slower than that of a larger concentration. When imaged at 48 hours, the normalized MGV of the 10^4 CFU/mL concentration was 1.06 ± 0.01 units, lower than the 1.08 threshold determined in section 4.5.1. Therefore, the data indicates that the capability of this system is sensitive enough to detect well concentrations of 10^3 bacteria. More studies need to be conducted with well concentrations between 1-10^3 bacteria in order to confidently determine the limits of this sensitivity, as well as extended trials to determine the precise point at which a single bacterium can be detected using the Rapid Culture Nanowell device and Methylene Blue. Additionally, increasing the ISO setting of the camera can help raise the sensitivity of the camera in detecting a change in well colour, however, this must be balanced with the shutter speed and amount of noise in the final image.

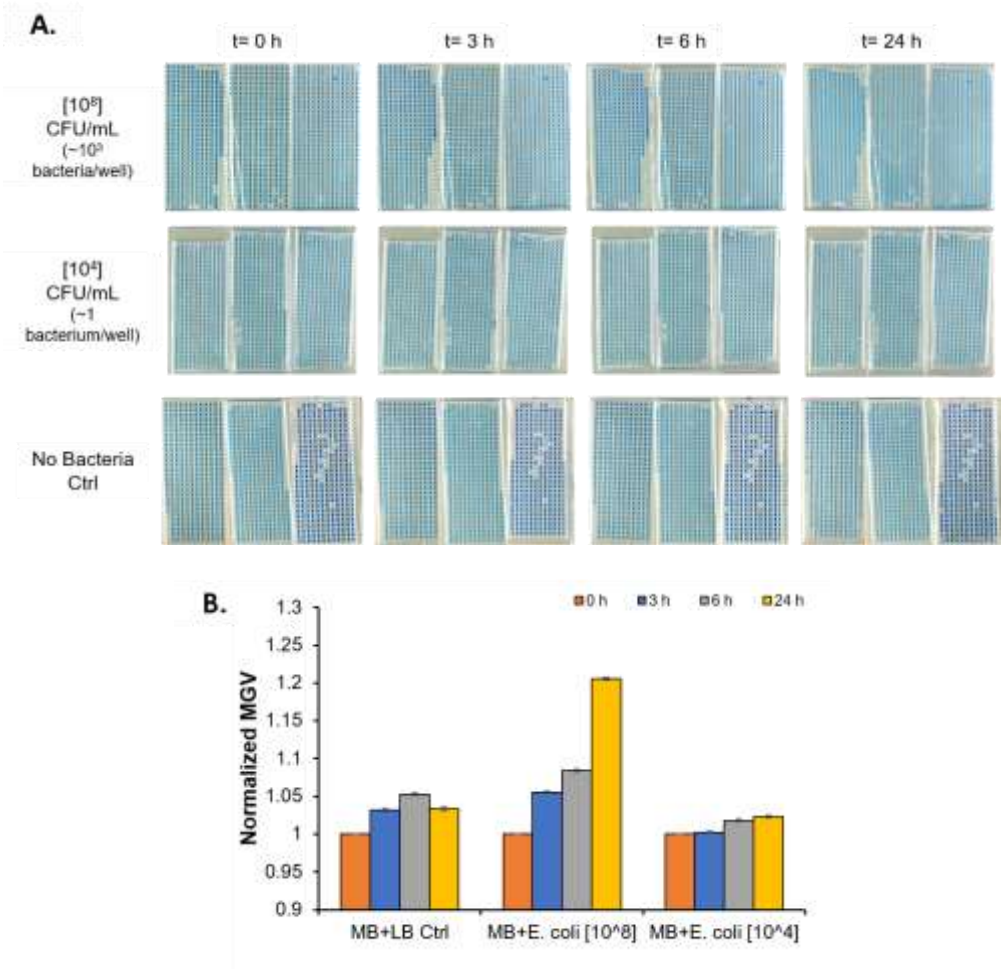

Figure 35: A.) Comparison of lithography mould nanowell devices with varying *E. coli* concentrations. After a period of 24-hours, the wells of 10^8 CFU/mL were visibly a different shade of blue compared to the control, whereas it is difficult to distinguish a difference in the lower concentration. LB *E. coli* [10^8 CFU/mL] n=817, LB *E. coli* [10^4 CFU/mL] n=685, and LB Control n= 664. B.) Normalized MGV were extracted using image analysis and compared at 3, 6, and 24-hour time-points. Data shown as mean ± SEM.

4.7 Effect of Human Milk on MB metabolism

4.7.1 Testing of Bacterial Metabolism Detection in Milk Samples

In order for the Rapid Culture Nanowell Device to be as widely applicable as the culture dish for diagnosing infections, various types of media needed to be tested to determine the suitability of the nanowell device with MB as the optical indicator. Human milk was chosen as a

media of interest due to the potential application of this device in the screening of bacterial contaminants in Human Milk Bank stores post-pasteurization. Samples of human milk acquired from the Rogers Hixon Toronto Milk Bank were artificially inoculated with 10^8 CFU/mL of *E. coli* K12 MG1655 and dispensed into three nanowell devices. These samples were compared to their LB counterparts and imaged at t=0, 3, 6, and 24 hours with the DSLR-Macroscope system (Figure 36.A).

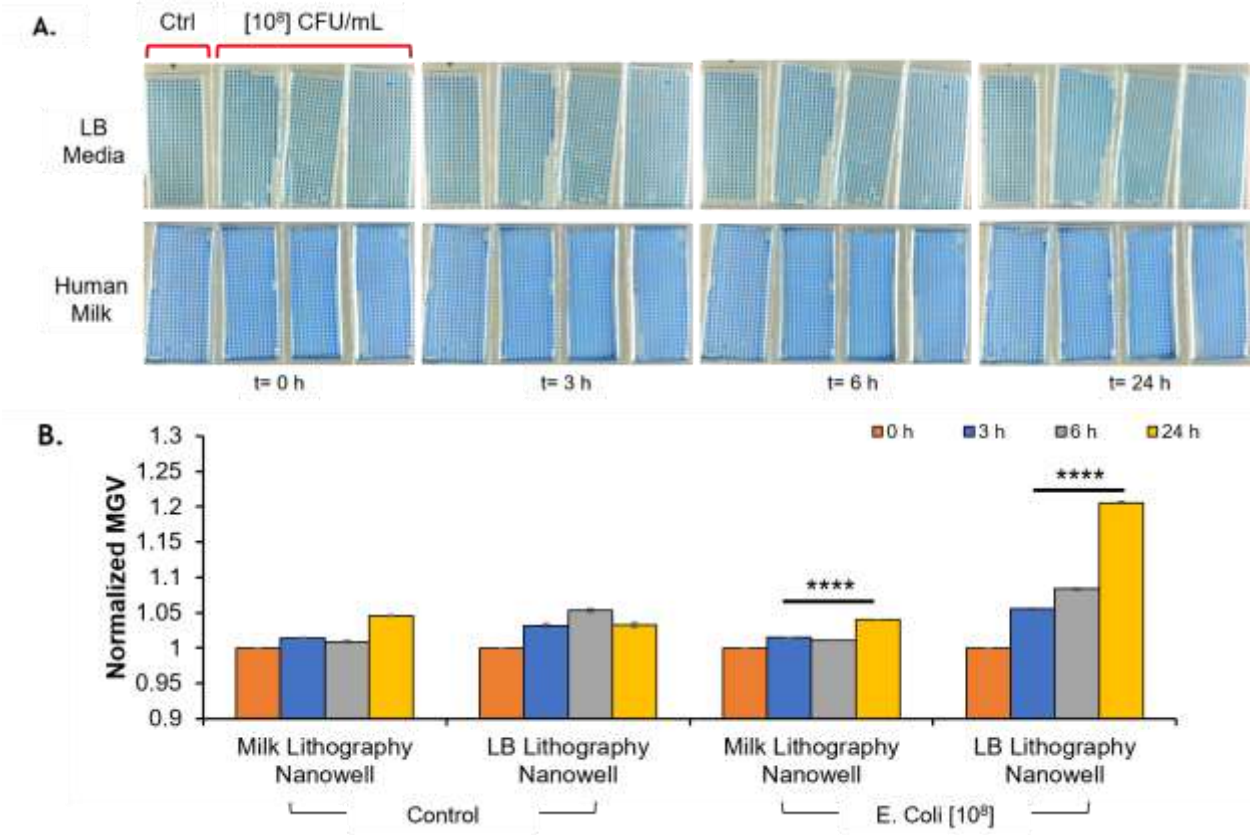

Figure 36: Time lapse measuring the MB colour change dependent on bacterial presence over 24 hours comparing the effect of different media. A.) Lithography nanowell devices filled with LB media and human milk as the nutrient media. Bacteria milk samples (n=635) were artificially inoculated with 10^8 CFU/mL of *E. coli*. Control milk n=266. LB *E. coli* [10^8] CFU n=817 and LB Control n= 664. B.) 96 well plate 300 µL wells filled with human milk and compared to LB as the nutrient media. Bacteria milk samples (n=9) were artificially inoculated with 10^8 CFU/mL of *E. coli*. Control n=3. LB control (n=9), LB bacteria (n=9). Data shown as mean ± SEM.

Although the differences between the two media at all time points were significant ($p<0.0001$), the overall increase in normalized mean gray value due to the presence of bacteria was more evident in LB media compared to human milk. LB media wells with bacteria were 17% less saturated than the LB sterile control after 24 hours. Milk media wells with bacteria, however, did not show a decrease in saturation compared to their sterile control. This phenomenon was also observed in the microscale where the colour change at 24 hours was more evident in LB compared to human milk (Figure 37). The differences between the media in non-bacterial wells were not significant, however, the milk bacteria well were significantly different from the LB bacteria wells at 24 hours ($p<0.0001$).

To confirm that the bacteria had not been destroyed by the immune factors naturally found in human milk, the wells were imaged to measure the fluorescence emitted from the GFP-tagged *E. coli* cells (Figure 38.A). Over the 5-hour incubation period for the nanowells, the fluorescent intensity increased by 453% (6.41 MGV units at t=0 hours, 35.49 MGV units at t=5 hours) indicating that the bacteria were alive and growing. However, the saturation of the bacteria wells was only 0.002 units higher than that of the control wells. The fluorescence in the microwells was approximately 11 times larger after 28 hours, and 37 times after 50 hours (Figure 38.B). The smaller colour change could be due to the presence of other proteins in the milk that increase the opacity of the well. The opaque milk would transmit less light back to be detected by the DSLR-Macroscope's sensors compared to the translucent LB media. Thereby the overall change in colour would be harder to detect in the milk samples. A more concentrated mixture of human milk with MB will need to be explored in future experiments.

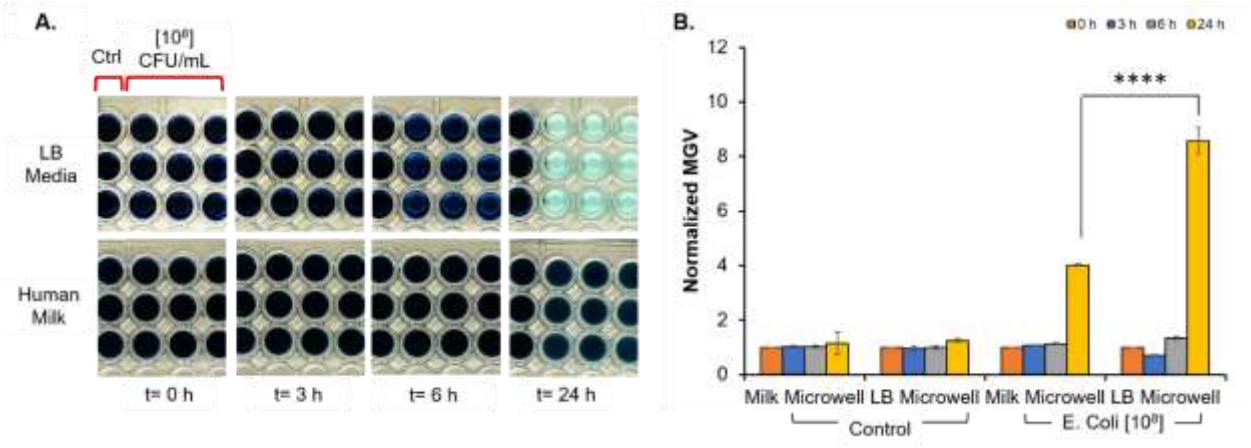

Figure 4.37: Comparison of colour change due to bacterial metabolism in LB media or human milk in microwells over 24 hours. A.) DSLR images of the microtiter wells filled with either LB or human milk and [10^8 CFU/mL]. Bacteria LB samples (n=9) and milk samples (n=9) were artificially inoculated with 10^8 CFU/mL of *E. coli*. Control LB (n=9) and milk (n=3). 96 well plate 300 µL wells filled with human milk and compared to LB as the nutrient media. B.) Comparison of the different media on the normalized MGV of the controls were not significant, however the difference between Milk and LB bacteria wells were highly significant ($p<0.0001$) at 24 hours. Data shown as mean ± SEM.

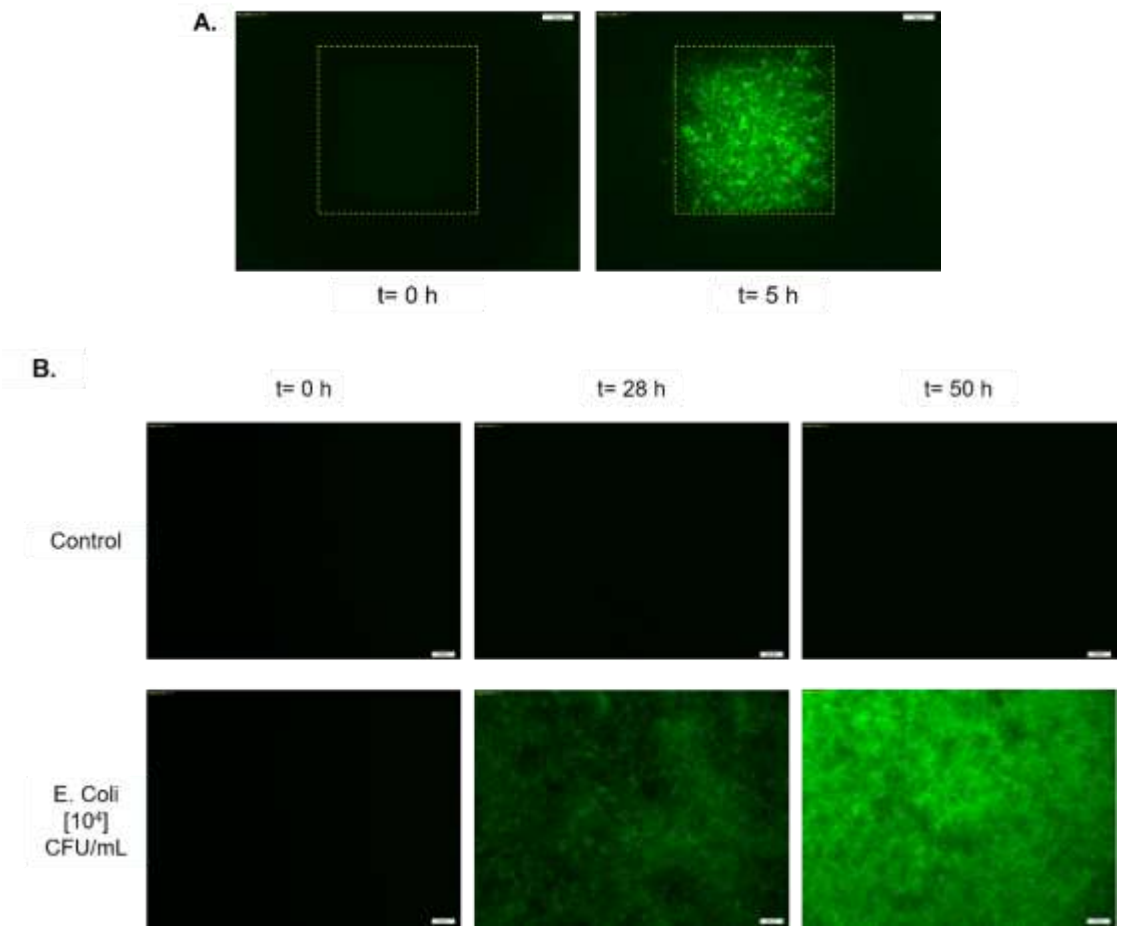

Figure 38: Fluorescent images tracking the growth of bacteria via GFP fluorescence. The increase in GFP intensity indicating viable growth of bacteria within A.) a single nanowell and B.) a microwell filled with human milk. (n=3)

4.8 Comparison of time required for detection of bacterial presence using Nanowell Device vs. Culture Plate

In order to accurately draw parallels between the efficacy of the nanowell device compared to the culture plate, LB agar dishes were streaked with *E. coli* K12 MG1655 and imaged with the DSLR-Macroscope system to determine the time at which colonies can be identified. LB agar dishes were prepared using the protocol in Appendix A. Three dishes were placed within the DSLR-Macroscope system and imaged every thirty minutes for 17.5 hours. This imaging frequency was chosen based on the typical doubling time of *E. coli* K12 found in the literature

[62]. The first presence of bacterial colonies can be distinguished in Figure 39 after 16 hours. This can be compared to the first point of bacterial detection in the nanowells at 3.33 hours.

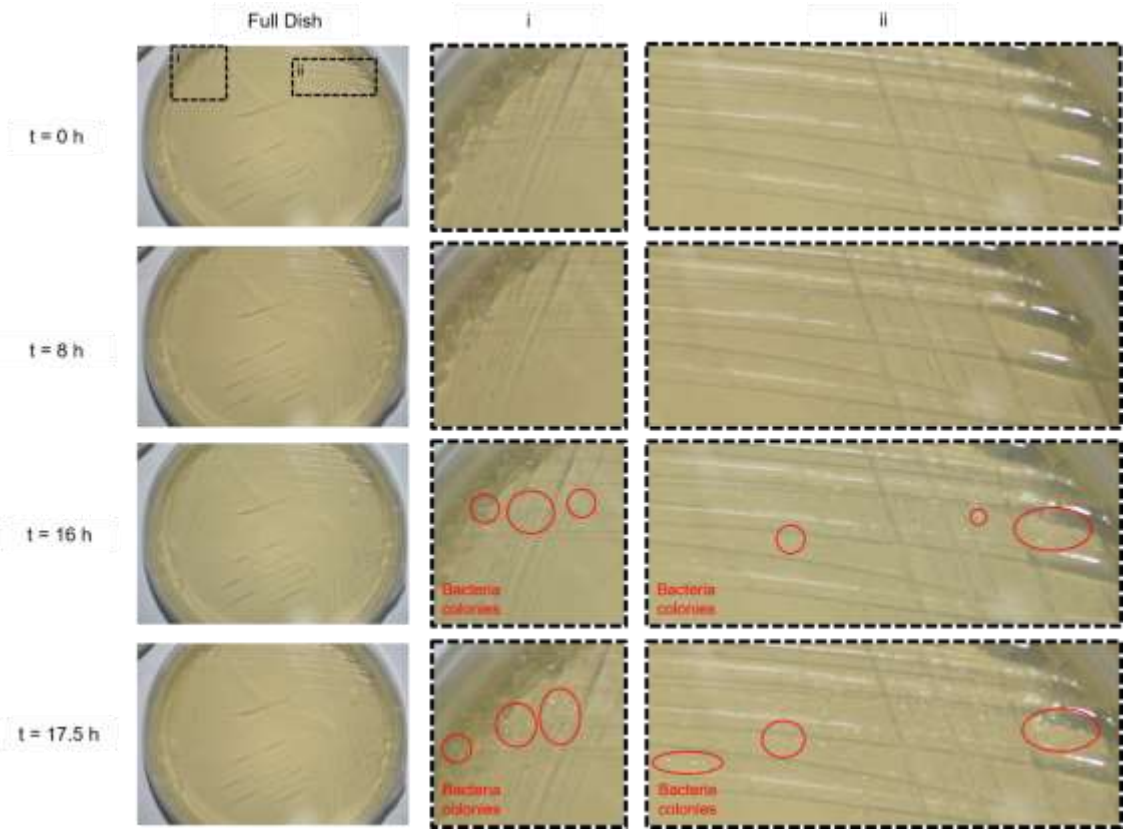

Figure 39: Images comparing appearance of bacterial colonies on LB Agar dish over time

Chapter 5 – Conclusion & Future Work

5.1 Conclusion

Donor milk banks who serve immunocompromised preterm infants depend on the culture plate to preventatively screen against pathogenic bacteria in post-pasteurization milk [4], [9]. Unfortunately, this method of detection involves long processing times that last several days, delaying the distribution of human milk to the infants who need it most [6], [10], [11]. By combining the concept of metabolite monitoring using a chromogenic optical dye to indicate bacterial viability and compartmentalized culture, this thesis explored the potential application of the updated Rapid Culture Nanowell Device and Methylene Blue as an alternative to the culture dish.

Initial characterizations were conducted to confirm the inverse relationship between DO concentrations within solutions and the saturation of MB in solutions and applied to volumes ranging from 10 mL to 75 nL. It was also demonstrated that the surface roughness from a Multi-Jet Modeling 3D printer hindered the sealing of individual wells and created leaks that allowed for external gaseous interactions. This led to inaccuracies which interfered with determining the rate of MB reduction by bacteria in these wells. Therefore, photolithography master moulds should still be the fabrication method of choice for these microfluidic devices. Lastly, the DSLR-Macroscope was developed and tested to be a reliable system that provided a controlled, automated imaging platform for the Rapid Culture Nanowell Device compared to the Tecan plate reader. Both systems identified the presence of bacteria after 8 hours. Therefore, the DSLR-Macroscope showed potential in being a more affordable method compared to the traditional microscope and is a stepping stone to the use of the mobile phone platform.

The point of detection in the nanowell devices when comparing the same distribution of bacteria was found to be faster than in the microwells. For concentrations of 10^3 bacteria/well, microwells showed a change in MB colour after 24 hours compared to 3.33 hours in the nanowells. By decreasing the well volume from 300 µL to 75 nL, the time of detection decreased by 620%. However, the degree of colour change was more evident in the microwells than nanowells. The threshold to determine the presence of micro-organisms was also higher in the microwells compared to the nanowells (1.3 normalized MGV units and 1.08 normalized MGV units, respectively). Further exploration into the time required for MB to fully convert into its colourless reduced state needs to be conducted. The preliminary results comparing human milk and LB media indicate that the time required to identify the presence of bacteria was longer in milk. Experiments were conducted to confirm the viability of bacteria throughout the imaging period. Further exploration is needed to further adapt the updated Rapid Culture Nanowell device for the application of detecting bacteria in human milk. Finally, when comparing the time of *E. coli* detection with the DSLR-Macroscope of the nanowell and LB agar dish, the nanowell was 380% faster at 3.33 hours compared to the 16 hours for the culture dish. This thesis has detailed the initial steps to the development of a quick, low-cost, easy-to-use bacterial detection system with Methylene Blue so to protect infants from foodborne infectious diseases and shorten the access time to the lifesaving nutrition.

5.2 Future Work

Although the current design of the Rapid Culture Nanowell Device and the use of Methylene Blue as an optical indicator has shown promise in detecting bacterial presence faster than the culture dish, improvements, as well as further experimentation, are required. This includes:

1. Further exploration of nanowell volumes

Based on the results presented in this thesis and those by Ayyash et al., nanowells between the dimensions of 100x100x100 - 500x500x300 µm (length x width x depth) need to be explored in order to determine the ideal volume that allows for the fastest detection in the required sample volume, while also providing sufficient nutrients for ideal bacterial metabolism [90]. Ayyash demonstrated that in a well volume of 1 nL (100x100x100 µm), *E. coli* at a concentration of 10^8 cells/mL could be detected in 38 minutes. However, in this thesis, the detection time was 3.33 hours for the same concentration of *E. coli* in a well volume of 75 nL. Experiments with nanowell sizes between these two sets of dimensions at a well aspect ratio of 1:1 needs to be systematically explored in order to determine the ideal well volume to decrease the time to detection. Based on Ayyash's experiments, a lower aspect ratio is recommended as it is easier to fill the shallow nanowells due to the larger contact angle between the liquid and solid interface, decreasing the likelihood of bubble formation that would hinder the filling [119]. This would also help to ensure an even distribution of bacteria as it would not allow for the butterfat found in milk to rise, concentrating the bacteria to the upper layer of the well [77].

2. Application and Characterization of other bacterial species and media

The behaviour of other bacterial species commonly found in contaminated human milk must be studied in the updated Rapid Culture Nanowell Device with Methylene Blue because the rate of

reduction could differ based on the bacterial species. Different species of bacteria have shown to have different reducing intensities and growth rates at a set temperature [129]. Additionally, the time spent in the lag phase of growth, in which bacteria consume oxygen, varies per species [129]. Oxygen consumption is also proportional to protoplasmic mass, therefore larger cells will generally consume more oxygen faster than those that were smaller [129]. It is hypothesized that coliforms are some of the most rapidly reducing species, followed by the Streptococci spp. [51]. The initial characterization detailed in this thesis has only explored the rate of reduction based on non-pathogenic *E. coli* MG1655. The behaviour of *B. cereus* in this device and set-up would be beneficial since *B. cereus* is the most common bacteria found in post-pasteurized milk due to its resistance to heat via sporulation.

3. Applications to measure other methods of bacterial metabolism

Methylene Blue is an indicator that indirectly measures the metabolism of bacteria by the absence of the metabolite oxygen. However, some bacteria are able to survive and grow without oxygen. Methylene blue would, therefore, not be effective in detecting the presence of these anaerobic bacteria. The Rapid Culture Nanowell device could then be combined with another metabolic indicator that would monitor changes in pH levels or aptamers that bind to specific receptors on the surfaces of bacterial membranes. This modification would allow for the identification of the microbial contamination.

4. Use of the Red channel to detect a faster change in colour

By monitoring the change in the saturation of MB via its red channel, there is the potential to detect the presence of bacteria faster than using the average of the RGB values. The DSLR-Macroscope system takes images of the Rapid Culture Nanowell device and the Methylene Blue indicator in a 24-bit RGB image format. Using the ImageJ analysis program, the image of the

nanowells can be split into the respective red, green and blue channel. As the MB reduces over time to indirectly monitor the presence and metabolism of bacteria, the blue wells decrease in saturation.

When these images were split into the different channels and analyzed, the point in time when wells with bacteria could be differentiated from those without in the red channel was seen at 2.67 hours ($p<0.001$). The normalized values for the bacterial wells were 1.15 ± 0.01 units compared to the sterile wells at 1.01 ± 0.01 units. This was faster than the point of differentiation using the green channel (3.33 hours with normalized MGV of 1.04 ± 0.01 units and 1.02 ± 0.01 in the bacteria and non-bacteria wells, respectively ($p<0.05$)) and the blue channel (5.0 hours with a normalized MGV of 1.07 ± 0.01 units and 1.04 ± 0.01, in respective bacteria and non-bacteria wells ($p<0.05$)). A greater and faster change in MB colour was detected through the red channel compared to the other channels due to MB's peak absorption at around 660 nm wavelengths, which coincides with the red visible spectrum (625-740 nm). The disappearance of the absorption peak when methylene blue is converted into its reduced leucomethylene blue state would result in the largest change in normalized mean gray value. In the red channel, the mean gray value extracted from the blue methylene blue was approximately 48.06 ± 0.36 units. As the saturation of blue decreased due to bacterial metabolism, the MGV increased to an average of 83.00 ± 0.33 units. Comparatively, the methylene blue was extracted to have an MGV range of 173.58 ± 0.30 – 202.91 ± 0.34 units in the blue channel and 132.59 ± 0.33 – 164.57 ± 0.37 units in the green channel. Therefore, further exploration into this finding could lead to alterations in the imaging system to facilitate the shortening of the detection time for MB colour change, indicating the presence of bacterial contamination.

References

[1] Foodborne Disease Burden Epidemiology Reference Group 2007-2015, "WHO estimates of the global burden of foodborne diseases," *World Heal. Organ. Geneva*, pp. VIII–265, 2015.

[2] Rogers Hixon Ontario Human Milk Bank, "Why Donate Breast Milk?," 2019. [Online]. Available: https://www.milkbankontario.ca/donate-milk/.

[3] J. Meinzen-Derr *et al.*, "Role of human milk in extremely low birth weight infants' risk of necrotizing enterocolitis or death," *J. Perinatol.*, vol. 29, no. 1, pp. 57–62, 2009.

[4] J. H. Kim and S. Unger, "Canadian Paediatric Society, Nutrition and Gastroenterology Committee. Human milk banking.," *Paediatr. Child Health (Oxford).*, vol. 15, no. 9, pp. 595–8, 2010.

[5] E. B. Froh, J. Vanderpool, and D. L. Spatz, "Best Practices to Limit Contamination of Donor Milk in a Milk Bank," *JOGNN - J. Obstet. Gynecol. Neonatal Nurs.*, vol. 47, no. 4, pp. 547–555, 2018.

[6] S. Landers and K. Updegrove, "Bacteriological screening of Donor Human Milk Before and After Holder Pasteurization," *Breastfeed. Med.*, vol. 5, no. 3, pp. 117–121, 2010.

[7] A. Lucas and C. D. Roberts, "Bacteriological quality control in human milk-banking.," *Br. Med. J.*, vol. 1, no. 6156, pp. 80–82, 2009.

[8] J. E. Tyson, W. H. Edwards, A. M. Rosenfeld, and A. E. Beer, "Collection methods and contamination of bank milk," *Arch. Dis. Child.*, vol. 57, no. 5, pp. 396–398, 1982.

[9] Human Milk Banking Association of North America (HMBANA), "Guidelines for the Establishment and Operation of a Donor Human Milk Bank," Fort Worth, TX, 2018.

[10] H. J. Chung, C. M. Castro, H. Im, H. Lee, and R. Weissleder, "A magneto-DNA nanoparticle system for target specific bacterial identification," *Nat Nanotechnol.*, vol. 8, no. 5, pp. 369–375, 2013.

[11] The Milk Bank of Indiana HMBANA, "Why do we pasteurize breast milk donations?," 2015. [Online]. Available: https://www.themilkbank.org/blog-2/why-do-we-pasteurize-breast-milk-donations.

[12] E. Scallan *et al.*, "Foodborne Illness Acquired in the United States - Major Pathogens," *Emerg. Infect. Dis.*, vol. 17, no. 7, pp. 1339–1340, 2011.

[13] A. B. John, E. A. S. A. Razak, E. E. M. H. Razak, N. Al-Naqeeb, and R. Dhar, "Intractable Bacillus cereus Bacteremia in a Preterm Neonate," *J. Trop. Pediatr.*, vol. 53, no. 2, pp. 131–132, 2006.

[14] N. Ramarao *et al.*, "Two unrelated episodes of Bacillus cereus bacteremia in a neonatal intensive care unit," *Am. J. Infect. Control*, vol. 42, no. 6, pp. 694–695, 2014.

[15] A. Ronnestad *et al.*, "Late-Onset Septicemia in a Norwegian National Cohort of Extremely Premature Infants Receiving Very Early Full Human Milk Feeding," *Pediatrics*, vol. 115, no. 3, pp. e269–e276, 2005.

[16] M. A. Hylander, D. M. Strobino, and R. Dhanireddy, "Human Milk Feedings and Infection Among Very Low Birth Weight Infants," *Pediatrics*, vol. 102, no. 3, pp. 1–6, 1998.

[17] P. Sakamoto, "Introduction Microbiology and Preservation of Breast Milk," 2018.

[18] J.-W. Decousser *et al.*, "Bacillus cereus and severe intestinal infections in preterm neonates: Putative role of pooled breast milk," *Am. J. Infect. Control*, vol. 41, no. 10, pp. 918–921, 2013.

[19] L. Hanson, "Human milk and host defence: immediate and long-term effects," *Acta Paediatr.*, vol. 88, pp. 42–46, 2010.

[20] M. K. Davis, "Breastfeeding and chronic disease in childhood and adolescence," *Pediatr. Clin. North Am.*, vol. 48, no. 1, pp. 125–141, 2001.

[21] A. Singhal, T. J. Cole, and A. Lucas, "Early nutrition in preterm infants and later blood pressure: two cohorts after randomised trials," *Lancet*, vol. 357, no. 9254, pp. 413–419, 2001.

[22] T. M. Ball and a L. Wright, "Health care costs of formula-feeding in the first year of life.," *Pediatrics*, vol. 103, no. 4 Pt 2, pp. 870–6, 1999.

[23] J. M. Riordan, "The Cost of Not Breastfeeding: A Commentary," *J. Hum. Lact.*, vol. 13, no. 2, pp. 93–97, 1997.

[24] R. J. Schanler, R. J. Shulman, and C. Lau, "Feeding Strategies for Premature Infants: Beneficial Outcomes of Feeding Fortified Human Milk Versus Preterm Formula," *Pediatrics*, vol. 103, no. 6, pp. 1150–1157, 1999.

[25] M. Bartick and A. Reinhold, "The Burden of Suboptimal Breastfeeding in the United States: A Pediatric Cost Analysis," *Pediatrics*, vol. 125, no. 5, pp. e1048–e1056, 2010.

[26] R. Seeley, C. VanPutte, J. Regan, and A. Russo, "Mammary Glands," in *Seeley's Anatomy & Physiology*, 9th Editio., New York: McGraw-Hill Publishing, 2011, pp. 1052–1054.

[27] A. A. H. AL Haleem, "Breastfeeding." pp. 1–49, 2016.

[28] R. Seeley, C. VanPutte, J. Regan, and A. Russo, "Lactation," in *Seeley's Anatomy & Physiology*, 9th Editio., New York: McGraw-Hill Publishing, 2011, pp. 1103–1104.

[29] M. Hamosh, "Bioactive factors in Human Milk," *Pediatr. Clin. North Am.*, vol. 48, no. 1, pp. 69–86, 2001.

[30] V. V. Serra, S. Teves, A. Lopez de Volder, F. Ossorio, N. Aguilar, and M. Armadans, "Comparison of the risk of microbiological contamination between samples of breast milk obtained at home and at a healthcare facility," *Arch. Argent. Pediatr.*, vol. 111, no. 2, pp. 115–119, 2013.

[31] C. R. Martin, P. R. Ling, and G. L. Blackburn, "Review of infant feeding: Key features of breast milk and infant formula," *Nutrients*, vol. 8, no. 5, pp. 1–11, 2016.

[32] N. J. Andreas, B. Kampmann, and K. Mehring Le-Doare, "Human breast milk: A review

on its composition and bioactivity," *Early Hum. Dev.*, vol. 91, no. 11, pp. 629–635, 2015.

[33] M. Kramer and R. Kakuma, "Optimal duration of exclusive breastfeeding (Review)," *Cochrane Database Syst Rev*, no. 8, 2009.

[34] C. Urbaniak, J. P. Burton, and G. Reid, "Breast, milk and microbes: a complex relationship that does not end with la...: Discovery Service for Endeavour College of Natural Health Library," *Women's Heal.*, vol. 8, no. 4, pp. 385–398, 2012.

[35] D. B. Tully, F. Jones, and M. R. Tully, "Currents in Human Milk Banking Donor Milk : What's in It and What's Not," *J. Hum. Lact.*, vol. 17, no. 2, pp. 152–155, 2001.

[36] M. F. Picciano, "Nutrient composition of human milk," *Pediatr. Clin. North Am.*, vol. 48, no. 1, pp. 53–67, 2001.

[37] Centers for Disease Control and Prevention (CDC), "What are the benefits of breastfeeding?," 2018. [Online]. Available: https://www.cdc.gov/breastfeeding/faq/index.htm.

[38] M. Gdalevich, D. Mimouni, M. David, and M. Mimouni, "Breast-feeding and the onset of atopic dermatitis in childhood: A systematic review and meta-analysis of prospective studies," *J. Am. Acad. Dermatol.*, vol. 45, no. 4, pp. 520–527, 2001.

[39] M. Gdalevich, D. Mimouni, and M. Mimouni, "Breast-feeding and the risk of bronchial asthma in childhood: A systematic review with meta-analysis of prospective studies," *J. Pediatr.*, vol. 139, no. 2, pp. 261–266, 2001.

[40] A. M. Bloch, D. Mimouni, M. Mimouni, and M. Gdalevich, "Does breastfeeding protect against allergic rhinitis during childhood? A meta-analysis of prospective studies," *Acta Paediatr. Int. J. Paediatr.*, vol. 91, no. 3, pp. 275–279, 2002.

[41] A. Lucas, R. Morley, T. J. Cole, G. Lister, and C. Leeson-Payne, "Breast milk and subsequent intelligence quotient in," *Lancet*, vol. 339, pp. 261–264, 1992.

[42] K. Simmer, S. Schulzke, and S. Patole, "Longchain polyunsaturated fatty acid supplementation in infants born at term," *Cochrane Database Syst. Rev. Database Syst. Rev.*, no. 1, 2008.

[43] S. Sen *et al.*, "Donor milk utilization for healthy infants: Experience at a single academic center," *Breastfeed. Med.*, vol. 13, no. 1, pp. 28–33, 2018.

[44] WHO and UNICEF, "Global Strategy for Infant and Young Child Feeding," 2003.

[45] N. E. Wight, "Donor human milk for preterm infants: Practice considerations," *J. Perinatol.*, vol. 21, no. 4, pp. 249–254, 2001.

[46] Rogers Hixon Ontario Human Milk Bank, "Facts about Donor Milk," 2019. [Online]. Available: https://www.milkbankontario.ca/about-us/facts-about-donor-milk/.

[47] R. J. Schanler, C. Lau, N. M. Hurst, and E. O. Smith, "Randomized Trial of Donor Human Milk Versus Preterm Formula as Substitutes for Mothers' Own Milk in the Feeding of Extremely Premature Infants," *Pediatrics*, vol. 116, no. 2, pp. 400–406, 2005.

[48] B. R. Vohr *et al.*, "Beneficial Effects of Breast Milk in the Neonatal Intensive Care Unit on the Developmental Outcome of Extremely Low Birth Weight Infants at 18 months of age." pp. 374–375, 2006.

[49] Human Milk Banking Association of North America (HMBANA), "Our Work," *HMBANA*, 2018. [Online]. Available: https://www.hmbana.org/our-work/.

[50] C. G. Sullivan, "Position statement regarding use of informally shared human milk," *Am. Acad. Nurs. Policy*, vol. 64, no. 1, pp. 98–102, 2016.

[51] University of Guelph, "Dairy Microbiology," in *Food Science*, University of Guelph.

[52] A. Fatima, "An Awareness Study on Human Milk Banks and Microbial Analysis of Human Milk," *Int. J. Res. Appl. Sci. Eng. Technol.*, vol. 6, no. 6, pp. 1358–1363, 2018.

[53] S. Wang, M. L. Hibberd, S. Pettersson, and Y. K. Lee, "Enterococcus faecalis from healthy infants modulates inflammation through MAPK signaling pathways," *PLoS One*, vol. 9, no. 5, pp. 1–12, 2014.

[54] B. J. Stoll *et al.*, "Early Onset Neonatal Sepsis: The Burden of Group B Streptococcal and E. coli Disease Continues," *Pediatrics*, vol. 127, no. 5, pp. 817–826, 2011.

[55] D. B. Haslam and J. W. St. Geme, "Other Infections," in *Principles and Practice of Pediatric Infectious Diseases*, 5th ed., S. S. Long, C. G. Prober, and M. Fischer, Eds. Elsevier Inc., 2018, pp. 732–735.

[56] V. B. Shete, D. P. Ghadage, V. A. Muley, and A. V Bhore, "Acinetobacter septicemia in neonates admitted to intensive care units," *J. Lab. Physicians*, vol. 1, no. 2, pp. 73–76, 2009.

[57] R. Kiu and L. J. Hall, "An update on the human and animal enteric pathogen Clostridium perfringens," *Emerg. Microbes Infect.*, vol. 7, no. 1, 2018.

[58] E. J. Asturias *et al.*, "Enterobacteriaceae: Gram-Negative Bacilli," in *Principles and Practice of Pediatric Infectious Diseases*, 5th Editio., S. S. Long, C. G. Prober, and M. Fischer, Eds. Elsevier Inc., 2018, pp. 819–851.

[59] J. M. C. Jefferies, T. Cooper, T. Yam, and S. C. Clarke, "Pseudomonas aeruginosa outbreaks in the neonatal intensive care unit - a systematic review of risk factors and environmental sources," *J. Med. Microbiol.*, vol. 61, no. 8, pp. 1052–1061, 2012.

[60] S. Freeman, M. Harrington, and J. Sharp, "How do Bacteria divide?," in *Biological Science: The Cell, Genetics, and Development*, 3rd Editio., Toronto: Pearson Learning Solutions, 2011, p. 239.

[61] F. Widdel, "Theory and Measurement of Bacterial Growth A. Basic and practical aspects," *Grundpraktikum Mikrobiol. Univ. Bremen*, pp. 1–11, 2010.

[62] G. Sezonov, D. Joseleau-Petit, and R. D'Ari, "Escherichia coli physiology in Luria-Bertani broth," *J. Bacteriol.*, vol. 189, no. 23, pp. 8746–8749, 2007.

[63] S. Freeman, M. Harrington, and J. Sharp, "Bacteria and Archaea," in *Biological Science: Evolution, Diversity, and Ecology*, 3rd Editio., Toronto, 2011, pp. 595–622.

[64] J. M.Willey, L. M. Sherwood, and C. J.Woolverton, "Microbiology - Prescott, Lansing M., Harley, John P., Klein, Donald A.," *Microbiology*, pp. 1023–1086, 2008.

[65] Cornell University Milk Quality Improvement Program, "Raw Milk Quality Tests," 2008.

[66] T. Bilkis, M. M. Islam, M. C. Sumy, M. N. Ali Mandal, and G. M. N. Uddin, "Rapid estimation of quality of raw milk for its suitability for further processing in the dairy industries of Bangladesh," *Int. J. Dairy Sci.*, vol. 8, no. 1, pp. 1–11, 2013.

[67] Rogers Hixon Ontario Human Milk Bank, "Nutritional analysis of donor milk," *The Rogers Hixon Ontario Human Milk Bank*, 2019. [Online]. Available: https://www.milkbankontario.ca/research-and-resources/nutritional-analysis-of-donor-milk/.

[68] MediCare Colgate, "T30 Human Milk Pasteuriser," 2019. [Online]. Available: https://medicarecolgate.com/catalog/t30-human-milk-pasteuriser/%0A.

[69] Cornel University College of Agriculture and Life Sciences, "Bacterial Endospores," 2019. [Online]. Available: https://micro.cornell.edu/research/epulopiscium/bacterial-endospores/.

[70] S. Aryal, "MacConkey Agar - Composition, Principle, Uses, Preparation and Colony Morphology," *Microbiology Info*, 2018. [Online]. Available: https://microbiologyinfo.com/macconkey-agar-composition-principle-uses-preparation-and-colony-morphology/%0A.

[71] S. Aryal, "Blood Agar - Composition, Preparation, Uses and Pictures," *Microbiology Info*, 2018. [Online]. Available: https://microbiologyinfo.com/blood-agar-composition-preparation-uses-and-pictures/.

[72] Biomerieux, "Blood Agar Culture Media," 2019. [Online]. Available: http://www.biomerieux-culturemedia.com/product/30-columbia-agar-+-5-percent-sheep-blood.

[73] D. M. Kasozi *et al.*, "The bacterial redox signaller pyocyanin as an antiplasmodial agent: comparisons with its thioanalog methylene blue," *Redox Rep.*, vol. 16, no. 4, pp. 154–165, 2011.

[74] K. P. Jorgensen, "Determination of the enzyme activity of activated sludge by methylene blue reduction," *Water Pollut. Control Fed.*, vol. 56, no. 1, pp. 89–93, 1984.

[75] P. Bapat, S. K. Nandy, P. Wangikar, and K. V. Venkatesh, "Quantification of metabolically active biomass using Methylene Blue dye Reduction Test (MBRT): Measurement of CFU in about 200 s," *J. Microbiol. Methods*, vol. 65, no. 1, pp. 107–116, 2006.

[76] C. K. John, "Place of the Methylene Blue and Resazurin Reduction Tests in a Milk Control Program," *Am. J. Public Heal. Nations Heal.*, vol. 29, no. 3, pp. 239–247, 1939.

[77] H. R. Thornton and E. G. Hastings, "Studies on Oxidation-Reduction in Milk," *J. Dairy Sci.*, vol. 13, no. 3, pp. 221–245, 2010.

[78] D. J. Wales, R. M. Parker, J. C. Gates, M. C. Grossel, and P. G. R. Smith, "Integrated planar Bragg grating oxygen sensor," *15th Eur. Conf. Integr. Opt.*, no. December, pp. 5–6, 2010.

[79] W. Lee *et al.*, "3D-Printed micro fluidic device for the detection of pathogenic bacteria using size-based separation in helical channel with trapezoid cross-section," *Sci. Rep.*, vol. 5, pp. 1–7, 2015.

[80] J. H. Wu, C. H. Wang, Y. D. Ma, and G. Bin Lee, "A nitrocellulose membrane-based integrated microfluidic system for bacterial detection utilizing magnetic-composite membrane microdevices and bacteria-specific aptamers," *Lab Chip*, vol. 18, no. 11, pp. 1633–1640, 2018.

[81] H. Etayash, M. F. Khan, K. Kaur, and T. Thundat, "Microfluidic cantilever detects bacteria and measures their susceptibility to antibiotics in small confined volumes," *Nat. Commun.*, vol. 7, pp. 1–9, 2016.

[82] S. Wang *et al.*, "Portable microfluidic chip for detection of Escherichia coli in produce and blood," *Int. J. Nanomedicine*, vol. 7, pp. 2591–2600, 2012.

[83] H. Zhang, F. Huang, G. Cai, Y. Li, and J. Lin, "Rapid and sensitive detection of Escherichia coli O157:H7 using coaxial channel-based DNA extraction and microfluidic PCR," *J. Dairy Sci.*, vol. 101, no. 11, pp. 9736–9746, 2018.

[84] A. C. Fernandes, C. M. Duarte, F. A. Cardoso, R. Bexiga, S. Cardoso, and P. P. Freitas, "Lab-on-chip cytometry based on magnetoresistive sensors for bacteria detection in milk," *Sensors (Switzerland)*, vol. 14, no. 8, pp. 15496–15524, 2014.

[85] N. Yamaguchi, H. Ohba, and M. Nasu, "Simple detection of small amounts of Pseudomonas cells in milk by using a microfluidic device," *Lett. Appl. Microbiol.*, vol. 43, no. 6, pp. 631–636, 2006.

[86] T. Preckel, G. Luedke, B. N. Wang, R. Dubrow, and C. Buhlmann, "Detection of Cellular Parameters Using a Microfluidic Chip-Based System," *JALA*, vol. 7, no. 4, pp. 85–89, 2002.

[87] A. M. Kaushik, K. Hsieh, L. Chen, D. J. Shin, J. C. Liao, and T.-H. Wang, "Accelerating bacterial growth detection and antimicrobial susceptibility assessment in integrated picoliter droplet platform," *Biosens Bioelectron*, vol. 97, pp. 260–266, 2017.

[88] J. Cao, S. Nagl, E. Kothe, and J. M. Köhler, "Oxygen sensor nanoparticles for monitoring bacterial growth and characterization of dose-response functions in microfluidic screenings," *Microchim. Acta*, vol. 182, no. 1–2, pp. 385–394, 2015.

[89] R. Gómez-Sjöberg, D. T. Morisette, and R. Bashir, "Impedance microbiology-on-a-chip: Microfluidic bioprocessor for rapid detection of bacterial metabolism," *J. Microelectromechanical Syst.*, vol. 14, no. 4, pp. 829–838, 2005.

[90] S. Ayyash, W. I. Wu, and P. R. Selvaganapathy, "Fast and inexpensive detection of bacterial viability and drug effectiveness through metabolic monitoring," *Sensors*, vol. 16, no. 11, pp. 1–14, 2016.

[91] Pearson Education Inc, "Metabolism," 2006. [Online]. Available: https://slideplayer.com/slide/10917648/.

[92] J. D. Schwartzman *et al.*, "A Guide to Utilization of the Microbiology Laboratory for Diagnosis of Infectious Diseases: 2013 Recommendations by the Infectious Diseases Society of America (IDSA) and the American Society for Microbiology (ASM)a," *Clin. Infect. Dis.*, vol. 57, no. 4, pp. e22–e121, 2013.

[93] L. Maturin and J. T. Peeler, "BAM: Aerobic Plate Count," *U.S. Food & Drug Administration*, 2001. [Online]. Available: https://www.fda.gov/food/foodscienceresearch/laboratorymethods/ucm063346.htm.

[94] KwaZulu-Natal Department of Health, "Standard Operating Procedures for the Operation of Human Milk Banks in Kwazulu-Natal," 2014.

[95] D. B. Weibel, W. R. DiLuzio, and G. M. Whitesides, "Microfabrication meets microbiology," *Nat. Rev. Microbiol.*, vol. 5, no. 3, pp. 209–218, 2007.

[96] A. Pimpin and W. Srituravanich, "Reviews on micro- and nanolithography techniques and their applications," *Eng. J.*, vol. 16, no. 1, pp. 37–55, 2012.

[97] R. Martinez-Duarte and M. J. Madou, "SU-8 Photolithography and Its Impact on Microfluidics," in *Microfluidics and Nanofluidics Handbook*, 2011, pp. 231–268.

[98] Microchem, "SU-8 2000 Permanent Epoxy Negative Photoresist," *Process. Guidel.*, vol. 20, 2015.

[99] B. Bhushan and M. Caspers, "An overview of additive manufacturing (3D printing) for microfabrication," *Microsyst. Technol.*, vol. 23, no. 4, pp. 1117–1124, 2017.

[100] N. Bhattacharjee, A. Urrios, S. Kang, and A. Folch, "The upcoming 3D-printing revolution in microfluidics," *Lab Chip*, vol. 16, no. 10, pp. 1720–1742, 2016.

[101] G. Mehta, M.-A. Mycek, D. Sud, J. Linderman, K. Mehta, and S. Takayama, "Optical imaging in microfluidic bioreactors enables oxygen monitoring for continuous cell culture," *J. Biomed. Opt.*, vol. 11, no. 5, p. 050504, 2006.

[102] K. Mehta *et al.*, "Quantitative measurement and control of oxygen levels in microfluidic poly(dimethylsiloxane) bioreactors during cell culture," *Biomed. Microdevices*, vol. 9, no. 2, pp. 123–134, 2006.

[103] S. M. Grist, L. Chrostowski, and K. C. Cheung, "Optical oxygen sensors for applications in microfluidic cell culture," *Sensors (Switzerland)*, vol. 10, no. 10, pp. 9286–9316, 2010.

[104] D. B. Papkovsky and R. I. Dmitriev, "Biological detection by optical oxygen sensing," *Chem. Soc. Rev.*, vol. 42, no. 22, pp. 8700–8732, 2013.

[105] Thermo Scientific, "Promoter Collection," 2012.

[106] Agile Manufacturing, "ProJet HD3000 Technical Specifications." 2008.

[107] Harrick Plasma, "What is Plasma Cleaning," 2019. [Online]. Available: https://harrickplasma.com/what-is-plasma/.

[108] D. J. Guckenberger, E. Berthier, E. W. K. Young, and D. J. Beebe, "Fluorescence-based assessment of plasma-induced hydrophilicity in microfluidic devices via Nile Red adsorption and depletion," *Anal. Chem.*, vol. 86, no. 15, pp. 7258–7263, 2014.

[109] S. H. Tan, N. T. Nguyen, Y. C. Chua, and T. G. Kang, "Oxygen plasma treatment for reducing hydrophobicity of a sealed polydimethylsiloxane microchannel," *Biomicrofluidics*, vol. 4, no. 3, pp. 1–8, 2010.

[110] F. J. de Bruijin, *Handbook of Molecular Microbial Ecology II: Metagenomics in Different Habitats*. Hoboken, New Jersey: John Wiley & Sons, 2011.

[111] S. Sutton, "Microbiology Topics. Accuracy of Plate Counts," *J. Valid. Technol.*, vol. 17, no. 3, pp. 42–46, 2011.

[112] Universal Wireless Repair, "Main Camera," 2017. [Online]. Available: http://uwrepair.com/product/main-camera-8/.

[113] Microscope.com, "Compound Microscope." [Online]. Available: https://www.microscope.com/omano-om136-monocular-compound-microscope.html.

[114] Google, "Google Pixel 2," 2019. [Online]. Available: https://store.google.com/product/pixel_compare.

[115] Nikon, "Nikon D810 User's Manual," 2014.

[116] Flinn Scientific Chem Fax!, "Blue Bottle Experiment," 2016.

[117] A. Olajire and A. Olajide, "Kinetic Study of Decolorization of Methylene Blue with Sodium Sulphite in Aqueous Media: Influence of Transition Metal Ions," *J. Phys. Chem. Biophys.*, vol. 2, no. 2, pp. 1–7, 2014.

[118] R. R. Cavano, "Sulfites for Oxygen Control," pp. 1–7, 2007.

[119] S. Ayyash, "Fast and inexpensive detection of bacterial viability and drug effectiveness through metabolic monitoring," McMaster University, 2016.

[120] D. Markov, E. M. Lillie, S. P. Garbett, and L. J. McCawley, "Variation in diffusion of gases through PDMS due to plasma surface treatment and storage conditions," *Biomed. Microdevices*, vol. 16, no. 1, pp. 91–96, 2014.

[121] I. Sunshine, *CRC Handbook of Analytical Toxicology*. Cleveland: The Chemical Rubber Co., 1969.

[122] K. E. Kram and S. E. Finkel, "Rich Medium Composition Affects Escherichia coli Survival, Glycation, and Mutation Frequency during Long-Term Batch Culture," *Appl. Environ. Microbiol.*, vol. 81, no. 13, pp. 4442–4450, 2015.

[123] T. M. Nosek, *Essentials of Human Physiology*. Gold Standard Multimedia, 1998.

[124] A. Lamberti, S. L. Marasso, and M. Cocuzza, "PDMS membranes with tunable gas permeability for microfluidic applications," *RSC Adv.*, vol. 4, no. 106, pp. 61415–61419, 2014.

[125] Y. Zhang, M. Ishida, Y. Kazoe, Y. Sato, and N. Miki, "Water-vapor permeability control

of PDMS by the dispersion of collagen powder," *IEEJ Trans. Electr. Electron. Eng.*, vol. 4, no. 3, pp. 442–449, 2009.

[126] T. C. Merkel, V. I. Bondar, K. Nagai, B. D. Freeman, and I. Pinnau, "Gas Sorption, Diffusion, and Permeation in Poly(dimethylsiloxane) The permeability of poly(dimethylsiloxane) [PDMS] to," *J Polym Sci B Polym Phys*, vol. 38, pp. 415–434, 2000.

[127] B. Jo, L. M. Van Lerberghe, K. M. Motsegood, and D. J. Beebe, "Three-Dimensional Micro-Channel Fabrication in," *J. Microelectromechanical Syst.*, vol. 9, no. 1, pp. 76–81, 2000.

[128] S. Halldorsson, E. Lucumi, R. Gómez-Sjöberg, and R. M. T. Fleming, "Advantages and challenges of microfluidic cell culture in polydimethylsiloxane devices," *Biosens. Bioelectron.*, vol. 63, pp. 218–231, 2015.

[129] C. K. Johns, "Concerning the Accuracy of the Methylene Blue Reduction Test," *J. Dairy Sci.*, vol. 21, no. 4, pp. 227–237, 1938.

[130] T. Cross *et al.*, "An Optimized Enrichment Technique for the Isolation of Arthrobacter Bacteriophage Species from Soil Sample Isolates," *J. Vis. Exp.*, no. 98, pp. 1–9, 2015.

Appendix A
Standard Operating Procedure for Preparation and Streaking of LB Agar Culture Dishes

Standard Operating Procedure for Preparation of LB Agar dishes

1. Prepare 750 mL of LB liquid (25 g broth powder per 1 L distilled water) in a 1000 mL glass bottle with cap.
2. Add 11.25 g (1.5%) bacteriological agar.
3. Swirl to mix. The powder will not dissolve completely.
4. Loosely cap the bottle to allow for venting of excess gas. Add a fresh piece of autoclave tape.
5. Autoclave on liquid cycle.
6. After the cycle is complete, remove to benchtop, tighten the cap, and cool to ~50°C. The media should still be liquid but should be just beginning to thicken. As a ballpark: still quite warm to the touch, but cool enough to leave your gloved hand on the outside of the flask for several seconds without burning it.
7. If antibiotics are to be added, add at this point (1:1000 dilution in LB agar) in a sterile environment, and swirl the flask vigorously for several seconds to mix.
8. In aseptic conditions, set plates out in stacks of 5, and label the bottom with the antibiotic added. Use the following key as an example: A=ampicillin, C=chloramphenicol, K=kanamycin, T=tetracycline, S=streptomycin.
   *Be careful not to damage the plastic sleeve that the dishes come in. Finished plates will be stored in this.
9. Remove the dish lid, and remove the cap from the bottle. Pour just enough LB agar into the petri dish to completely cover the bottom of the dish, then replace the lid such that the dish isn't fully covered.
   *Work quickly!! The agar will harden soon once it is cool enough to add antibiotics. You should finish pouring dishes within 5 minutes of adding the antibiotic.
10. Allow agar to set. When the agar becomes translucent, replace the lid on the dishes and stack them. Store plates back in the plastic sleeve that the Petri dishes came in. Ensure that dishes are stored upside down in a 4°C refrigerator. Label the sleeve and date stamp it.

Standard Operating Procedure for Bacterial Streaking of Agar Dish

1. In sterile conditions, use a sterile pipette tip to pick up a single colony from a previously cultured bacterial dish or scrap the top layer of a frozen glycerol bacterial stock.
2. Gently streak out a zig-zag pattern on top of the LB agar dish close to the edge. Stick to one section of the agar dish. Refer to Figure A40. Appropriately dispose of the tip.
3. With a fresh sterile tip, gently drag through streak #1 and spread the bacteria in a zig-zag motion over another section of the dish. Repeat this at least two more times, each time with a new tip. With each streak, lines should be spaced further and further away from each other. This is to ensure the appearance of single colonies.
4. Cover the agar plate with its lid. Incubate overnight at 37°C, upside down.
5. Colony growth should be seen after incubation.

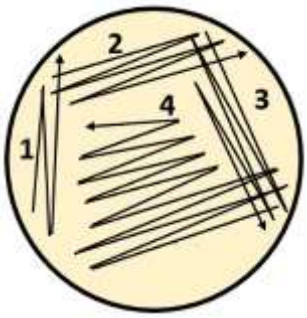

Figure A40: Streaking pattern on LB agar plate. Adapted from [130].

Appendix B
Standard Operating Procedure for ImageJ Processing & Analysis

1. Collect desired images and put in a separate folder.
2. Open ImageJ program. Open a sequence of photos: "File" → "Import" → "Image Sequence" → Select the first image of the sequence to be analyzed.
3. Save the image sequence as a .tiff file to retain all the changes made.
4. To align wells in the images, use the StackReg plugin.
    a. Download from the ImageJ website, unzip, and copy into the Plugin folder of ImageJ (via Programs). "Plugins" → "StackReg" → "StackReg" → Select "Rigid Body" when asked which type of Translation is required and press "OK". Depending on the image, you may need to run the plugin multiple times on different settings – i.e. Scaled Rotation or Translation.
5. Select ROI using the "Microarray Profile" plugin. This plugin allows you to adjust the ROI, the number of rows and columns required to measure all the wells in the device.
    a. In the pop-up window, click "Reset Grid" to modify the number of well rows and columns. Can also modify the ROI in this pop-up window.
    b. Once the grid has been superimposed onto the image, you can modify it to match the well grid.
        i. Hold down shift, select the top-left corner square and drag it towards the bottom right corner. This will shrink the spacing between rows and columns.
        ii. While holding down 'alt', drag the grid to match the top-left square with the top-leftmost well in your image.
        iii. While holding down 'shift', adjust the top-right square to match the top-right well in your image. This should align all the squares in the grid to the wells in the image.
    c. Click "Measure RT". A window will pop-up with the mean gray value for each of the wells and for each of the images in the series.
6. Copy and paste this data or export into Excel under the file name indicated in the code in Appendix A. Save as .CVS format.
7. Open R and the code. Edit code to match the scenario of the image series: the number of images taken will translate to the number of columns required in the final matrix. Enter this number after "ncol =" in the code (2 instances). The number of data points collected by ImageJ divided by the number of images will be the number of rows. Enter this number after "nrow=" (1 instance).
8. Select the whole code, then run.
9. Open the Excel file "export" as indicated in the code. This is the raw mean gray intensities of each well, organized such that each row is a specific well. Copy and paste the data into the appropriate Excel document for further processing.
10. Open the Excel file "exportNormal". This is the normalized intensities values of each well, organized such that each row is a specific well. Again, copy and paste the data into the appropriate Excel document for further processing.

11. From R, transfer the averages of each measure time point and the standard deviations to your Excel document.
12. Normalize the data against an image taken of the empty and sealed wells to control for background noise and potential irregularity of light distribution.
13. Graph the data and analyze for trends.

Appendix C
Code for organizing ImageJ Data into columns for Excel

A short code was written for use in the program R to quickly systematize the data extracted from ImageJ and export it into an Excel file. "ncol" represented the number of pictures taken in the time-lapse and "nrow" indicated the number of wells within the device. Additionally, the code helped to normalize the data for each individual well (x_n/x_0; where $n =$ picture number in the stack, $x_n =$ Mean Gray Value at $n, x_0 =$ Initial Mean Gray Value) to determine trends, find the average behaviour within condition sets, and determine the standard deviation.

```
normalize = function(x) {
   x/x[1]
}

data = read.csv(file="milk.csv", header=FALSE, sep=",")
v = as.vector(data[,9])
m = matrix(v, ncol = 147,byrow=TRUE)
head(m, n=10)
dim(m)
dim(n)

normalized = matrix(, nrow=348, ncol=147)
for (i in 1:(dim(m)[1])) {
   n = normalize(m[i,])
   normalized[i,] = n
}
head(normalized)

avg = apply(normalized, 2, mean)
standardDev = apply(normalized, 2, sd)

avg
standardDev

write.table(m, file="export.csv", sep=",")
write.table(normalized, file="exportNormal.csv", sep=",")
```

Appendix D
Effect of bacterial concentration on rate of MB colour change using older stock of MB

The point of differentiation between the sterile well controls and those with varying concentrations were as follows: 8 hours (1.22 ± 0.02 normalized MGV units) for 10^8 CFU/mL or 10^7 bacteria/well concentration ($p<0.01$), 24 hours (1.21 ± 0.03 normalized MGV units) for 10^4 CFU/mL or 10^3 bacteria/well ($p<0.05$), and 36 hours (1.22 ± 0.04 normalized MGV units) for 10^2 or 10 bacteria/well ($p<0.01$) (Figure A41). Although the exact point at which bacterial wells of each concentration could be differentiated from the control varied when comparing older and newer stocks of MB, similar behaviours were noted with the varying concentrations. The maximum normalized MGV for 10^7 bacteria/well was noted to be lower than that for 10^3 bacteria/well. This is hypothesized to be due to the overcrowding leading to greater competition to resources, and ultimately slower growth and reduction of MB.

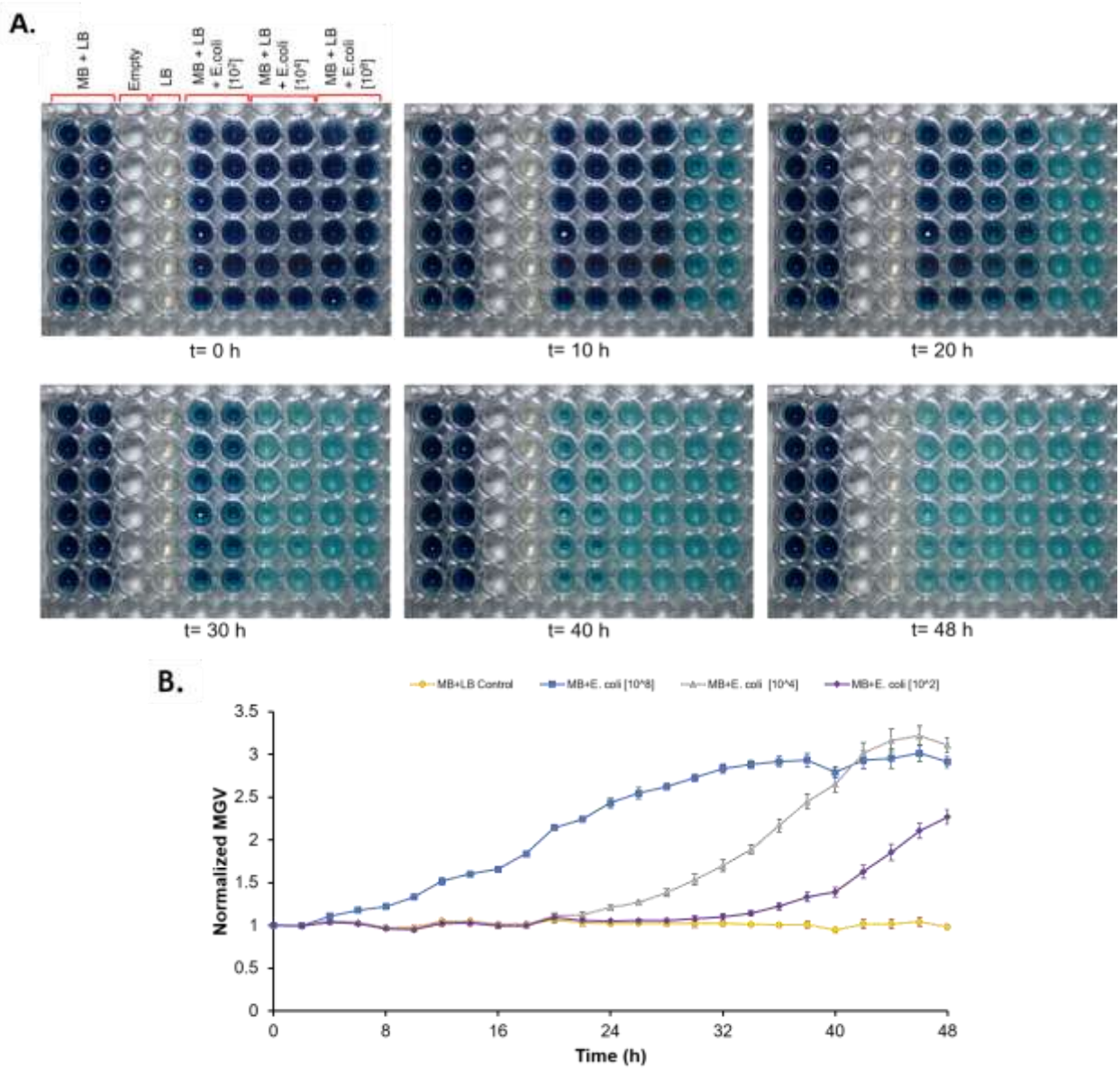

Figure A41: Effect of bacterial concentration on time of MB colour change due to metabolism. A.) Selected images taken from the 48-hour imaging period that show the colour change progression of varying E. coli concentrations. [MB] = 2.5 mg/mL. B.) Wells of *E. coli* [10^8 CFU/mL] (n=36) show increase in normalized MGV that differentiates from the control at 8 hours. Concentrations of [10^4 CFU/mL] (n=36) differentiate from the controls at 24 hours, and for [10^2 CFU/mL] (n=36), 36 hours. Data shown as mean ± SEM.

Appendix E
MB Concentration Comparison in Nanowell Devices

To determine which concentration of MB would allow for ideal imaging and differentiation between control and inoculated wells in nanowell volumes, MB at 1.0 mg/mL and 1.5 mg/mL were compared. These concentrations were chosen based on the concentrations and colourations tested in microwell volumes. It was expected that the visible saturation of MB would be paler in the nanowells compared to the microwells due to a decrease in volume depth. Therefore, a higher concentration may be required to be able to distinguish between bacteria and no bacteria conditions. Refer to Chapter 3 for protocols for preparation of sample solutions, filling of devices, and imaging. *E. coli* K12 MG 1655 was used at 10^8 CFU/mL. Figure A42 shows timed images of the devices over a 24-hour period and the extracted data.

Over time, the control devices of both concentrations (device ii. and iv.) remained constant at a normalized value of around 1. However, the inoculated devices (device i. and iii.) showed an increase in normalized MGV at the 24-hour mark to 1.25 ± 0.005 units for 1.5 mg/mL MB and 1.27 ± 0.005 units for 1.0 mg/mL MB (Figure A42.B-C). Within each concentration of MB, a clear distinction can be visually detected between the device with bacteria and the one without. The normalized MGV of the sterile and inoculated devices within each concentration were significantly different at 24-hours ($p<0.0001$). Image analysis indicated that the difference between the 1.5 mg/mL MB devices (i. and ii.) was 0.22 units whereas, for the 1.0 mg/mL devices (iii. and iv.), the change was 0.25 units (Figure A42.D). This higher value for 1.0 mg/mL MB could be explained by there being less MB for the bacteria to reduce. Therefore, in the same length of time, the final colouration will be lighter in the solution with less MB when all other factors are the same. An MB concentration of 1.0 mg/mL was chosen over 1.5 mg/mL because of its greater detectable change within 24 hours.

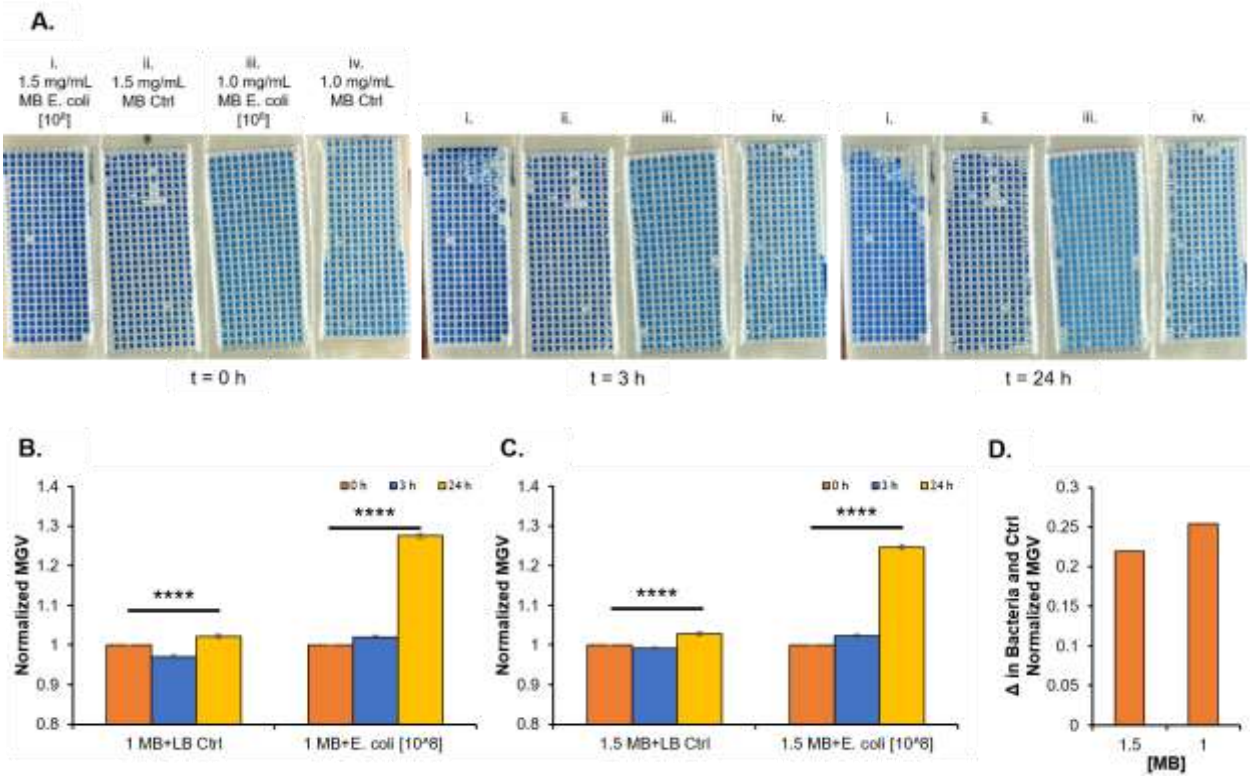

Figure A42: Comparison of MB concentrations in nanowell devices to determine ideal concentration for use. A.) Time lapse images of devices with bacteria and those without. MB at B.) 1.0 mg/ml and C.) 1.5 mg/mL were chosen based on experiments in microwell volumes. Sample sizes for each of the conditions follow: 1.0 mg/mL MB no bacteria, n=187; 1.0 mg/mL MB bacteria, n=252; 1.5 mg/mL MB no bacteria, n=199; and 1.5 mg/mL MB bacteria, n=202. Data shown as mean ± SEM. D.) Comparison of the difference in colour based on concentration showing greater change in 1.0 mg/mL than 1.5 mg/mL.

Appendix F
Preliminary Experiment testing a higher MB Concentration in LB Nanowells

As a preliminary test to increase the saturation and overall colour change of the nanowells, the same MB concentration used in the microwells was applied to the nanowells. The concentration was increased from 1.0 mg/mL to 2.5 mg/mL. The point of bacterial detection was determined by comparing a device filled with *E. coli K12* at a concentration of 10^8 CFU/mL and another with only the MB+LB control solution (Figure A43.A). Images were taken in half-hour intervals for 46 hours. Over the imaging period, the differences between the inoculated and controls wells were significant ($p<0.0001$). After one hour, the bacterial wells were significantly different from the sterile wells ($p<0.01$) at normalized MGV of 0.95 ± 0.0003 units compared to the controls at 0.93 ± 0.0005 units (Figure A43.B). After 46 hours, the average saturation of the bacterial well was 48% paler than the control well. Despite the definitive increase in overall saturation, the MB did not completely reduce into its colourless state and the overall change in MB colour did not surpass a normalized MGV of 1.09 units. This could indicate that the ideal concentration of MB that would balance is between 1.0-2.5 mg/mL.

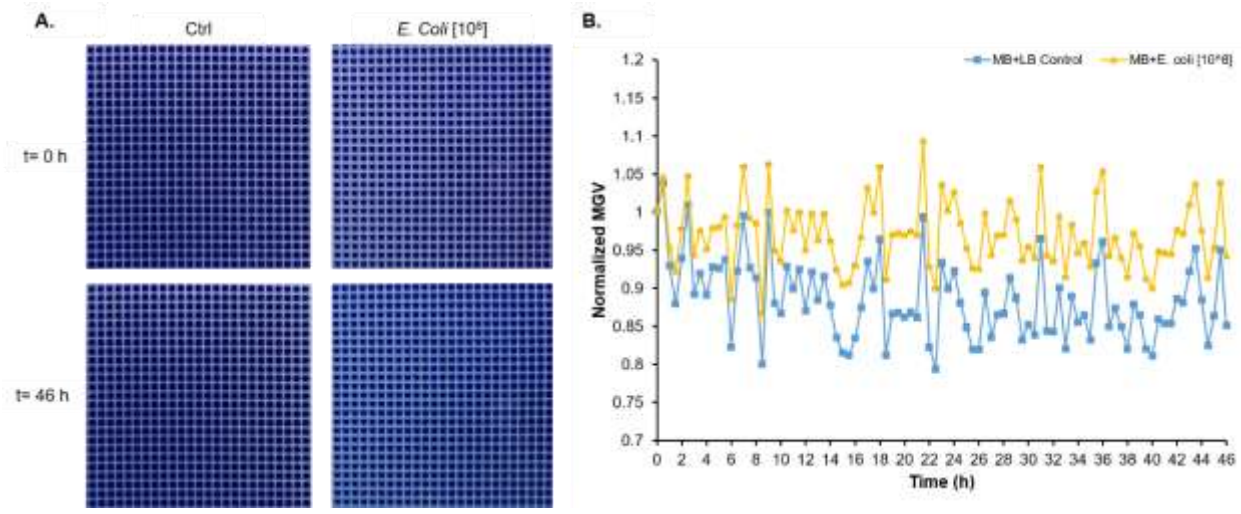

Figure A43: Nanowells filled with 2.5 mg/mL MB as a preliminary test to increase saturation and colour change. A.) Images of wells filled with 10^8 CFU/mL bacteria (n=625) and those without (n=625) taken at t=0 and 46 hours. B.) The normalized saturation of the bacteria wells was not significantly different from the sterile wells. Data shown as mean ± SEM.